SELF-ORGANIZED NANOSTRUCTURED PARTICLES FABRICATED FROM SPRAY-DRYING OF COLLOIDAL NANOPARTICLES

(コロイドナノ粒子の噴霧乾燥による
自己組織化ナノ構造体微粒子の合成)

by

ASEP SUHENDI

HIROSHIMA UNIVERSITY
SEPTEMBER 2013

SELF-ORGANIZED NANOSTRUCTURED PARTICLES FABRICATED FROM SPRAY-DRYING OF COLLOIDAL NANOPARTICLES

A Dissertation Submitted to
Department of Chemical Engineering
Graduate School of Engineering
Hiroshima University

by

ASEP SUHENDI

In Partial Fulfillment of the Requirements
For the Degree of
Doctor of Engineering (Dr. Eng.)

Hiroshima University
September 2013

Approved by

Professor Kikuo Okuyama
Advisor

Acknowledgments

Abstract

Self-organized nanostructured particles fabricated from spray-drying of colloidal nanoparticles has received a great amount of attention recently. Study on the structurization of nanostructured materials under effects of droplet charge is not available. To meet this demand, this dissertation is mainly divided into four sections cover the study on self-organized nanostructured particle under various droplet charges by spray-drying of colloidal nanoparticles.

Section 1 (*i.e.*, **Chapter 1**) is the introduction. Two kinds of droplet generation using spray drying methods (i.e. ultrasound-assisted and electrospray-assisted spray-drying methods) with their basic theoretical explanation and current progress in the production of particles are discussed.

Section 2, consisting of two chapters, describes the self-organization of colloidal nanoparticles under uncharged droplet condition. The synthesis of colloidal nanoparticles and its application in the fabrication of various self-organized hollow particles are described in detail, corresponding to **Chapter 2 and 3**, respectively.

In **Chapter 2**, the effect of nanoparticle charges on the self-organized nanostructured particles is described. Preparation of spherical-dense PS particles with controllable outer diameter and its application for particle templating application are reported. Particle formation and several parameters manipulation are also discussed. The prediction equation as a simple theoretical model on the effect of several parameters was also described to support the experimental result.

Chapter 3 describes effects of colloidal nanoparticles charge, size and concentration on fabrication of self-organized porous silica particles become the main

focus of the study. Self-organization of colloidal nanoparticles in the formation of porous film form was studied. Comparison between theoretical calculation and experimental results on the arrangement of the particles was also presented. The calculation results were used for production of particles with controllable morphology.

Section 3, presenting the study self-organization of colloidal nanoparticles under charged droplet condition, comprises four chapters (Chapter 4, 5, 6 and 7). The production of self-organized nanostructured particles with controllable size and morphology using a specific parameter manipulation under charged droplet condition becomes the main objective in this section.

In Chapter 4, a high stability and controllability charged droplet generation system is developed. Control of charge over volume delivered to the system is essential for generation of stable and monodisperse charged droplets.

Chapter 5 explains the effects of droplet size and colloidal nanoparticles composition on the formation of core-shell silica/PS particles. Adjustment of colloidal nanoparticles composition and its effect on the core-shell particle morphology is the main focus of this chapter.

Chapter 6 describes the effects of droplet size and concentration on the formation of spherical hollow silica particles. Control of agglomeration-free condition of the produced hollow particles is achieved by adjustment of several parameters including the droplet size. The effectiveness of the hole size control by adjusting template hole size is also described.

Chapter 7 describes the effects of droplet charge on fabrication of self-organized hollow silica particles from electrospray-drying of colloidal nanoparticles. Self-organization of nanoparticles inside a charged droplet and self-organization parameters (i.e. flow rate, charge, size, and composition of the colloidal nanoparticles)

are also thoroughly investigated. The availability of the charge in the droplet surface provides possibility in formation of various morphologies in the fabricated particle with controllable outer shape, hole number, shell thickness, and internal structure.

Finally, **Section 4 (Chapter 8)** contains general conclusion of all topics, which has been described in the previous sections and chapters.

Contents

2. Effect of colloidal nanoparticle charge on the fabrication of various self-organized porous and hollow particles   33

Technology Transfer on Nanotechnology at Hiroshima University

1.1. Introduction

Technology is knowledge of tools, techniques, system or method of organization in order to solve a problem or serve some purpose.[1] Technology significantly affected our daily life become easier, simpler, and more convenience. Development of technology is a consequence of science and engineering. For example, science might study the flow of electrons in electrical conductors, by using already-existing tools and knowledge. This new found knowledge may then be used by engineers to create new tools and machines, such as semiconductors, computers, and other forms of advanced technology.

Development of technology takes place every day, wherever in the world, in each country, university, factory, research institute, etc. In each country, development of technology maybe differ each other depend on many factors, e.g. economy, society's demand, government policy etc. Development of technology in someplace may be required in other places at different time. Therefore, in order to make a shortcut in research and development, and also to obtain economic gain, transfer technology between countries is necessary.

Technology transfer is the movement process of science, engineering, and technology among governments and other institution to ensure that scientific and technological development are accessible to a wider range of users, who can then further develop and exploit the technology into new products, process, applications, materials or service. Technology transfer is including transfer of knowledge, skill, method of manufacturing, and even transfer of a group of people to train and educate other people. It is a commonplace that technological innovation in developed

countries and the transfer of technology to less developed countries both play an important role in determining the pattern of world trade and changes in that pattern over time[2]. A technological innovation is an idea, practice or object that is perceived as new by an individual or some other unit. Therefore, technology transfer is the application of information (a technological innovation) into use. The technology transfer process usually involves moving a technological innovation from a research and development organization to a receptor organization (such as a private company). A technological innovation is fully transferred when it is commercialized into a product that is sold in the marketplace.[1] So, technology transfer is a special type of communication processes in two way directions which give advantages each other.

In general there are three phase of transfer technology which are selection of transfer technology, decision of move technology, and technology transfer education and training to local person. To do technology transfer smoothly, the agent of transfer technology, so called technology broker is necessary. Technology brokers are people or organization, provide a way and facilitate communications between donor and receiver of transfer technology. Technology broker plays an important role in the process of transfer technology. According to Hargadon, technology brokers, at least, do the following tasks: (i) capture good ideas, keeping ideas alive, imagining new uses for old ideas, and putting promising concepts to the test.[3]. Although the markets and settings of different brokers are diverse, their approaches are same. Indeed, the four intertwined process are remarkably alike across companies and industries.[3]

Development of technology innovation is a linear process, from basic research, to applied research, to development, to commercialization, to diffusion, and to consequences of the innovation.[1] A linear model of the innovation-development

process may not fully take into account external environmental factors, such as market demand or regulatory changes, which may influence the technological innovation process. The technology transfer process spans the stage from research and development to commercialization and beyond, but with particular focus on the interface between research and development (often by a university research center, a corporate unit, or by a government laboratory) and commercialization (often carried out by a private company).[3]

Technology, as widely accepted, is essential for improving the economy of a nation, especially in developing countries where industrial growth is assigned a very important role. In this aspect, the technical institutes and universities play essential roles not only as the creators of new technology but also as the providers of much needed skilled-personnel and as the media players who match the economic changes with the change in society. But the universities cannot just develop the technology, hand it over to the industry sector and wash their hands off it. They have to collaborate with industry to make full use of the transferred technology from the adoption stage to the commercialization stage. In turn the university needs the industry's knowledge of the market to come up with more and more new, applicable and successful technology development.[4]

In order to support Japan to accelerate the transfer technology to the developing countries, Graduate School of Engineering of Hiroshima University conducted a Special Doctoral courses for international student, namely "Fostering Program for Practical Researchers and Engineers Distinguished in Technology Transfer". This program is supported by Ministry of Education, Culture, Sports, Science and Technology (MEXT) of Japan. It cultivate researchers and engineers with the capability to accommodate themselves to worldwide transfer of engineering and

_____

technology taking place in research and development, and manufacturing situations of this era of borderless operations, as well as professional research and development capability.

This thesis described the activity of technology transfer from Hiroshima University to Indonesia, in the term of a special doctoral course. The research and development of self-organized nanoparticles was conducted at Thermal Fluid Engineering Laboratory of Graduate School of Engineering of Hiroshima University.

1.2. Implementation

1.2.1. Laboratory Description

At thermal fluid engineering laboratory, I did the research on self-organization of nanostructured particles fabricated from spray-drying of colloidal nanoparticles. I have successfully fabricated various morphologies of nanostructured particles and have studied the effects influencing the self-organization process.

I did research on the synthesis of colloical nanoparticles with controllable size and its application in the formation of self-organized hollow-structured particles. Particle formation and effects of several parameters manipulation are also described.[5]

Development of high stability and controllability of elecrospray system for generating monodisperse charged droplets was reported. Controllable cone-jet geometry resulted in the production of controllable monodisperse droplets and particles.[6]

Effects of droplet size and concentration on the production of single and aggregated hollow particles has been studied. Successful control in the number of holes of the produced hollow particles was achieved by the Adjustment in the droplet

_____

size, which can be easily realized by flow rate control in the electrospray-assisted spray-drying process.[7]

Effects of droplet and colloidal nanoparticles properties on the self-organization process in the spray-drying process was studied. Introduction of droplet charge affecting the electrostatic interaction between the colloidal nanoparticles. Control of these parameters can produced hollow particles with controllable outer shape, hole number, shell thicknes, and internal structure.

The results of these research have been published in internationally-renowned peer reviewed journal and international scientific meeting such as Colloids and Surfaces A: Physicochemical and Engineering Aspects, Langmuir, Advanced Powder Technology, and Materials Letters.

1.2.2. Special Course Program

Technology transfer class was held at Hiroshima University for all foreign students involved in special doctoral course program. The class covers description on theory and case study of technology transfer from Japan to developing countries in Asia, including China, Thailand, Iran, Vietnam, Bagladesh, and Indonesia. Practical example and theoretical analysis of the transfer of research and development and manufacturing technology both domestic and abroad are explained using teaching materials developed in the "MOT Educational Program on Technology Transfer for Developing Countries". The class discussed the general theory of technology transfer, the importance and issues for both transferring and receiving partners. The issues on learning curve and the use of learning curve on the information flow in manufacturing, technology transfer and human resource development in developing countries.

1.2.3. Strategy and Characteristics of Transfer Technology

There are six technology strategies with their own characteristic points of management technology, which are offensive strategy, defensive strategy, imitative strategy, dependent strategy, traditional strategy, and opportunity strategy. The characteristics of offensive strategy are: develop various technologies in the company, Lead technology innovation in industry continuously, dominate market, and possess profits exclusively, much resources of enterprise are allocated to technology development, not afford to develop technology for quality improvement and cost reduction in rapid growth and maturation stages, and licensing developed technology and to other companies to get license fees.

The characteristics of defensive strategy are: develop various technologies like offensive strategy, avoid to lead technology innovation, observe technology trend and develop technology efficiently, not fundamental and unique research, but experimental development and design, less research and development investment than offensive strategy by avoiding develop risk, possible to allocate resources to management technologies, possible to improve quality and reduce cost for maintain competitiveness.

The imitative strategy shows characteristics as follow: install the developed and introduces technology, research and development on production management technologies for quality improvement, cost reduction, or technology service and training, after maturation, efficient production processes and high quality products with less price are developed, receiver of new product technology in technology transfer, no need to product development, delay in entering competition in market, and enter market with severe competition.

On the dependent strategy show characteristics as follow: less or no technology

development, as a member of high technology company, supply parts or other services, try to improve efficiency in producing assigned parts and services or the company itself becomes dependent without considering the improvement, necessary to improve efficiency and show uniqueness and particularity in producing parts and services.

The traditional strategy show characteristics as follow: develop technology based on skilled workers, technologies in skilled workers and engineers, all technologies are accumulated in workers and engineers as skill and know-how, tacit technologies in workers and engineers should be visualized, clarified, and digitalized, of transferred to next workers and engineers for continuing and enhancing the technologies.

Last, the opportunity strategy show these characteristics: in market with less technology but rapid changes, seek new opportunity of business, market survey to seek opportunity and management technology on product quality are important.

1.2.4. Advantages of Transfer Technologies

In the perspective of receiving side, technology transfer is the process of sharing knowledge, skills, technologies, methods of manufacturing, samples of manufacturing, and facilities among governments and other institutions to ensure that scientific and technological developments are accessible to a wider range of users who can then further develop and exploit the technology into new products, processes, applications, materials or services. Basically, Technology transfer from the receiving side can contribute to economic development, improvement technology, and provide large-scale of job opportunities.

Transferring technology is profitable to the business management. It means that technology which a certain economic subject holds is used for the same purpose and

production activity is performed by other economic subject. Background of technology transfer are: appreciating yen, high wages, and young workers decrease, and diminishing international competitiveness including overseas transfer of production plan, additional value improvement of existing industry, and new industrial creation (expansion market). Based on those backgrounds, transferring technology is profitable to the business management because they can reduce the production cost; wages cost, and also expand the new market. Finally, it will improve their income.

1.2.5. Internship at Japanese Company

Internship program dispatches foreign students to Japanese companies and cultivates their comprehension capability related to issues about cooperation between domestic development-manufacturing departments and overseas production sites and technology transfer, and problem-solving capabilities in connection with them. The "internship" coordinates industry-university cooperation type educational activities in which practical training by engineers of host companies and theoretical instruction by academic instructors specializing in manufacturing technology transfer are combined. Internship program was done at a chemical Japanese company, namely Toda Kogyo Corp. Toda Kogyo Corp. was established in 1823, started the production of red iron oxide pigment. Toda Kogyo Corp. has developed a fine-tuned and successful synergy between innovative material processing and high quality product, resulting in new dimensions in the production of functionalized-materials for the emerging technologies such as energy storage and nanotechnologies.

Toda Kogyo has four main products which are magnetic recording powder, magnetic parts materials, electrophotographic materials, and color materials. Magnetic recording powder has been developed for the next-generation materials which are

being perfected for use in applications of the emerging digital multimedia age. Applications: Video tape, audio tape, computer storage, various disks. Magnetic parts materials has been developed as ultrafine ferrite particles can be applied directly onto PET films and papers to create prepaid cards and magnetic tickets. Applications: prepaid cards, magnetic tickets, magnetic rolls. Electrophotographic materials have been developed as a toner particle that can create beautiful, vivid colors ideal for the next generation of high-speed color units. Applications: Printer, copy machines, fax machines. Iron oxide particles has been developed as coloring agents or pigments with beautiful color and good physical properties (e.g. anti-corrosive, coated perfectly) and could be applied as paint, ink, resin, cement.

Internship was conducted on October 3-7, 2011 at Toda Kogyo Co., Ltd., located in Otake City, Hiroshima, Japan. The activity during internship was synthesis of magnetic nanoparticle by liquid phase method. Magnetic nanoparticles (i.e., Barium Ferrite) has been successfully synthesized using liquid phase method. The synthesized Barium Ferrite nanoparticle was dispersed in water; the Vibrating Sample Magnetometer (VSM) measurement shows that it had a high coercivity. This type of particles is appropriate for frequenty used recording media.

1.2.6. Problem Based Learning for Technology Transfer

The Graduate School of Engineering of Hiroshima University organized a special doctoral course, namely "Fostering Program for Practical Researchers and Engineers Distinguished in Technology Transfer". The curriculum of special course is very unique, because it covers the research, coursework on transfer technology, internship at Japanese companies, and exercises on technology transfer which is called as PBL (Problem Based Learning). Therefore, every student who was accepted as

"special course student" should join the internship at Japanese company as well as exercise on technology transfer (PBL).

On 26th and 27th December 2011, The Graduate School of Engineering organized the annual meeting of "PBL for Technology Transfer". This meeting was attended by some professors and all special course students. There are seven PhD students who were finished the internship at Japanese company, presented their experiences. They are: Mr. Li Gang, Ms. Phothisantikul Phacharakamol, Mr. Noman Abdullah, Mr. Tran Tu Anh, Mr. Xu Rong, Mr. Soltaniasl Mohammad, and myself Asep Suhendi. There are also two Master students (Mr. Meng Zhuo and Mr. Lee Zhezeng) presented the same experiences.

On the first day, all presenters presented their experiences about cultural exchanges experiences from their daily life in Japan. Generally, students choose Japan because Japan is modern and well-developed country, and Japan has been known as one of the leading countries in high technology. The students choose Hiroshima University because of the uniqueness curriculum of the special course. All presenters have many unique experiences, because the Japanese culture is different with their own culture. At the first time their coming to Japan, all presenters have a deep impression to Japanese culture, everything seen wonderful and new. After several months, we found difficulties of Japanese life. One of the greatest barriers for us is language problem. Most of special course students do not understand Japanese and most of Japanese people do not understand English. So that, very difficult to communicate with Japanese students. To solve this problem, most of us use sign language in a primitive way to communicate to Japanese people, and fortunately, Japanese people show great respect to our effort.

On the second day, all presenters presented their experiences about internship in

_____

Japanese Company. Many Japanese companies participate in this internship which are: Mitsubishi Rayon, Keisoku Research Consultant Corporation, Fujikasui Engineering Co., Ltd., Toyo Koatsu, Sanei Co., Toda Kogyo corp., and Ondo Corp. Most of presenter got a lot of good experiences during the internship in Japanese Company. They can compare the habit in Japanese company with the company in their own country. Again, the barrier for us is communication. It was very difficult to communicate to company people in English.

1.3. Conclusions

A special doctoral course, namely "Fostering Program for Practical Researchers and Engineers Distinguished in Technology Transfer", has been conducted at Hiroshima University. The purpose of this program is to support the technology transfer process from Japan to the developing countries. The program includes the research in the laboratory, internship program, and problem-based learning. Overall, this program is very good not only to support technology transfer process, but also to produce high-quality research which is very useful for development of science and technology and for industrial application.

1.4. References

[1] E.M. Rogers, S. Takegami, J. Yin, Lessons learned about technology transfer, Technovation, 21 (2001) 253-261.

[2] P. Krugman, A model of innovation, technology transfer, and the world distribution of income, The Journal of Political Economy, (1979) 253-266.

[3] A. Hargadon, R.I. Sutton, Technology brokering and innovation in a product development firm, Administrative science quarterly, (1997) 716-749.

[4] J. Lee, H. Win, Technology transfer between university research centers and industry in singapore, Technovation, 24 (2004) 433-442.

_____

[5] A.B.D. Nandiyanto, A. Suhendi, T. Ogi, T. Iwaki, K. Okuyama, Synthesis of additive-free cationic polystyrene particles with controllable size for hollow template applications, Colloids and Surfaces A: Physicochemical and Engineering Aspects, 396 (2012) 96 - 105.

[6] A. Suhendi, M.M. Munir, A.B. Suryamas, A.B.D. Nandiyanto, T. Ogi, K. Okuyama, Control of cone-jet geometry during electrospray by an electric current, Advanced Powder Technology, 24 (2013) 532-536.

[7] A. Suhendi, A.B.D. Nandiyanto, M.M. Munir, T. Ogi, K. Okuyama, Preparation of agglomeration-free spherical hollow silica particles using an electrospray method with colloidal templating, Materials Letters, (2013 (In press)).

Chapter 1

Introduction

1.1. Background

Nanostructured particles have received a great amount of attention recently.[1] They possess excellent properties both chemically and physically, which are significantly different from those in bulk form.[2] As a result, they are potential for a variety of application, ranging from electronic devices, ceramics, magnetic materials, drug delivery, catalysts, chemical and sensors, etc.[3-5]

Effective strategies to tailor nanomaterial reliably and predictably are important.[6] Interest in the control of different characteristics, such as size distribution, morphology, purity, crystallinity, and composition has been increasing. Investigations toward the functionalization, the formulation, and the production of self-organized nanostructured particles have focused on making them available for industrial application.

Fabrication of nanostructured particles has been widely reported, with combination of self-organization and templating method is the main key in the process. Successful preparation of nanostructured particles and their scale-up formulation have been reported. Controllable particle size and morphologies within the desired range is also achievable under specific conditions. However, problems and limitations associated with the above methods remain: (i) agglomeration in the final product; (ii) multi-step preparation; (iii) contamination; (iv) high-cost process; (v) difficult in process; and, (vi) scaling-up the process.[7]

Among the above processes, a spray drying method of colloidal nanoparticles is most promising. The advantages of this method are facile yet simple process and

_____

potential for many applications. Because of that demands, in this dissertation, this method is described in detail, which will be crucial for the improvement of particle science and technology.

1.2. Spray-drying method

A spray-drying process is an effective and efficient method to produces dry powder from either a liquid or slurry. This method has many advantages and has potential to be used in many applications. Spherical-shaped particles with agglomeration-free, relatively monodisperse size, and high-purity can be produced simply using a rapid, a cheap, and a continuous process.[4] Great attention come from scientist and industrialist due to its simple design and easy-to-scaling-up process of the spray-drying method.[8] Many form of spray-drying have been reported[4, 9], which can be characterized using their atomization process. The atomization process involves physical or electrical forces to atomize solution input into droplets. Ultrasonic nebulizer, twin fluid nozzle, and electrospray are among the widely used methods. In this dissertation, we choose ultrasonic nebulizer and electrospray apparatus as an atomizer, which representing physical and electrical forces, respectively. Throughout this thesis, silica nanoparticles and PS spheres are used as typical host material and template, respectively.

1.2.1.   Ultrasound-assisted spray-drying method

A schematic of a typical ultrasound-assisted spray-drying apparatus used to produce and collect the nanostructured particles is shown in **Figure 1.1**. The main equipment consists of (i) a nebulizer that converts the starting solution into micro-droplets, (ii) the carrier gas, (iii) a tubular, laminar flow aerosol reactor, and (iv) a

_____

filter for sample collection. The starting solution was atomized by an ultrasonic nebulizer, which usually cooled with running water. The constant level of the spray solution ensures a uniform generation rate of droplets. The average equivalent diameter of solution droplets is 4.5 µm.[10] Water is usually used as the solvent. Typical tubular furnace is a glass tube of 13-mm inside diameter and about 1000 mm long.[11] The furnace consists of several (in this example five) independently controlled heating zones, each 200 mm in length, enabling flexibility in the production of the experimental temperature distributions. The temperature of each heating zone can be controlled to within 2 °C. A previous numerical evaluation of the reactor showed that the flow in the reactor is laminar for gas flow rates between 0.5 to 2 l / min.[12] Laminar flow is necessary for comparison with the results of the numerical simulations. The carrier gas used is usually nitrogen or air.

_____
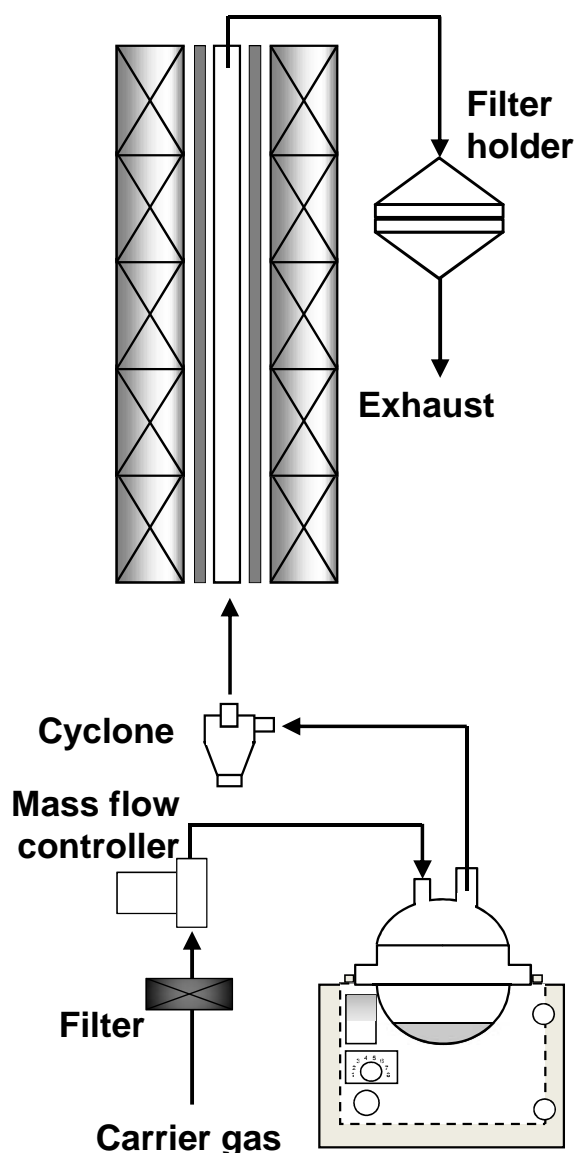
Figure 1.1. An ultrasound-assisted <u>spray</u>-drying apparatus

Several developments have been suggested to achieve particle control, in which adjustment of colloidal composition in the system is the easiest alternative.[11] Difference in the composition determines change in the number of nanoparticles in the droplet. This change allows self-arrangement particles with a specific morphology. After adjustment of solution compositions, templating method with the use of colloidal nanoparticles is the next well known technique to be applied using spray-drying process. Adjustments of these parameters provide control to the particle size and structure.[9, 11]

_____

1.2.2. Electrospray-assisted spray-drying method

Electrostatic spraying, is a technique capable of producing near-monodisperse droplets in the super-micrometer, sub-micrometer, and nanometer size ranges.[13, 14] In the electrospray system, a stream of charged droplets is produced by applying a potential difference of several thousand volts between a plate and the tip of a capillary supplied with a liquid.[15] **Figure 1.2** shows a basic apparatus used in the electrospray process. The apparatus consists of a metallic syringe needle, a high voltage power supply and a conductive plate. The metallic syringe capillary serves both as a liquid supplier and an electrode for applying high voltage. The collection electrode (conductive plate) is used as a grounded electrode as well as for collecting the produced particles. In the electrospray process, a conducting liquid flows through a capillary and pulled by the high voltage different between the needle and the collection electrode. Due to the presence of the strong electric field at the capillary outlet, and with a balance of surface tension and gravity, the liquid meniscus takes the shape of a Taylor cone, which in turn emits an electrically driven jet[15]. Jets of non-viscoelastic liquids break up into droplets with high amount of charge.[16]
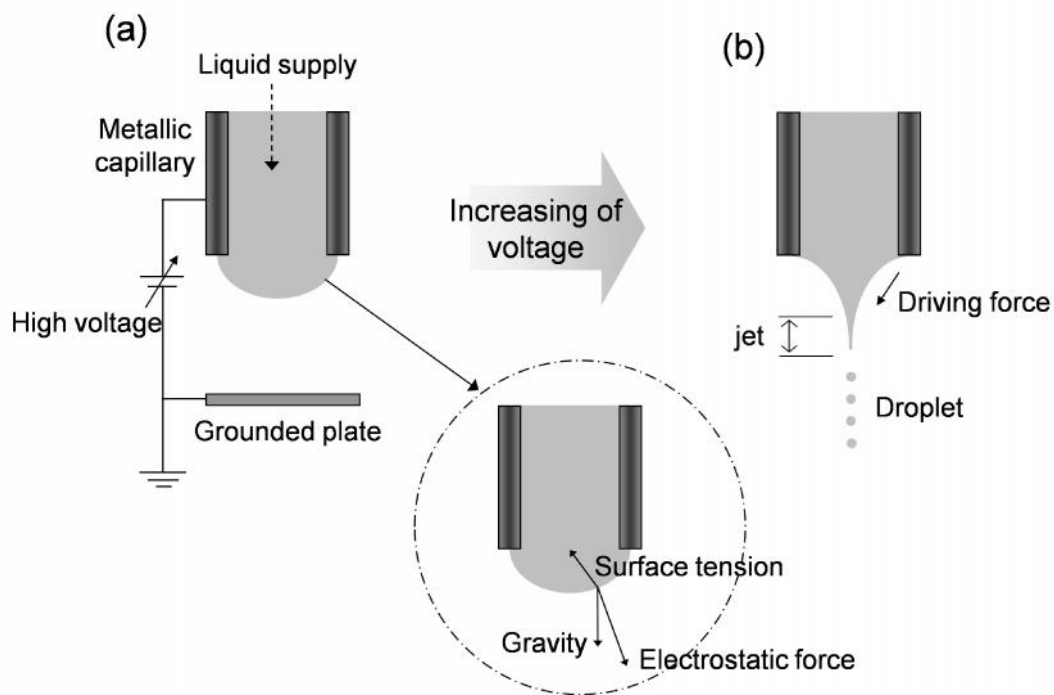
Figure 1.2.   Illustration of droplet formation in electrospray method.

Several scaling law, which relate process parameters and liquid properties to the size of the produced droplets have been developed for droplets produced by electrospray in the cone-jet mode.[17, 18] **Table 1.1** shows comparison of the scaling law proposed by Fernandez de la Mora, and Ganan-Calvo. Rosell-Llompart and Fernandez de la Mora[13], as well as Chen and Pui[19] developed a semi-empirical model to predict the initial droplet size for electrospray in the cone jet mode.

_____

Table 1.1. Comparison of the scaling law proposes by de la Mora, and Ganan-Calvo.

D_d: produced droplet size	…: liquid density
I: current emitted	Q: flow rate
‡: charge relaxation time ($|v_0/K$)	K: liquid electrical conductivity
x: surface tension	|: dielectric constant
$G(|)$: dimensionless function of $|$	k_I; k_d: 1.66; 6.46 (constants)
$G(|)=-10.9|^{-6/5}+4.08|^{-1/3}$	Q_{min}: minimum flow rate

	Fernandez de la Mora (1994)		**Ganan-Calvo (1994)**	
D_d	$G(|)(Q‡)^{1/3}$	(1)	$k_d|^{-1/6}(Q‡)^{1/3}$	(4)
I	$f(|)\left(\dfrac{xKQ}{|}\right)^{1/2}$	(2)	$k_I|^{1/4}\left(\dfrac{xKQ}{|}\right)^{1/2}$	(5)
Q_{min}	$\dfrac{|v_0 x}{…K}$	(3)	$\dfrac{|^{1/2}v_0 x}{…K}$	(6)

Produced droplet size can be predicted using equation (1) or (4). Both equations depend on the flow rate and relaxation time. The difference in constant used was based on experiment which relates each other.

1.3.   Influences of components properties

There are many components influencing the formation of self-organized nanostructured particles.[20] However, information about influences of self-assembly parameters (i.e., surface charge, size, and concentration of colloidal nanoparticles) on the formation of porous materials is still lacking. In fact, optimization of these parameters provides significant information toward producing highly ordered self-organized materials. In this dissertation, two main components will be focused on: colloidal nanoparticles properties (i.e., size, composition, and surface charge) and droplet properties (i.e., size, concentration surface, and charge).

_____

1.3.1. Colloidal nanoparticle properties

In the spray-drying process, self-organization of colloidal nanoparticles is affected mainly by its properties. Currently, no detailed information on the influences of self-assembly parameters (i.e., surface charge, size, and concentration of colloidal nanoparticles) in the formation of nanostructured materials is available. In fact, optimization of these parameters provides significant information toward producing highly ordered self-organized materials. In this dissertation, the influences of self-assembly parameters on the structuralization in the particle form were examined.

1.3.1.1 Size

Successfulness of particle formation is based on the size ratio of the host nanoparticles and the template spheres. The host nanoparticles and the template sizes provide the change in the hole size and the shell thickness of the produced hole structured particles, respectively. In addition, although the size ratio can be used as a modified parameter for controlling hole size and shell thickness, the adjustment of size ratio have some limitations. If the size of silica and PS are almost the same, it results the fail in maintenance of silica to be arranged on the PS surface.[20]

1.3.1.2 Composition

Typically, in order to control morphology, the adjustment of composition is essential. The increase of silica nanoparticles composition allowing to the production of particles with separated holes inside. On the contrary, the low composition of silica nanoparticles cause to the formation of kissing holes in the final particles, permitting to the flow of gas through the particles. However, further deviation from this condition

_____

leads unsuccessful particle development, due to the deficient of silica nanoparticles.[20]

1.3.1.3 Charge

When silica nanoparticles and anionic PS particles were used, porous structure was produced. On the contrary, when silica nanoparticles and cationic PS spheres were used, hollow particle with smooth surface and spherical shape is obtained. Successful porous structuralization was achieved when using silica and PS particles with negative zeta values, while successful hollow structuralization was obtained when using silica and positive PS. The successful formation of porous particles and film are due to repulsive interactions between the colloidal components (i.e., silica and PS), whereas formation of hollow particles and film are caused by the attractive interaction between the colloidal particles.

1.3.2. Droplet properties

Droplet as the container of the self-organization process also has many important properties that can affect the self-organization process. Properties of the droplet influencing the self-organization process are surface charge, size and concentration of the droplet.

1.3.2.1 Size

The control of self-organization process can also be achieved by controlling the droplet size. The droplet size determines the particle size, which controls the number of template particles inside the droplet. In electrospray method, droplet size control can be achieved mainly through the control of nanoparticles flow rate. Modification in the outer shape of the particles can be achieved only by the adjustment of nanoparticles feed

_____

rate.

1.3.1.2 Concentration

The control of morphology using the first way is the easiest approaches. Many researchers have been reported this technique due to its potential tendency. Number of concentration can determine the dominating components in the nanostructured particle formation during self-organization.

1.3.1.2 Charge

In the electrospray, droplets are ejected from the nozzle due to the electric force between the needle and the collection electrode. Droplets travel from the needle to the collection electrode while solvent evaporates. Droplet charge remained, whereas droplet mass reduces. This will increase the charge to mass ratio. When the charge to mass ratio exceeds the Rayleigh limit, coulomb explosion occurs.

1.4. Particle formation during spray-drying

During spray-drying, droplets travel and experiencing evaporation. The droplet size will be reduced and the nanoparticle inside the droplet will self-organize into their most stable condition. During self-organization, the nanoparticles are experiencing electrostatic interaction, which depend on the charge of colloidal nanoparticles and droplet. From the self-organization and electrostatic interaction of the colloidal nanoparticles, nanostructured particles with various size and morphologies can be produced.

_____

1.4.1. Particle formation under uncharged droplets

Because the spray-drying method provides the atomization process by physical forces only, no charge exists on the generated droplet. Therefore, self-organization of components in the formation of particles is based on charge of colloidal nanoparticles only. For instance, when particles were prepared from spray-drying of precursor containing silica nanoparticles and PS spheres, possible particle formation mechanism can be classified by two routes. Combination of precursor containing negatively charged silica and anionic PS results in the production of porous-structured particles, whereas those combination of silica nanoparticles with cationic PS spheres allows the creation of hollow particles.

1.4.2. Particle formation under charged droplets

When the spray-drying method is processed under charged droplet condition, additional factors in the colloidal self-assembly phenomena should be considered. Droplet charge adds electrostatic interactions to the colloidal nanoparticles during the self-organization process. Therefore, in addition to the solvent evaporation and the colloidal-to-colloidal interactions, several phenomena happen: attractive-and-repulsive interactions between colloidal particle and droplet surface, ion emission, and mass reduction due to Rayleigh limit theory.[21, 22] Combination of those factors can result particles with unique morphologies, which are different from common spray-drying method.

_____

1.4.3. Summary of possibly produced particles from spray-drying of colloidal nanoparticles

Figure 1.4. shows the summary of the self-organized nanostructured particles fabricated from spray-drying of colloidal nanoparticles under charged and uncharged droplet condition. Droplet containing colloidal nanoparticles are generated from atomizers and evaporated. The droplet evaporation reduces the volume size of the droplet. During the decreasing in droplet size, the colloidal nanoparticles are electrostatically interacting and self-assembling. Different electrostatic interaction phenomena occur for charged and uncharged droplets condition.

In the case of uncharged droplet condition, colloidal nanoparticles plays important role in the self-organization. The use in the different colloidal nanoparticle charges determine the hole structure of the final product. Combination of negatively charged silica and anionic PS spheres resulted in the formation of porous structure, while the combination of negatively charged silica nanoparticles and cationic PS spheres resulted in the generation of hollow structure.

Different from uncharged condition, in the charged droplet condition, more parameters can be controlled (i.e., droplet size and droplet charge polarity). Production of small droplet size makes the production of controlled number of hole in the formation of hole structured particles available (i.e., core-shell, single hollow, and multi-numbered hole hollow structure). Low droplet size can contain single template particle. This technique can be used to create single cores-hell and hollow particles. More increase in droplet size can increase more number of template particles, which resulted in the formation of multi-nuberedf hollow particles.

Introduction of droplet charge adds electrostatic interaction to the self-organization process. When silica nanoparticles and cationic PS spheres were used

for producing hollow particles under different droplet charges, different types of hollow particles were obtained. When positively charged droplet was applied, grape-like hollow particles were produced. While for negatively charged droplet, aggregated hollow particles were created. The attractive interaction between silica and PS are strong enough to maintain the hollow structure against droplet charge.
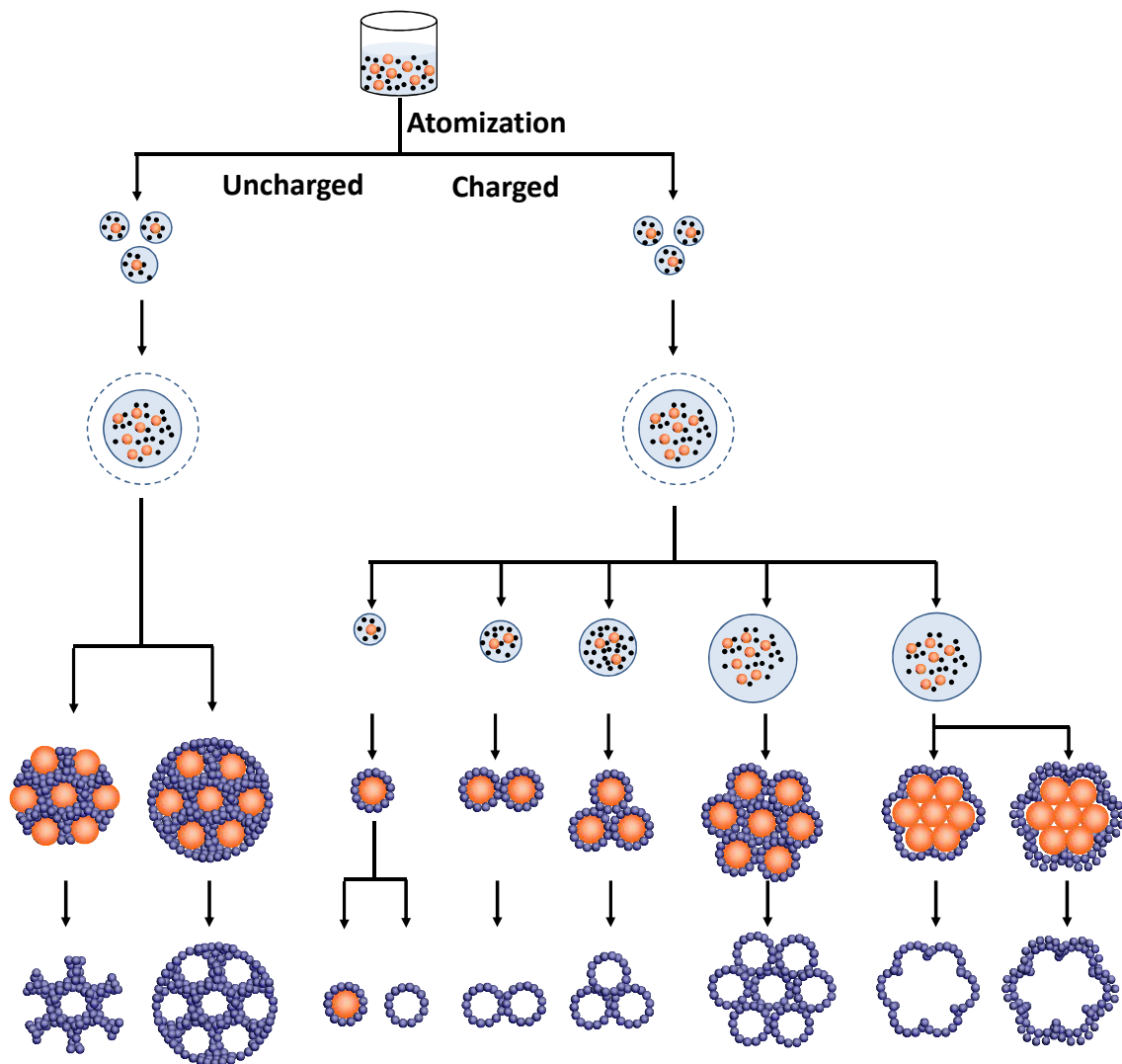

Figure 1.3. A summary of the self-organized nanostructured particles using the spray-drying method.

_____

1.5. Motivation, objectives, and outline of the dissertation

1.5.1. Motivation and objectives

The various self-organized nanostructured particles obtained from spray-drying methods exhibit many potential applications for their uses in future technology. Control in the particle morphology is enhancing the particle performance. This reason insists in the requirement of further studies in the self-organized nanostructured particles with controllable size and morphologies.

Because size- and morphological-controllability of nanostructured particles from colloidal nanoparticles is of both great significance and challenge, this dissertation was to prepare self-organized nanostructured particles fabricated from spray-drying of colloidal nanoparticles. I hope that with this study, new findings will be gained and can bring to the improvement of particle technology, especially concerned to the fields of chemical, material, and medical engineering.

1.5.2. Outline

An overview of my current research on the self-organized nanostructured particles fabricated from spray-drying of colloidal nanoparticles is described in this dissertation, which is believed to be the first detailed study on the structurization of nanostructured materials under effects of droplet charge. This dissertation is mainly divided into four sections, in which some section comprises several chapters (**Figure 1.4**). The adjustment of several parameters to realize particles of varying morphologies is explained. Illustrations mechanism as well as theoretical explanation, is also described to support and clarify the design of particles.
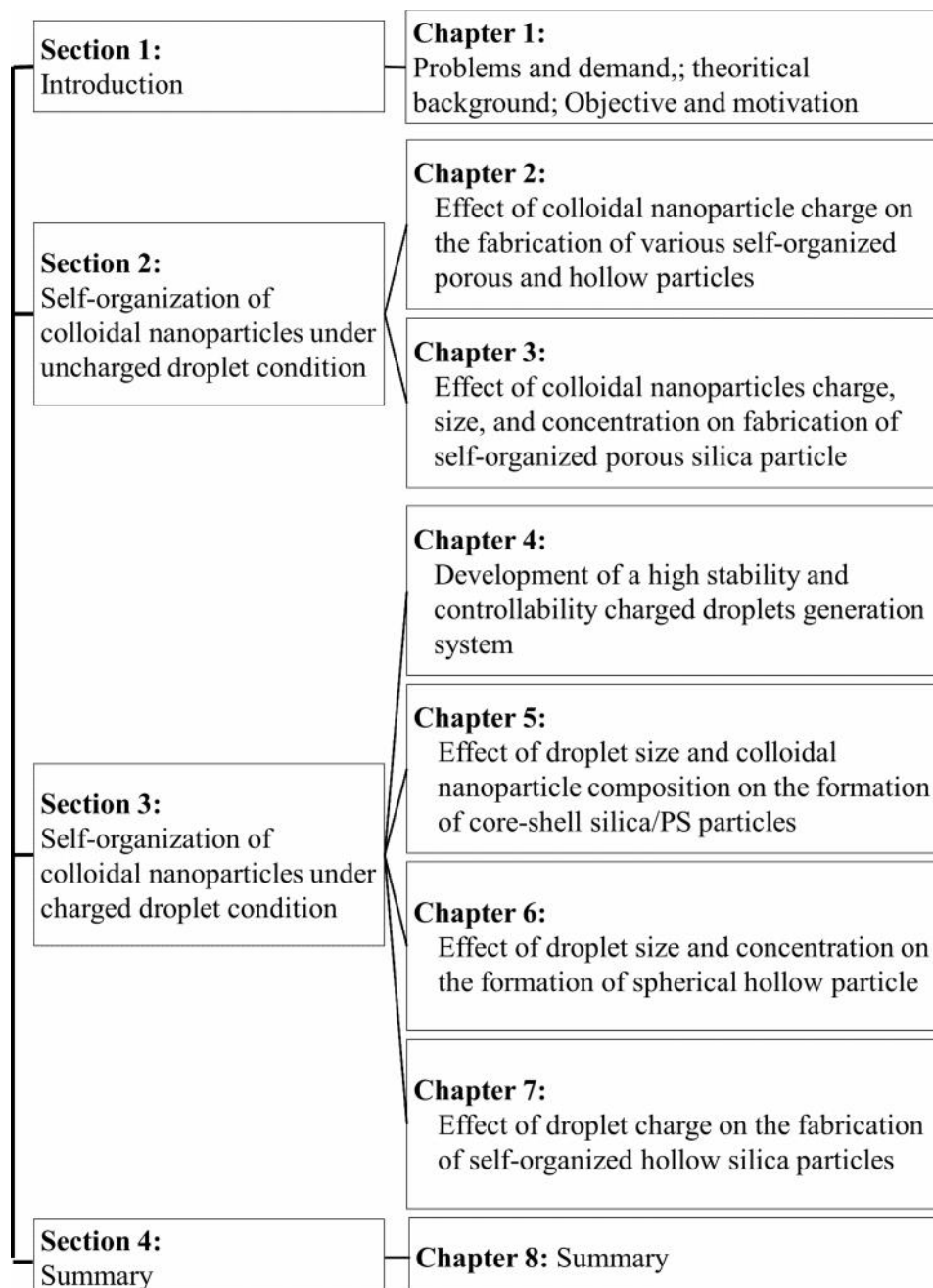
Section 1:
Introduction

Chapter 1:
Problems and demand,; theoritical background; Objective and motivation

Section 2:
Self-organization of colloidal nanoparticles under uncharged droplet condition

Chapter 2:
Effect of colloidal nanoparticle charge on the fabrication of various self-organized porous and hollow particles

Chapter 3:
Effect of colloidal nanoparticles charge, size, and concentration on fabrication of self-organized porous silica particle

Section 3:
Self-organization of colloidal nanoparticles under charged droplet condition

Chapter 4:
Development of a high stability and controllability charged droplets generation system

Chapter 5:
Effect of droplet size and colloidal nanoparticle composition on the formation of core-shell silica/PS particles

Chapter 6:
Effect of droplet size and concentration on the formation of spherical hollow particle

Chapter 7:
Effect of droplet charge on the fabrication of self-organized hollow silica particles

Section 4:
Summary

Chapter 8: Summary

Figure 1.4. A summary of dissertation outline

Section 1 (*i.e.*, Chapter 1) is the introduction. Two kinds of methods (i.e. ultrasound-assisted and electrospray-assisted spray-drying methods) with their basic theoretical explanation and current progress in the production of particles are discussed.

Section 2, consisting of two chapters, describes the self-organization of colloidal nanoparticles under uncharged droplet condition. The synthesis of colloidal

_____

nanoparticles and its application in the fabrication of various self-organized hollow particles are described in detail, corresponding to **Chapter 2 and 3**, respectively.

In the first part of the **Section 2** (**Chapter 2**), the effect of nanoparticle charges on the self-organized nanostructured particles is described. Preparation of spherical-dense PS particles with controllable outer diameter and it's application for particle templating application are reported. Particle formation and several parameters manipulation are also discussed. The prediction equation as a simple theoretical model on the effect of several parameters was also described to support the experimental result.

In the second part of **Section 2** (**Chapter 3**), effects of colloidal nanoparticles charge, size and concentration on fabrication of self-organized porous silica particles become the main focus of the study. Self-organization of colloidal nanoparticles in the formation of porous film form was studied. Comparison between theoretical calculation and experimental results on the arrangement of the particles is also presented. The calculation results were used for production of nanostructured particle. [20]

Section 3, presenting the study self-organization of colloidal nanoparticles under charged droplet condition, comprises four chapters (**Chapter 4, 5**, **6** and **7**). The production of self-organized nanostructured particles with controllable size and morphology using a specific parameter manipulation becomes the main objective in this section.

In the first part of **Section 3** (**Chapter 4**), a high stability and controllability charged droplet generation system is developed. Control of charge over volume delivered to the system is essential for generation of stable and monodisperse droplets.[23]

_____

Chapter 5 explains the effect of droplet size and colloidal nanoparticle composition on the formation of core-shell silica/PS particles. Adjustment of colloidal nanoparticles composition and its effect on the core-shell particle morphology is the main focus of this chapter.[24]

Chapter 6 explains the effect of droplet size and concentration on the formation of spherical hollow particle preparation of spherical hollow silica particles. Control of agglomeration-free condition of the produced hollow particles is achieved by adjustment of several parameters including droplet size. The effectiveness of the hole size control by adjusting template hole size is also described.[25]

Chapter 7 is the final chapter for **Section 3**. It describes the effects of droplet charge on fabrication of self-organized hollow silica particles from electrospray-drying of colloidal nanoparticles. Self-organization of nanoparticles inside a charged droplet and self-organization parameters (i.e. flow rate, charge, size, and composition of the colloidal nanoparticles) are also thoroughly investigated. The availability of the charge in the droplet surface provides possibility in formation of various morphologies in the fabricated particle with controllable outer shape, hole number, shell thickness, and internal structure.

In **Section 4** (**Chapter 8**), the summary of all chapters is presented.

1.6. References

[1] W.H. Suh, A.R. Jang, Y.H. Suh, K.S. Suslick, Porous, hollow, and ball‐in‐ball metal oxide microspheres: Preparation, endocytosis, and cytotoxicity, Advanced Materials, 18 (2006) 1832-1837.

[2] H.-K. Chan, Dry powder aerosol drug delivery—opportunities for colloid and surface scientists, Colloids and Surfaces A: Physicochemical and Engineering Aspects, 284 (2006) 50-55.

[3] F. Iskandar, Nanoparticle processing for optical applications–a review, Advanced

_____

Powder Technology, 20 (2009) 283-292.

[4] K. Okuyama, I. Wuled Lenggoro, Preparation of nanoparticles via spray route, Chemical Engineering Science, 58 (2003) 537-547.

[5] R. Vehring, Pharmaceutical particle engineering via spray drying, Pharmaceutical research, 25 (2008) 999-1022.

[6] J.H. Bang, K.S. Suslick, Applications of ultrasound to the synthesis of nanostructured materials, Advanced Materials, 22 (2010) 1039-1059.

[7] F. Iskandar, A.B.D. Nandiyanto, W. Widiyastuti, L.S. Young, K. Okuyama, L. Gradon, Production of morphology-controllable porous hyaluronic acid particles using a spray-drying method, Acta biomaterialia, 5 (2009) 1027-1034.

[8] P. Thybo, L. Hovgaard, J.S. Lindeløv, A. Brask, S.K. Andersen, Scaling up the spray drying process from pilot to production scale using an atomized droplet size criterion, Pharmaceutical research, 25 (2008) 1610-1620.

[9] A.B.D. Nandiyanto, K. Okuyama, Progress in developing spray-drying methods for the production of controlled morphology particles: From the nanometer to submicrometer size ranges, Advanced Powder Technology, 22 (2011) 1-19.

[10] W.-N. Wang, A. Purwanto, I.W. Lenggoro, K. Okuyama, H. Chang, H.D. Jang, Investigation on the correlations between droplet and particle size distribution in ultrasonic spray pyrolysis, Industrial & Engineering Chemistry Research, 47 (2008) 1650-1659.

[11] F. Iskandar, L. Gradon, K. Okuyama, Control of the morphology of nanostructured particles prepared by the spray drying of a nanoparticle sol, Journal of Colloid and Interface Science, 265 (2003) 296-303.

[12] I.W. Lenggoro, T. Hata, F. Iskandar, M.M. Lunden, K. Okuyama, An experimental and modeling investigation of particle production by spray pyrolysis using a laminar flow aerosol reactor, Journal of Materials Research, 15 (2000) 733-743.

[13] J. Rosell-Llompart, J. Fernandez De La Mora, Generation of monodisperse droplets 0.3 to 4 μm in diameter from electrified cone-jets of highly conducting and viscous liquids, Journal of Aerosol Science, 25 (1994) 1093-1119.

[14] D.-R. Chen, D.Y. Pui, S.L. Kaufman, Electrospraying of conducting liquids for monodisperse aerosol generation in the 4 nm to 1.8 μm diameter range, Journal of Aerosol Science, 26 (1995) 963-977.

[15] M. Cloupeau, B. Prunet-Foch, Electrohydrodynamic spraying functioning modes: A critical review, Journal of Aerosol Science, 25 (1994) 1021-1036.

[16] J. Suh, B. Han, K. Okuyama, M. Choi, Highly charging of nanoparticles through electrospray of nanoparticle suspension, Journal of Colloid and Interface Science, 287 (2005) 135-140.

_____

[17] A. Ganan-Calvo, J. Davila, A. Barrero, Current and droplet size in the electrospraying of liquids. Scaling laws, Journal of Aerosol Science, 28 (1997) 249-275.

[18] D. La Mora, J. Fernandez, The current emitted by highly conducting taylor cones, Journal of fluid mechanics, 260 (1994) 155-184.

[19] D.-R. Chen, D.Y. Pui, Experimental investigation of scaling laws for electrospraying: Dielectric constant effect, Aerosol Science and Technology, 27 (1997) 367-380.

[20] A.B.D. Nandiyanto, A. Suhendi, O. Arutanti, T. Ogi, K. Okuyama, Influences of surface charge, size, and concentration of colloidal nanoparticles on fabrication of self-organized porous silica in film and particle forms, Langmuir, (2013).

[21] D.C. Taflin, T.L. Ward, E.J. Davis, Electrified droplet fission and the rayleigh limit, Langmuir, 5 (1989) 376-384.

[22] A. Gomez, K. Tang, Charge and fission of droplets in electrostatic sprays, Physics of Fluids, 6 (1994) 404.

[23] A. Suhendi, M.M. Munir, A.B. Suryamas, A.B.D. Nandiyanto, T. Ogi, K. Okuyama, Control of cone-jet geometry during electrospray by an electric current, Advanced Powder Technology, 24 (2013) 532-536.

[24] A. Suhendi, A.B.D. Nandiyanto, T. Ogi, K. Okuyama, Agglomeration-free core-shell polystyrene/silica particles preparation using an electrospray method and additive-free cationic polystyrene core, Materials Letters, 91 (2013) 161-164.

[25] A. Suhendi, A.B.D. Nandiyanto, M.M. Munir, T. Ogi, K. Okuyama, Preparation of agglomeration-free spherical hollow silica particles using an electrospray method with colloidal templating, Materials Letters, (2013 (In press)).

31

_____

Chapter 2

Effect of colloidal nanoparticle charge on the fabrication of various self-organized porous and hollow particles

2. 1. Introduction

Recently, hollow-structured particles have attracted tremendous attention due to their excellent performances: larger surface area, lower density, lower dielectric, etc. Excellent performance makes this material potential for many applications: catalysts, coating and composite materials, fillers, and drug delivery uses.[1-3]

Several approaches for the synthesis of hollow particles have been reported, in which most of them use an organic template-driven self-assembly technique. One of the template candidates is polystyrene (PS). PS is effective because it is easily removed (either with heat treatment or solvent dissolution)[4] and available as a homogeneous sphere. Due to its homogenous sphere, its removal results in the formation of a spherical hole in the host material[5]. This replication phenomenon also offers the possibility in the control of hole size by changing the PS size[6], driving the need of further study in the synthesis of PS particles with controllable size.

Effectiveness of the assistance of PS on the synthesis of hole-structured material in different forms (i.e. film, particle, fiber, etc) has been reported, informing that the PS is compatible with many self-assembly techniques and various host materials. However, when using PS as the template, several problems have been still noted: (i) most of the reports do not consider the existence of additives in the PS solution (i.e. surfactant, salt, polymer, etc). These additives can give undesirable effects on the structure of holes[7, 8]. The exist of additive also causes the formation of

mesoporous structure in shell[2]. This mesoporous structure is avoided for some applications (i.e. lens and optical-related uses) because it can absorb some chemicals[9], leading to change material structure and performance (e.g. refractive index); (ii) most do not concern on the charge of PS. In fact, the charge allows the formation of different hole configurations (i.e. porous and hollow structure)[10]; (iii) most of the current PS particles are synthesized by employing an anionic initiator that typically consists of inorganic component (K, Na, etc)[11], affecting to the purity of the PS itself. Further, this type of initiator allows the synthesis of PS with a negative zeta charge[10], in which this charge creates conflicts for some PS coating processes[12]; and, (iv) current PS particles that available in the market are typically expensive (10 mL (10 wt%) 100-500 USD)[13], making problems when employing a large volume of template.

To circumvent the above problems, studies on the synthesis of PS particles that are pure and have a positive zeta charge are important, especially when the PS is purposed to assist the production of hollow materials. Although several researchers reported the possibility in the use of negatively zeta charged PS for the production of hollow particles[1-3, 12], the assistance of additive for changing the PS charge and pasting the material shell onto template surface could not be avoided. Several methods to the synthesis of pure and cationic PS particles have been developed. Ramos et al[14] and Covolan et al[15] reported the preparation of PS particles by the use of cationic initiator that was free of inorganic component. However, their methods can not be separated from the use of surfactant to stabilize the PS particles. Against to the surfactant problems, Goodwin et al[16] reported the synthesis of PS particles under the surfactant-free condition and the use of cationic initiator. Control of PS size can be effectively achieved by adjusting several parameters only. However, their methods have limited to the production of submicrometer particles, which is far from the demand of

_____

current technologies: the preparation of nanometer-sized particles. Nano-sized template is important because it would presumably create smaller hole in the host material than submicron template, which would be effective to increase material performance (higher surface area and porosity, lower density, etc)[6]. Moreover, although it has been known that the use of cationic initiator could produce PS particle with a positive zeta charge[10], in the above reports, there is no information about the confirmation of zeta charge and applications of the synthesized PS (e.g. template).

The comprehensive studies on the preparation of cationic PS polymer particles (positive zeta charge) with size of down to the nanometer range and controllable size in the nanometer scale under an additive-free condition is virtually non-existence, especially related to the particle charge and the detailed explanation and comparison between experimental result and theoretical analysis. Moreover, most of the studies reported the synthesis of PS particles only but included no mention of the application of PS itself. For this reason, the purpose of this study was to spotlight the synthesis of pure cationic PS particles with controllable size in the nanometer scale using a single step and relatively simple and cheap process under the additive-free condition and to demonstrate their application as the template for facilitating the production of hollow inorganic particles.

In this chapter, we reported the synthesis of cationic PS particles with controllable size for investigating effect of colloidal nanoparticles charge on the fabrication of various self-organized porous and hollow particles. Different from other methods, the synthesis was based on the polymerization of styrene monomer in the absence of any additional components (polymers, surfactants, chemicals, etc) and in an aqueous solution system. A single step and relatively simple and cheap process could be achieved using the present method. A cationic initiator (i.e. 2,2-azobis

_____

(isobutyramidine) dihydrochloride (AIBA)) was used to produce cationic PS particles with a positive zeta charge. Besides, free of inorganic compound was also the advantage of the use of this type of initiator. In addition, we purified the styrene using a basic solution instead of a vacuum distillation method[19], which is simpler and more cost effective for the total synthesis process. Spherical-shaped and well-controlled particle size from 30 to 300 nm in the nanometer scale using the present method was achieved by the adjustment of several reaction parameters (temperature and monomer and initiator concentrations), in which to the best of my knowledge, this is the first documented synthesis of well-controlled size in the nanometer scale under the additive-free condition. The size of the PS particles was proportional to the composition of styrene and the amount of initiator concentrations but had an inverse-proportional trend to the temperature. In addition, we also found that the styrene amount had more effect than the initiator (more than 4 times) on controlling PS size. Due to use of neither surfactant nor other additives, pure and homopolymer PS particles could be obtained, confirmed by an FTIR and a Raman spectrum analysis. Derivation of an equation from experimental scaling law to predict particle size control was also added in this chapter. We believe that this novel equation would be useful for further applications, especially related to the scaling-up process.

The ability of the PS as the template to assist the production of hollow particles was also reported along with the hole-structured particle formation mechanism. Comparison of the prepared and commercial available PS was investigated. The result showed that the prepared PS was compatible to support the production of various hollow-structured particles (i.e. tungsten oxide, zirconia, and silica), in which this production could not be obtained when using commercial PS particles.

_____

2.2. Experimental method

2.2.1. Synthesis of PS Particles

PS particles were synthesized using a liquid-phase synthesis method, involving a simple polymerization of styrene monomer (styrene, Aldrich, USA) in an aqueous solution (ultrapure water, generated by Millipore, US) and in the absence of additives (polymers, surfactants, chemicals, etc) under AIBA (Sigma-Aldrich, USA) as the initiator. The polymerization was conducted in the batch-process reactor-system, which was similar to the previous works[9, 18]. The reactor system itself consisted of a batch-glass reactor (300 mL of a four-necked reactor), a magnetic stirrer, a mantle heater, a condenser, and a nitrogen gas inlet.

Firstly, an aqueous solution was put into the reactor system, vigorously stirred (600 rpm), and heated at a specific temperature under a nitrogen atmosphere. The heating process was then kept for 15 minutes to remove diluted oxygen in the solution. After the oxygen-free condition was reached, styrene monomer was added to the reactor subsequently. The system was then maintained for another 10 minutes to ensure that the styrene was dispersed homogenously in the aqueous solution. In addition, prior to adding into the aqueous solution, purchased styrene was previously washed by a base solution (NaOH (2.5 M)) to remove its inhibitor. In order to start the polymerization process, AIBA that previously dissolved in water was added to the mixed styrene-water solution. The mixtures were subsequently kept at this temperature for 10 hours under a nitrogen atmosphere. The reacted solutions were then cooled to room temperature.

2.2.2. Application of PS particles as a template

To confirm application of the prepared PS, the preparation of hollow inorganic particles using a spray-drying method and employing the prepared PS as the template

was reported. The hole-structured inorganic particles were prepared from a precursor, which was a mixture of colloidal nanoparticles (i.e. tungsten oxide (WO_3; Nishin Engineering Inc., Tokyo, Japan; an average size of 7 nm), silica (SiO_2; Nissan Chem. Ind., Ltd., Japan; an average size of 5 nm)), and zirconia (ZrO_2; Sumitomo Osaka Cement Co., Ltd., Japan; an average size of 7 nm)) and the synthesized PS particles (an average size of 273 nm) in an aqueous solution. To produce hollow inorganic particles with a good structure, the composition of inorganic host nanocolloid and PS in the initial precursor was fixed at a specific mass ratio: (i) WO_3/PS of 0.80; (ii) SiO_2/PS of 0.40; and (iii) ZrO_2/PS of 1.00. The precursor was then introduced to a spray-dried apparatus system (an ultrasonic nebulizer with a two-fixed zone electrical furnace reactor (200 and 500°C); a flow of carrier gas (N_2) of 1 L/min), which was similar to the previous works[1-4]. The commercial inorganic nanoparticles were used to simplify the process because their preparation methods have been well-known using the current technologies. Further, the other purpose from the use of commercial inorganic nanoparticles that were relatively monodispersed was to achieve the objective in the formation of highly ordered hollow particles. When monodispersed particles are self-assembled, the possibility in the formation of highly ordered particles is high; otherwise, it will be impossible.[5] In addition, to compare the prepared PS application, we also used a commercial PS (spherical particles with an average size of 250 nm, Japan Synthetic Rubber Co., Japan).

2.2.3. Characterizations

The prepared particles were characterized using a scanning electron microscope (SEM, Hitachi S-5000; operated at 20 kV) to examine their size and morphology. From SEM images, the size of the prepared particles was measured using a

Ferret analysis of about 150 individual particles[6]. In order to verify the particle charge, we analyzed the prepared PS, commercial PS, and WO_3 particles using a zeta potential measurement (Malvern Zetasizer, Nano ZS, UK).

2.3. Result and discussion

2.3.1. Synthesis of PS particles with controllable size

The work reported from the present study was primarily directed towards investigation of the temperature and the concentration of reactants effects in the synthesis of monodispersed PS particles. This study used a single-step process and performed in the absence of additives (e.g., chemicals, surfactants, polymers, salts, etc).
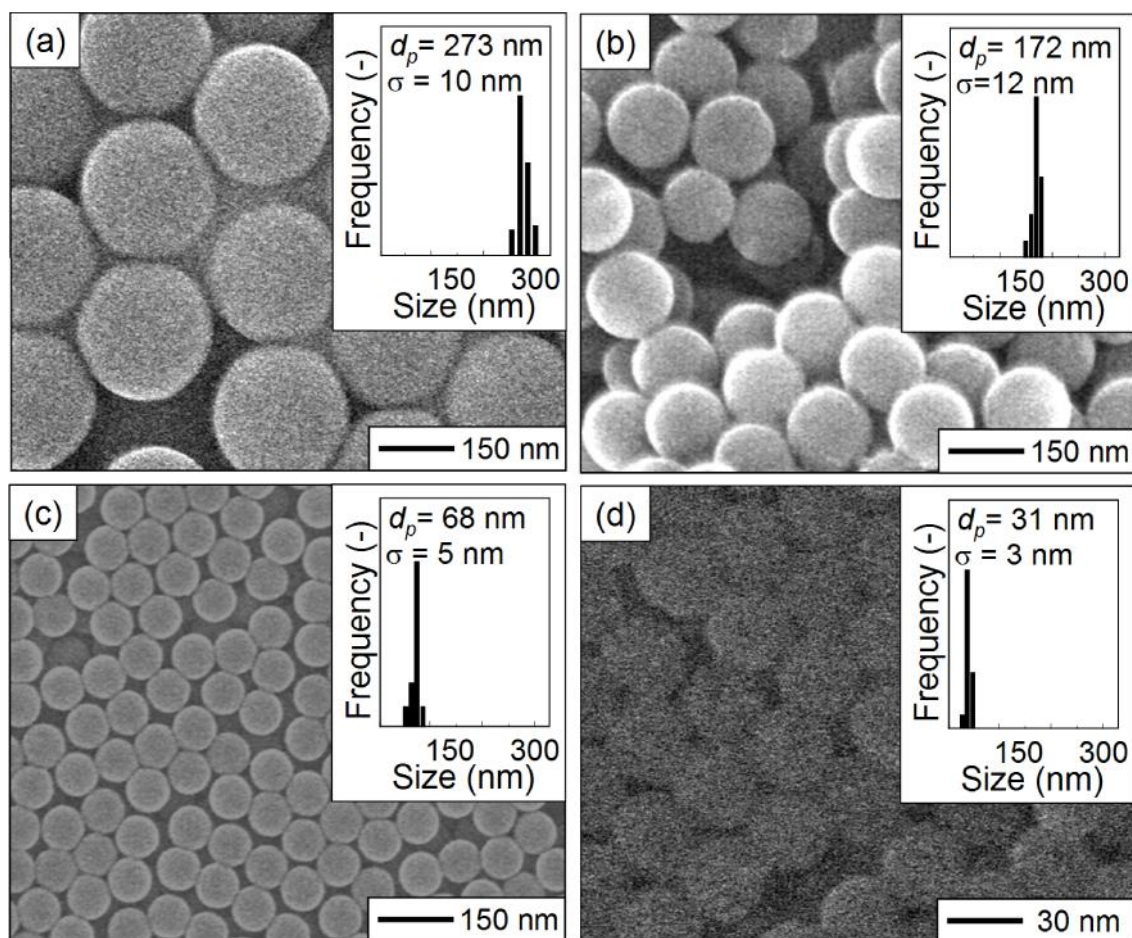
Figure 2.1.   SEM images of prepared particles produced with various reaction parameters.

Chapter 2: Effect of colloidal nanoparticle charge on the fabrication of various self-organized porous and hollow particles

_____

Figure 2.1 shows the SEM images of prepared particles produced with various reaction parameters. Relatively monodispersed particles with a spherical shape were examined in all cases. A strong relationship between particle size and several parameters was revealed. Particles with a mean size of 273 nm were formed when conducting with styrene of 2.00 wt%, initiator of 0.04 wt%, and temperature of 55 °C (**Figure 2.1a**). When several parameters were manipulated, different results were obtained. Decreases in monomer concentration (down to 0.80 wt%) allowed the production of particles with a size of 172 nm (**Figure 2.1b**). Adding combination of "decreasing styrene concentration" and "increasing temperature" caused the preparation of particles with a size of down to nanometer range (**Figure 2.1c**). Then, by decreasing initiator amount in the combination in **Figure 2.1c**, the production of particles with a size of down to 31 nm was obtained (**Figure 2.1d**). From all results, no effect of these reaction parameters on the particle shape was found because the prepared PS particles were consistent in their spherical form. Due to use of process in the absence of additives (e.g., chemicals, surfactants, polymers, salts, etc), the process was reliable with respect to the quality of the homopolymer PS product, confirmed by the FTIR and the micro-Raman spectra analysis.

An FTIR spectroscopy analysis results of different PS samples (samples of S01 (D_P = 273 nm), S37 (D_P = 165 nm), S08 (D_P = 136 nm), and S45 (D_P = 31 nm)) is shown in **Figure 2.2**. The results showed that different reaction parameters did not lead to change in material patterns and properties. All patterns were the same. The appearance of PS-related peaks (in the range of 600-900, 1011-1130, and 1600 and 2200 cm^{-1}) was observed[9, 10], confirming that all samples were pure PS. The intensity of alkyl groups and benzene ring peaked in the range of 600-900 and 1011-1130 cm^{-1}, respectively[10, 11]. The specific patterns in the range of 1600 and

_____

2200 cm^{-1} that would be found only in homopolymer PS structure[10] was appeared in all samples. The OH vibration and stretching patterns were also found in the range of 1500 and 3000 cm^{-1}, respectively, indicating that PS had a polar structure[11]. The intensity of polar hydroxyl peak in the range of 3000 increased with the decrease of PS size, indicating that smaller-sized particles had more interaction number with OH due to their larger surface area per unit volume.
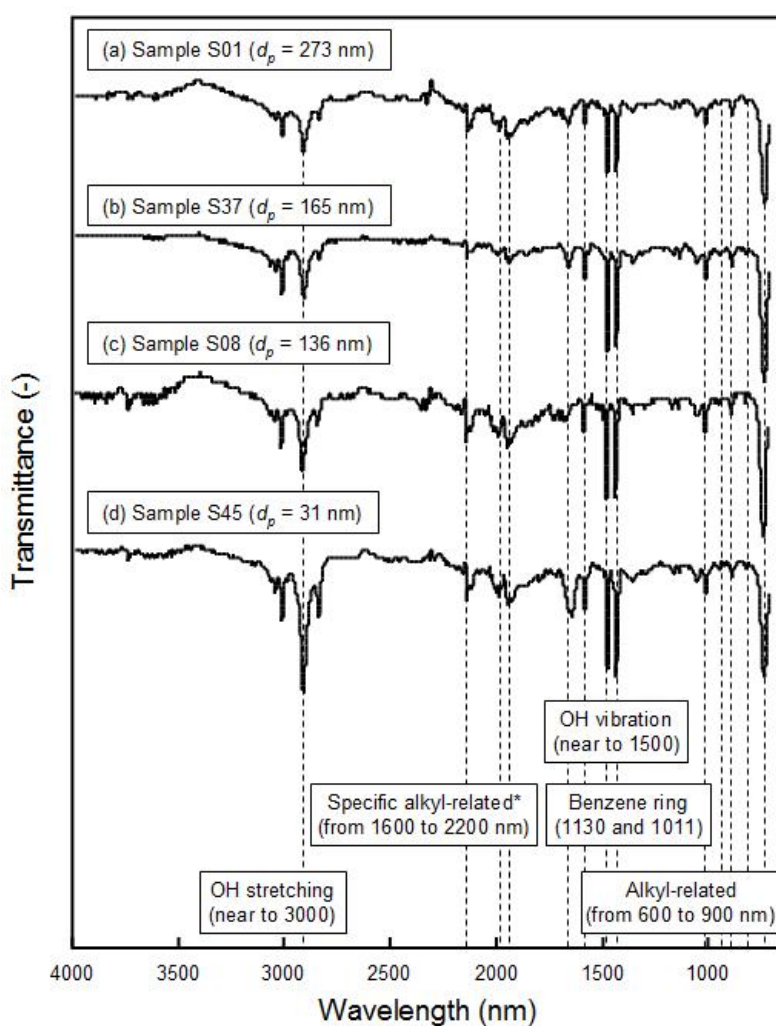
Figure 2.2. An FTIR analysis of several samples of S01 (D_P = 273 nm), S37 (D_P = 165 nm), S08 (D_P = 136 nm), and S45 (D_P = 31 nm). Note asterisk (*) shows the peak that typically appeared only in PS component (homopolymer).

A micro-Raman spectrum analysis of the prepared particles with mean size of 31 nm (Sample S45) is presented in **Figure 2.3**. The frequency in the range of 400, 800,

and 1600 cm^{-1} was observed, confirming the PS type frequency[12]. There were several strong signals that were characteristic of PS at about 400 (ring deformation), 800 (breathing ring), and 1600 (ring stretch) cm^{-1}[13]. No peak in the range of 1300 and 1500 cm^{-1} was obtained, confirming almost no existence of free styrene in the suspension[12].
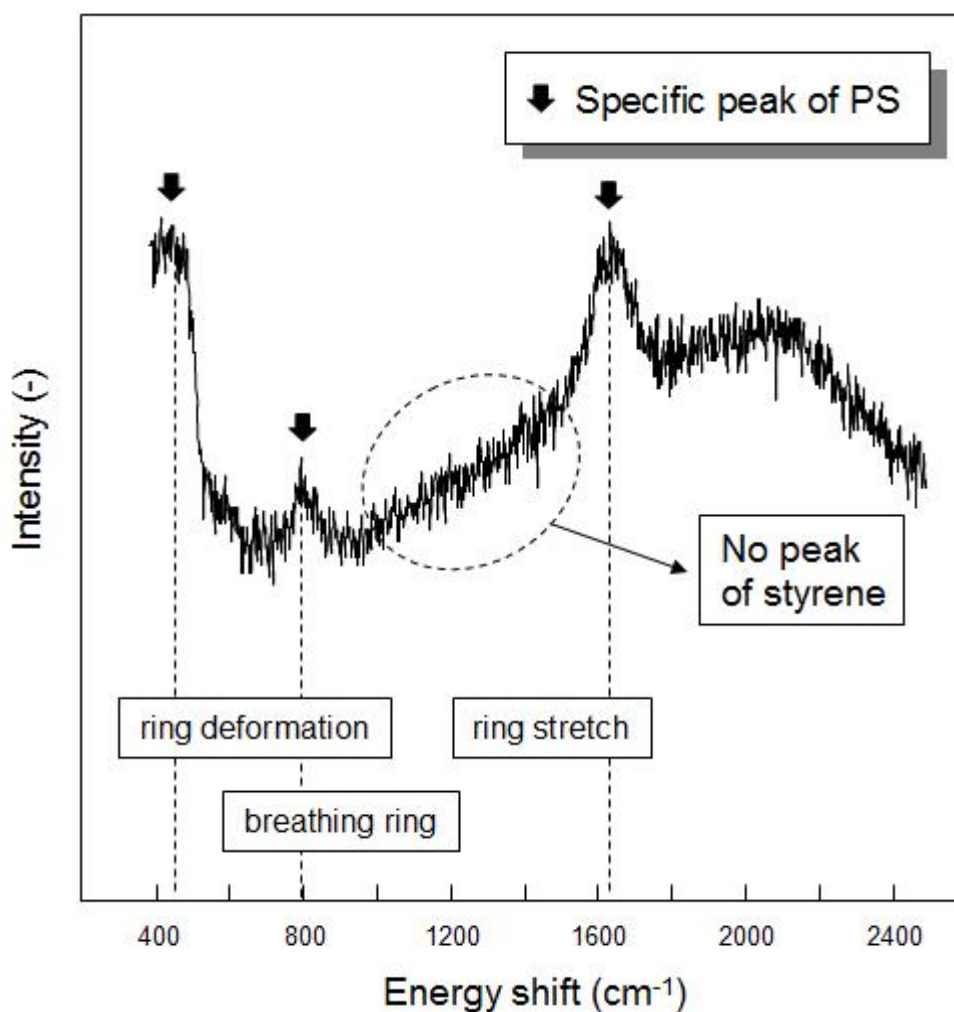
Figure 2.3. A Raman spectrum analysis of sample S45 ($D_P = 31$ nm).

The chemical composition of the prepared particles (as-synthesized particles; suspension type) was investigated using a Fourier transform infra red (FTIR, Shimadzu FTIR 8700) and a micro-Raman spectrum analysis. The micro-Raman spectroscopy, used a similar apparatus to other reference works[7, 8], was conducted with a

_____

Horiba-Jobin Yvon T64000 system equipped with an Ar^+ laser and a microscope with 100 times magnification. The incident laser beam was the 514.5 nm laser line with a power of 200 mW. The spectrometer was composed of a single-grating monochrometer of 600 g mm^{-1} and a charge coupled device detector. The spectrometer was calibrated using the 520 cm^{-1} silicon wafer of the 514.5 nm laser line before the measurements. The resolution of the spectrometer was 0.7 cm^{-1}.

2.3.1.1. Effect of temperature

Figure 2.4. shows the impact of temperature to particle size. An increase of temperature can lead the high interaction/conversion of reaction components, resulting in the good progress in the particle formation[14]. Final particle sizes as a function of the processing temperature, when performed at different amounts of styrene and initiator, are shown. To clarify the effect of the temperature, figures were classified into the styrene amount constant of 2.00, 0.80, and 0.40 wt%, corresponding to the **Figure 2.4a, b, and c**, respectively. A strong correlation between the particle size and the temperature was revealed. The size decreased significantly with the increase of temperature.
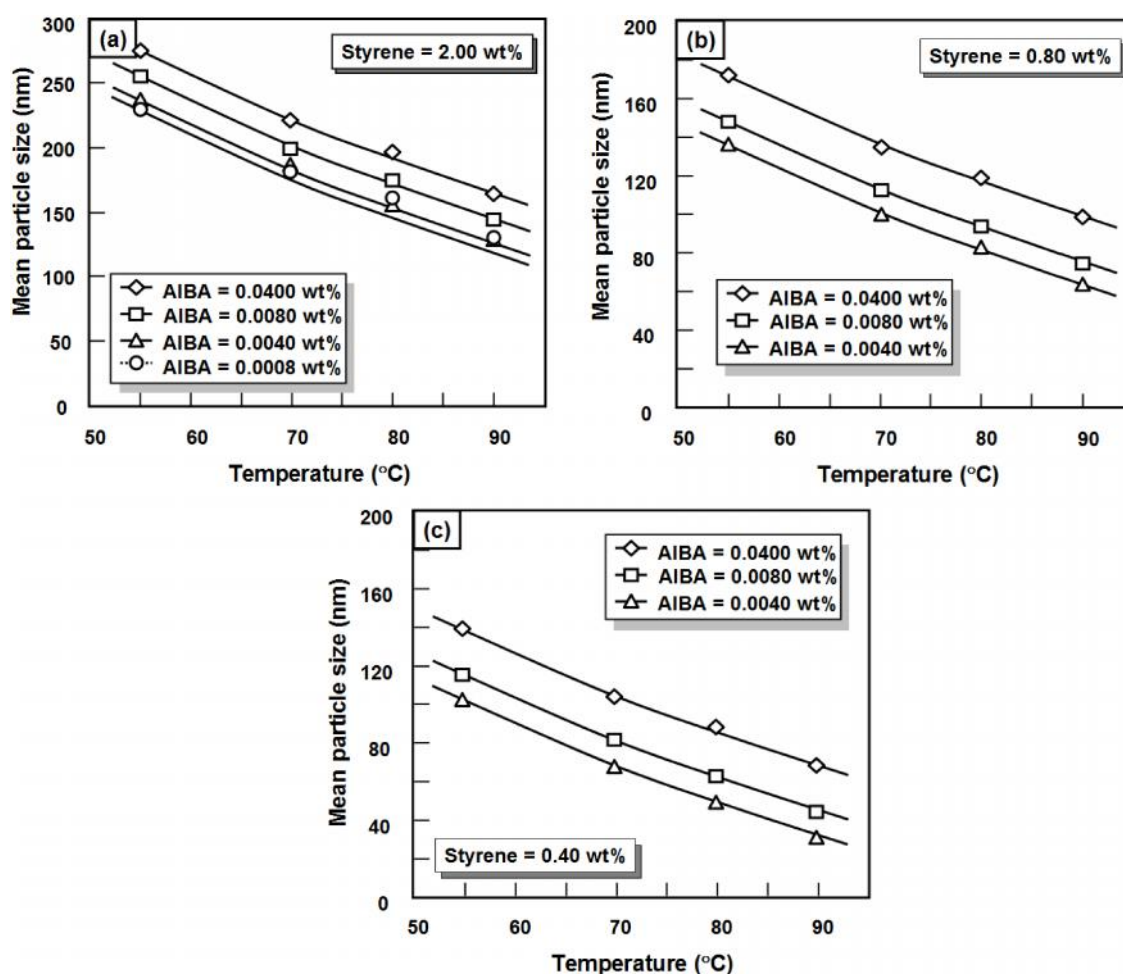
Figure 2.4. Mean particle size against detailed data on temperature under different styrene concentrations: (a) 2.00, (b) 0.80, and (c) 0.40 wt%. Samples were also conducted with different initiator concentrations, ranging from 0.0008 to 0.0400 wt%.

The interesting phenomenon in the control of PS size was probably due to the fact that the increase of the temperature allowed to enhance initiation efficiency and make high contact, interaction, and collision among the reactants (i.e. styrene monomer and initiator). The propagation rate of the styrene might considerably increase, while the radical termination reduced.[15] This condition led the rapid progress of oligomer and nucleus formation[14]. Further, the variation of reaction condition (i.e. temperature) influenced the styrene solubility in the aqueous medium[16]. Increase of temperature caused the increase of styrene solubility, making higher conversion of reactants and resulting in a good progress in the formation of oligomer and nucleus. However,

because most of the monomers and the oligomers were consumed for the nucleus construction, the availability of the free monomers and oligomers for further particle growth were limited, leading the retardation of the particle growth step and resulting in the synthesis of particles with a smaller size. Conversely, when the temperature was low, creation of larger size of droplet found and a slow decomposing initiator occurred, resulting in a slow-rate formation of oligomeric radical and creating fewer nuclei number[17]. As a consequence, it allowed the nuclei to catch more monomers/oligomers and increase their weight in the particle growth stage, resulting in the production of larger PS particles.

2.3.1.2. Effect of styrene concentration

Figure 2.5 shows the effect of styrene concentration on particle size. Particle sizes as a function of the styrene concentration under a specific temperature, when performed at the initiator amount of 0.0400, 0.0080, and 0.0040 wt%, are shown. **Figure 2.5a, b, c, and d** show the preparation of particles under different variations of temperature, corresponding to 55, 70, 80, and 90 °C, respectively. From above figures, the average diameter of PS particles increased from several tens to hundreds nanometers as the increase of the monomer concentrations. Similar positive gradient values in the same processing temperature were found, informing direct correlation between the styrene amount and the PS size.
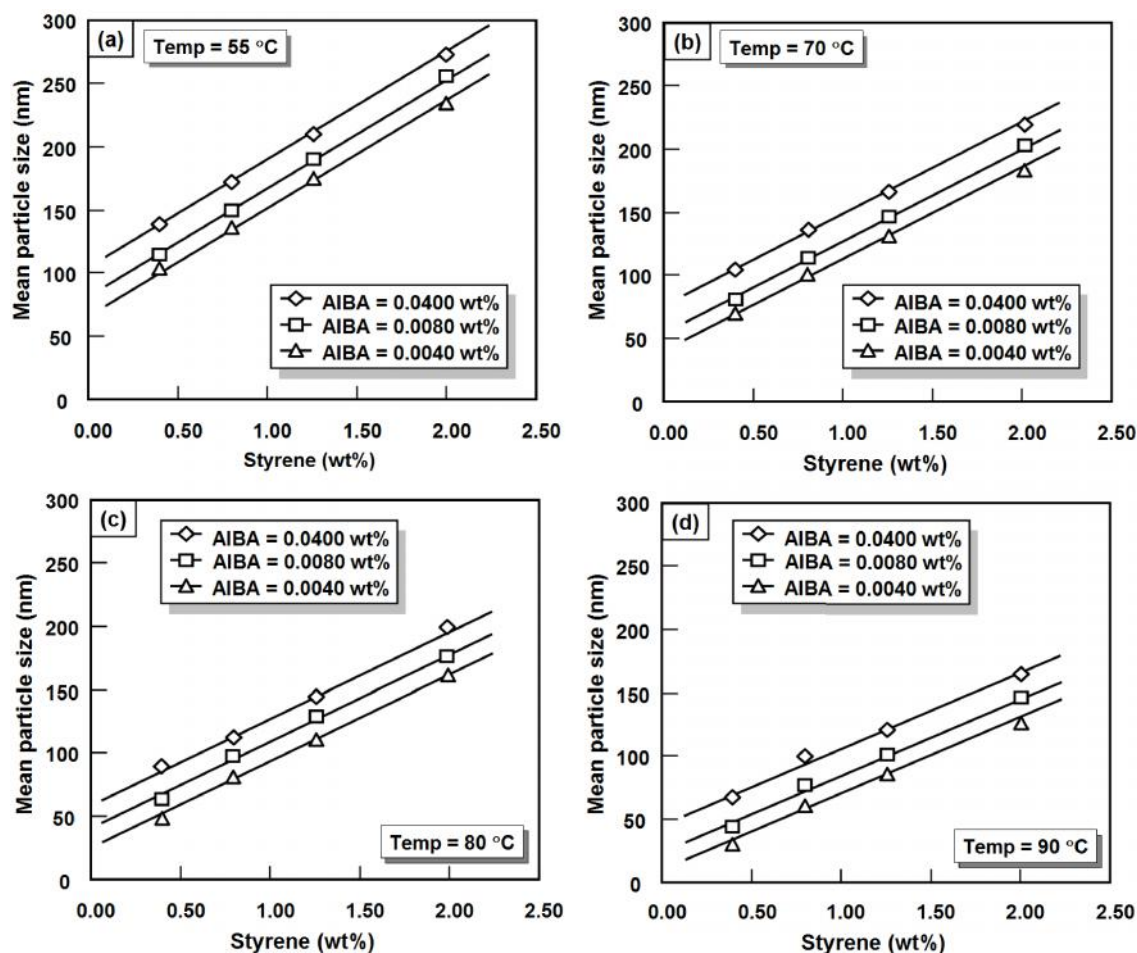
Figure 2.5. Mean particle size against detailed data on styrene concentration under different temperature variations: (a) 55, (b) 70, (c) 80, and (d) 90 °C. Samples were also conducted with different initiator concentrations, ranging from 0.0040 to 0.0400 wt%.

In the common dispersion polymerization (e.g. surfactant-added, water-alcohol system), monomer added can be completely dissolved. The concentration of dissolved monomer in the reaction medium changes directly with the amount of initial monomer[17]. However, in the present cases, the system was in the aqueous solution under the additive-free condition. The amount of the dissolved monomer (namely aqueous-phase monomer) was constant and independent to the initial concentration of monomer itself. The monomer can only be partially dissolved, creating most monomers exist as monomer droplets (namely oil-phase monomer). Because the aqueous-phase monomer is easily attacked by the initiator radical [18] and the rate of consumption of

46

aqueous-phase monomer is faster than the rate of diffusion of monomer (from oil to aqueous phase), the available active monomer was limited, retarding the nucleation stage. Further, due to the different Brownian motions (nuclei have slower Brownian motion than other components)[1], the initiator radicals and the free monomers/oligomers would prefer to interact and coalesce with the formed nuclei to increase nuclei weight, rather than create new nuclei via interaction of monomer-monomer and construction of longer oligomeric chain themselves[19].

In addition, in this study the amount of the styrene concentration was limited to the concentration of 2.00 wt%. Further increasing would make a problem in the polymerization process. A broad particle size distribution and a massive coagulum can be obtained[17], which is avoidable in the synthesis of monodispersed particles.

2.3.1.3. Effect of cationic initiator concentration

Figure 2.6 shows the effect of cationic initiator concentration on particle size. Changes in initiator amount seemed to have an impact to the change of PS size. **Figure 2.6a, b, c, and d** show the synthesis of PS conducted at the temperature of 55, 70, 80, and 90 °C, respectively. A strong effect as the increase of the initiator concentration on the increase of the particle size was obtained. However, further additional initiator amount (more than 0.0080 wt%) had a slight effect to the further production of larger particles. This reason drove us to the investigation of initiator amount of up to 0.0400 wt% in this study.

Chapter 2: Effect of colloidal nanoparticle charge on the fabrication of various self-organized porous and hollow particles

_____
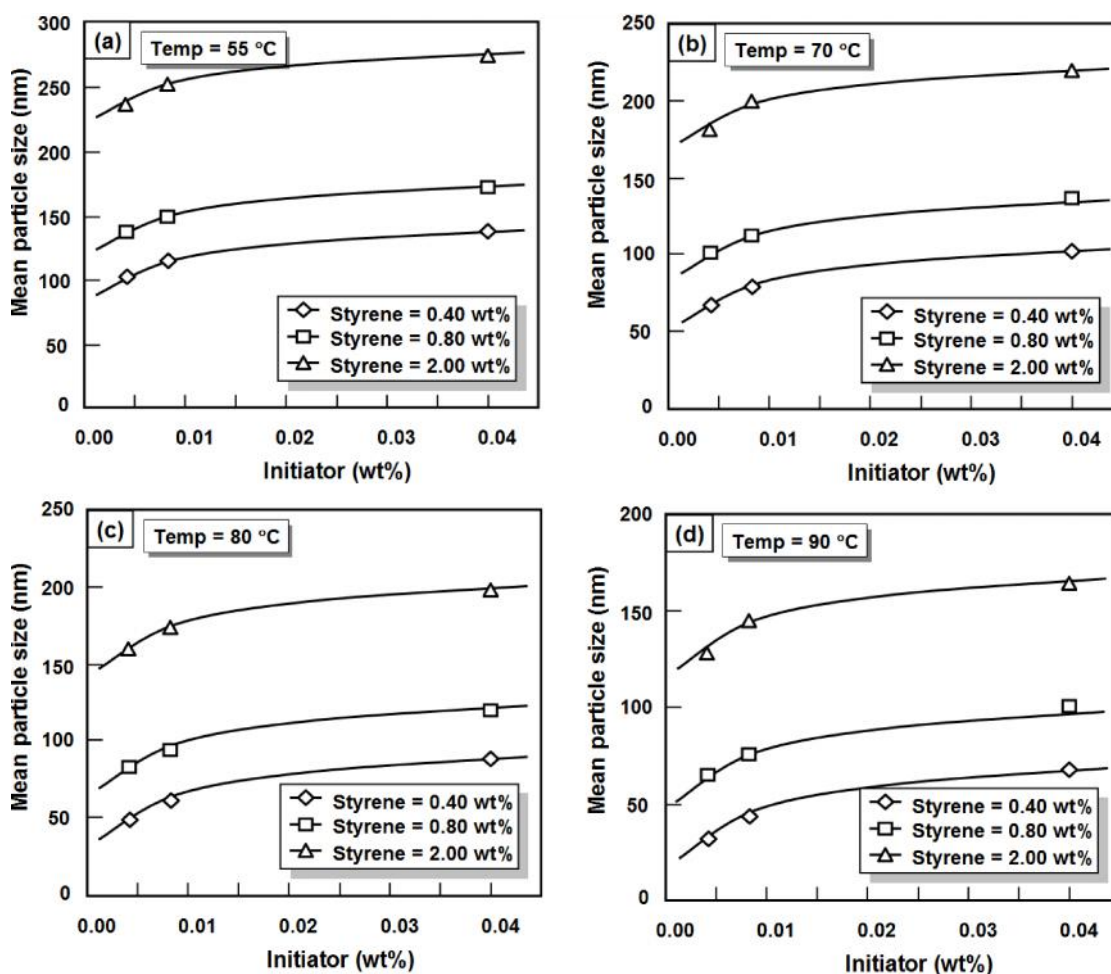
Figure 2.6. Mean particle size against detailed data on initiator concentration under different temperature processes: (a) 55, (b) 70, (c) 80, and (d) 90 °C. Samples were also conducted with different styrene concentrations, ranging from 0.40 to 2.00 wt%.

As the increase of the initiator amount, the polymerization rate should be increasing. Number of ionic groups produced from the decomposition of initiator increased[20], changing the stabilization of monomer (forming unstable monomer). The creation of these unstable components resulted in a good progress in the construction of longer oligomeric chain and larger nuclei and particles[15, 17]. For this reason, larger particles were obtained when a high concentration of initiator was employed. However, too high concentration of initiator did not make more efforts on the synthesis of larger particles. Although increase of initiator amount can increase the possibility of initiator to attack and radicalize styrene monomer, the number of styrene that could be

radicalized is limited to the solubility of monomer itself, as described in the above styrene effect discussion. In another possible reason, too high concentration caused the uncontrolled production of initiator radicals, allowing the higher degree of terminations between monomer radicals, monomers, and low molar mass oligomeric radicals in the early stages and resulting in that the growth process could not be further progressed[15].
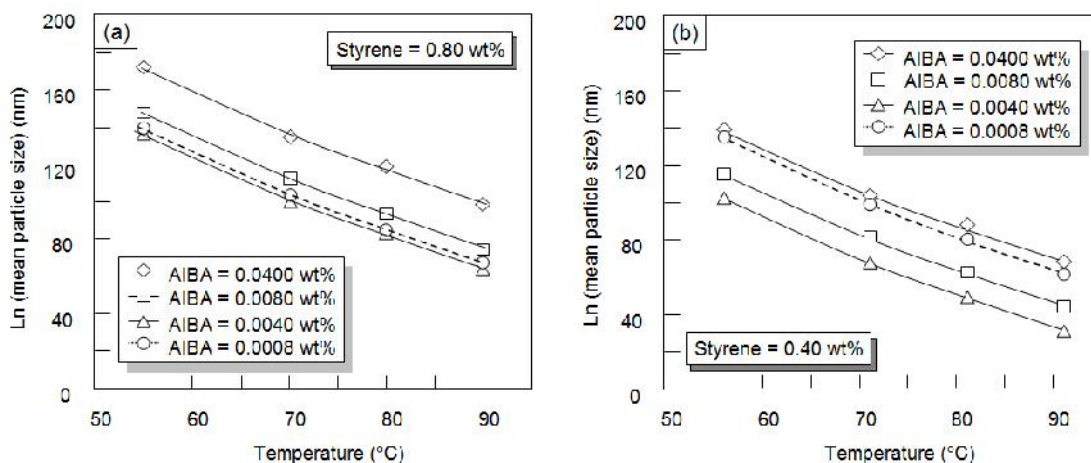
Figure 2.7. Appearance of error results (dash line; AIBA = 0.0008 wt%) in the mean particle size against detailed data on temperature graphs. Figures were classified under different styrene concentrations: (a) 0.80 and (b) 0.40 wt%. Samples were also conducted with different initiator concentrations, ranging from 0.0008 to 0.0400 wt%.

As shown in **Figure 2.6**, less initiator concentration permitted the synthesis of smaller particles. However, for some cases when using too low concentration of initiator (less than 0.0040 wt%), anomaly results were found, which did not follow the above trend of initiator on the particle size (**Figure 2.7** and **2.8**). Less concentration of initiator seemed to have an effect on the different particle formation rates. When the initiator was in the small amount, the production of initiator radical was limited, resulting in the less conversion of styrene[15]. Creation of nucleus was limited, while the free monomer was in the high number. This huge number of free monomer allowed the good progress in the growth process, making particle size larger. Other possible reason that made the experimental results far from the theoretical explanation was

because some reaction components were not converted or reacted completely when less concentration of initiator was used.
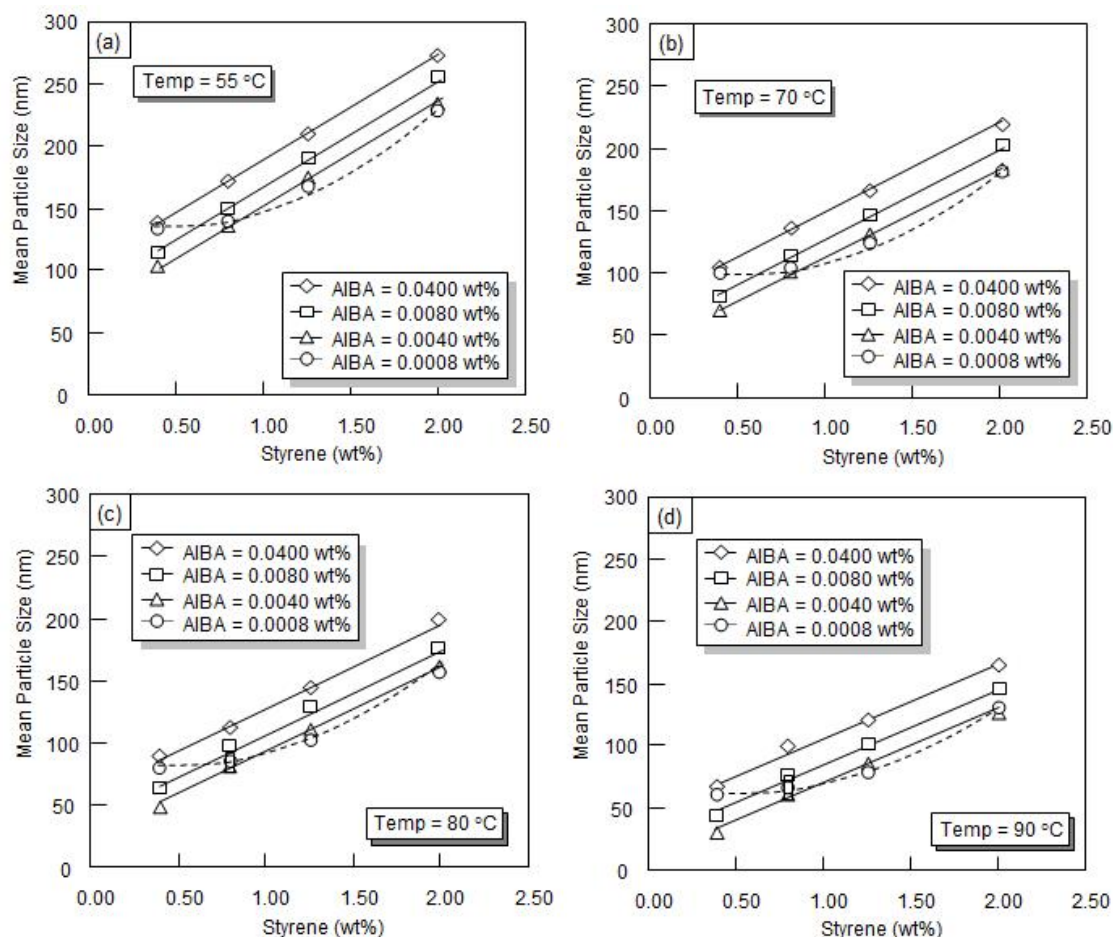
Figure 2.8. The appearance of error results (dash line; AIBA = 0.0008 wt%) in the mean particle size against detailed data on styrene concentrations graphs. The figure was classified under different temperature processes: (a) 55, (b) 70, (c) 80, and (d) 90 °C. Samples were also conducted with different initiator concentrations, ranging from 0.0008 to 0.0400 wt%.

2.3.1.4. Prediction equation as effect of several parameters

Experimental results showed that the control of particle size could be achieved by adjusting the temperature and the composition of reactants (i.e. monomer and initiator), driving the need of further investigations of these parameters. Using multiple regression analysis from **Figure 2.6-2.8**, we obtained that within the range of specific parameters, the final particle size (D_P) could be interpreted as a wide range of

preparative conditions: the temperature (T), the concentration of styrene (S), and the amount of initiator (I). Interestingly, all parameters could be treating as an independent variable, which was the same trend with Goodwin et al. analysis[20]:

$$dD_P = \left[\frac{\partial D_P}{\partial T}\right]_{S,I} dT + \left[\frac{\partial D_P}{\partial S}\right]_{T,I} dS + \left[\frac{\partial D_P}{\partial I}\right]_{T,S} dI \qquad (1)$$

Adopting the data analysis using equation (1), an overall equation representing the experimental parameters could be derived:

$$D_p = 71.80 \cdot S + 15.85 \cdot \ln(I) - 170.30 \cdot \ln(T) + 847.87 \qquad (2)$$

The above regressed data showed that the final size of the particles was proportional to the composition of styrene and the amount of initiator concentrations but had an inverse-proportional trend to the temperature. In addition, based on above equation, we found that the styrene amount had more effect than the initiator (more than 4 times).

Although this representation is purely empirical (from experimental data plot), it offers a useful guide to the selection and the adjustment of reaction parameters to provide a specific particle size. For example, when we intend to synthesize the PS with a size of 120 nm in the fixed temperature of 80 °C and the initiator concentration of 0.0400 wt%, the concentration of styrene that should be used is 1.00 wt%.

Based on above calculation results, the temperature and the composition of the reactants (i.e. monomer and initiator) could be used as parameters to control particle size precisely although the process was conducted in the absence of additives (**Figure 2.9**). The results demonstrated that some combinations of these parameters resulted in the successful formation of smaller particles (sizes of down to several tens nanometers; lied below "red-and-dashed" line), while the others were larger particles (sizes of up to submicrometer; lied above "red-and-dashed" line). This figure clearly showed that the

_____

particle size could be controlled by adjusting the temperature, in which increasing this parameter caused the production of smaller particles. To make clear the effect of other parameters (i.e. the styrene and the initiator amounts), we classified the figure into four zones of styrene concentration: 0.50; 1.00; 1.50; and 2.00 wt%. Each zone was conducted by the initiator concentration from 0.0040 to 0.0400 wt%. In each zone, the initiator with concentration of 0.0040 wt% was lied in the bottom zone, while 0.0400 wt% was in the top of zone, in which the increment of the initiator amount was illustrated by the "blue" arrows. The result showed that the increase of the styrene concentration led the positive trend in production of larger particles and in all styrene concentration zones, the increase of the initiator concentration had an impact to the formation of larger particles.
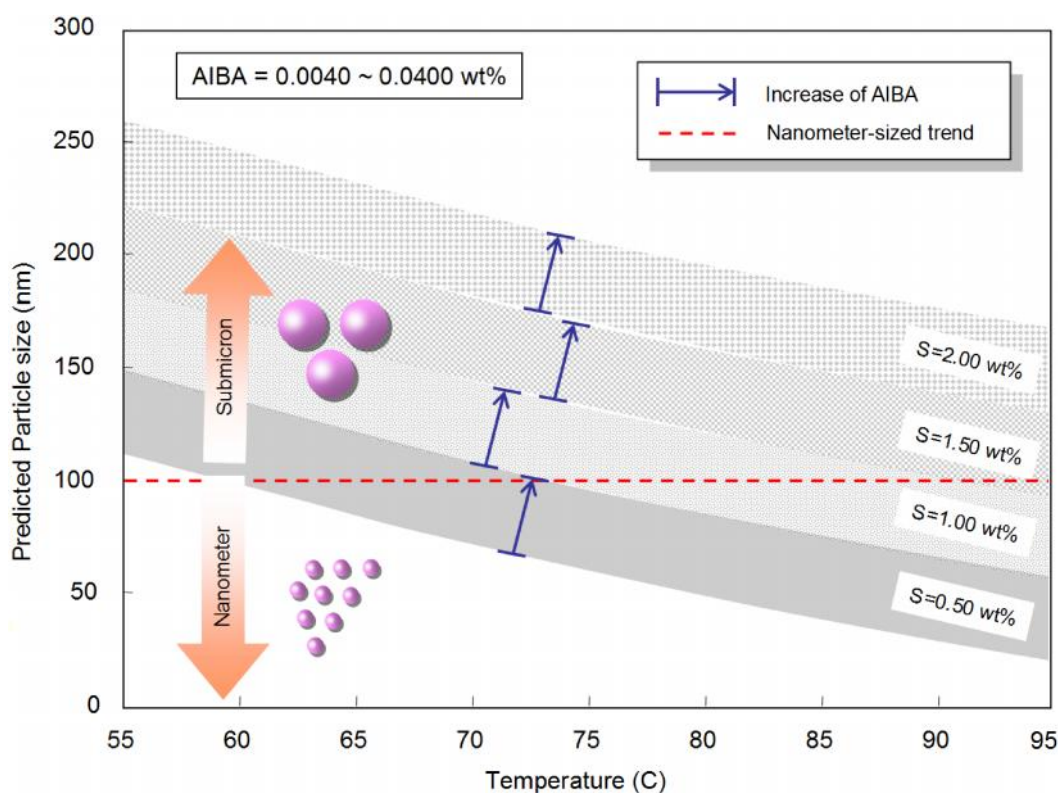
Figure 2.9. Summary of the effect of variation of temperature and styrene and initiator concentrations on PS particlesize.

Recognition of the prediction equation (scaling law) came from the experimental results, in which the variation was within strictly specified reaction parameters (styrene = 0.40 – 2.00 wt%; initiator = 0.0008 – 0.0400 wt%; temperature = 55 – 90 °C; and processing time = 10 hours).

2.3.2. Application of PS particles as the template

Since we have experiences in the preparation of particles with controllable morphology using a spray method[1-4], the potential advantage of this technique is investigated. Based on this technique, a possible formation mechanism of the hole-structured particle as an effect of template charge is deduced in **Figure 2.10**. Initial precursor was prepared by mixing host nanoparticles and PS particles in an aqueous solution. All particles at the very beginning of the process are distributed homogeneously in the precursor. Then, as a result of different charges of the particles, attraction and repulsion phenomenon happens. Because most of the host nanoparticles have a negative zeta charge, the phenomenon when using different charges of PS can be divided into two ways: (i) porous particle formation; (ii) hollow particle formation.
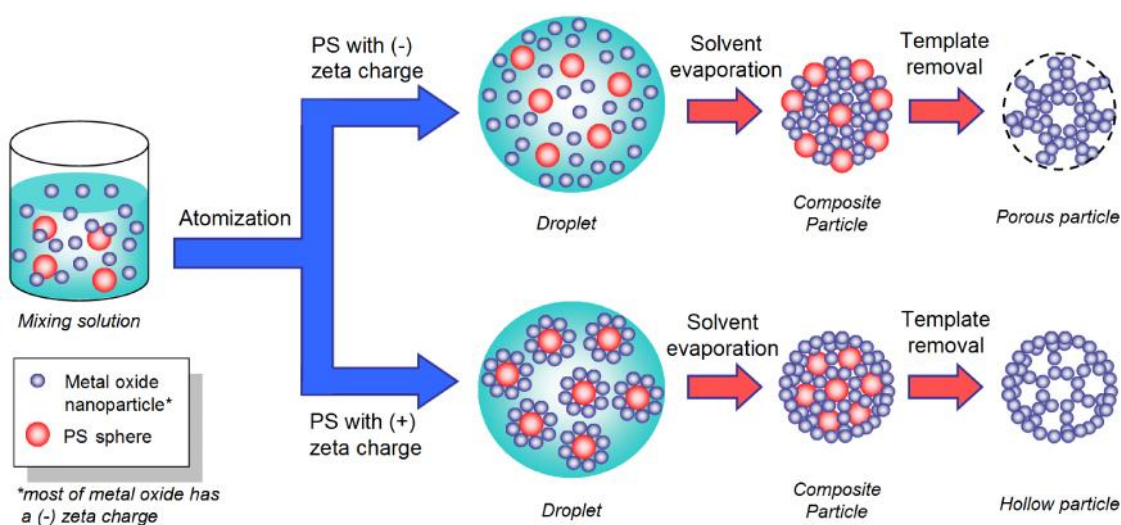
Figure 2.10. Illustration of self-assembly template mechanism using organic particle templates with different charges via a spray-drying route.

_____

In the first way, when the PS with a negative zeta charge is used, porous particles can be prepared. The reason is considerably because the host nanoparticles are characterized to have a similar surface charge to the PS particle. Repulsion process among both types of particles happens, resulting in that the PS and the host material are flying individually in the precursor. When the precursor is spray dried, the PS and the host particles are self-assembled under the repulsion phenomenon, forming a stable structure of PS and host materials. Finally, after further heat treatment for removing the template, the PS is removed, leaving the PS/host composite and remaining a pore structure in the final product. This formation mechanism can describe the reason that in the common use of PS template (most of PS particles have a negative zeta charge), porous particles are typically produced.

In the second way, when the PS with a positive zeta charge is used, different hole configurations can be obtained. Opposite charges between the PS and the host particles make the attraction phenomenon since mixing in the precursor. The partnership of the PS and the host particles is so attractive and favorable for host colloids to (i) attach on the surface of PS particle, and then (ii) form the aggregation of host nanoparticles onto the PS particle surface since in the precursor, creating core-shell-like structure (PS=core; host particle=shell). When the precursor is sprayed, aggregated PS/host are arranged inside the droplet and forming PS/host particle composite particles. Further drying travel (reaching the template removal drying processing zone), the PS was released, and the coexisting of the composite PS/host particle turned on the material with a hollow structure.

To confirm the role of PS charge in the preparation of hollow particles, we initially analyzed the charge of PS using a zeta potential measurement (**Figure 2.11**). The result showed that the prepared PS particles had a positive zeta potential ($\zeta_{pot} = $

+40 mV; **Figure 2.11a**), while commercially available PS was negative (ζpot = -39 mV; **Figure 2.11b**). With this reason when host material with a negatively zeta charge (e.g. ζpot for WO_3 is -39 mV) was added to the PS solution, different particle interactions could be occurred. Repulsion phenomena would have happened in the case of the commercial PS, while attraction would have been in the synthesized PS solution.
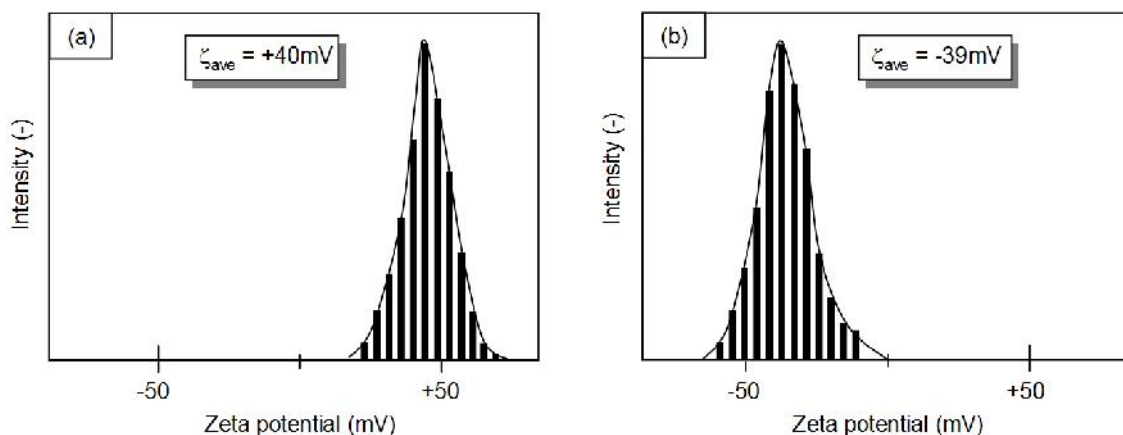
Figure 2.11. Zeta potential analysis of the synthesized PS (a) and commercial PS particles (b).

Figure 2.12 shows the SEM images of various spray-dried particles produced by various host materials and different PS particles. **Figure 2.12a-c** are SEM analysis images of WO_3 particles, while **Figure 2.12d and e** are ZrO_2 and SiO_2 particles, respectively. In the case of the effect of PS charges, figures are classified as follows: (i) **Figure 2.12a** shows the particles produced with no addition of PS; (ii) **Figure 2.12b** is for the addition of commercial PS; and (iii) **Figure 2.12c-e** are for the addition of the synthesized PS.

Spray-dried particles with no addition of PS were nonporous and spherical (**Figure 12a**). These results suggested that the aggregated particles were produced from an aggregation of inorganic nanoparticles during the spraying process. However, when the PS was added, particles with a hole structure were produced (**Figure 2.12b-c**). Small nanoparticles induced an attractive depletion-interaction between the PS templates during drying process[1], arranging and compacting the PS and the host materials in the

stable condition and resulting in the preparation of composite PS/host particles. Because the temperature process of the spray drying method (temperature of the second zone = 500°C) was higher than the thermal degradation of PSL (270 °C[21]), the PS would have been removed from the composite, remaining hole structure in the final product. Good skeleton patterns in **Figure 2.12b-c** confirmed that small host nanoparticles were self-assembled and located in the space between PS templates. The size and shape of holes for all hole configurations was identical to the initial PS template, informing that the PS could be effectively used as the template and giving a potential way for further developments (e.g. control of pore size).
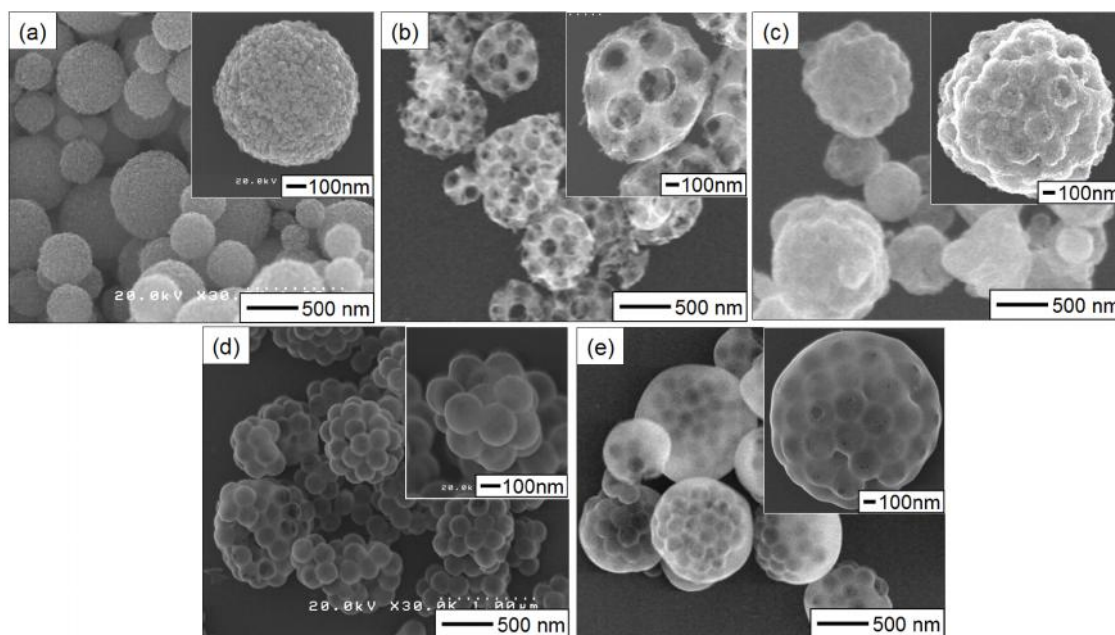
Figure 2.12. SEM images of spray-dried precursors with different compositions of initial precursor: (a) WO3 only; (b) WO3/the synthesized PS (270 nm); (c) WO3/commercial PS(250 nm). (d) and (e) are spray-dried particles prepared from zirconia/the synthesized PS and silica/the synthesized PS, respectively.

The effect of the use of the commercial PS and the synthesized PS on hole-structured particle types is shown in **Figure 2.12b-c**. Different results in the hole structure were obtained when using different types of PS. The addition of commercial PS particles into the precursor allowed the production of porous particles (**Figure**

2.12b), while the synthesized PS permitted the formation of hollow particles (**Figure 2.12c**). These results were in a good agreement with the above hypothesis in **Figure 2.10**. When a PS with positive zeta charge was used, high interaction between WO_3 and PS particles happened. The PS particles were easily attached by WO_3 nanoparticles, producing an aggregation of WO_3 and PS (a core/shell of PS/WO_3) in the precursor. When the aggregated composites were sprayed, they self-assembled in the droplet, forming hollow particles in the final product. However, when the PS with a negative zeta potential was employed, no aggregation phenomenon happened. The PS was difficult to be covered completely due to the repulsion effect between WO_3 and PS. This phenomenon resulted in the production of porous particles.

To confirm the hypothesis, we also prepared various hollow particles prepared from various host materials with the prepared PS template: zirconia (**Figure 2.12d**) and silica (**Figure 2.8e**). As expected, hollow particles could be obtained for all cases. The low magnification of SEM images also showed a group of identical collected hollow particles (in particle outer diameter and hole size), confirming that the morphology and dimensions of all particles are similar and the PS was effective in assisting the preparation of particles with a hollow structure.

2.4. Conclusion

We successfully examined the synthesis of homopolymer, pure, and cationic PS particles with controllable size (from 30 to 300 nm) and demonstrated their application as the template to facilitate the production of hollow inorganic particles. The PS synthesis process was conducted in the aqueous solution and under the additive-free condition. The effectiveness of this method in the precise control of particle size down to the nanometer scale was relied on changes in the temperature and the concentration

_____

of reactants. An increase of the temperature caused the production of smaller particles, while an increase of the amount of the reactants (i.e. monomer and initiator) resulted in the larger-sized particle synthesis. The derivation of the scaling particle size was also examined, which would be important for further applications, especially related to the scaling-up process. The change of the reaction parameters had no effect on the chemical structure of PS, confirmed by the FTIR and the micro-Raman spectrum analysis. Zeta measurement analysis showed that the prepared PS had a positive zeta charge, which was different from commercial PS particles, due to use of a cationic initiator (i.e. AIBA). The excellent ability from the synthesized PS as the template to assist the preparation of various hollow inorganic particles (i.e. WO_3, silica, and zirconia) was also reported, in which this hollow particle preparation could not be achieved when the commercial PS particles were used. Finally, due to the simple preparation procedures, the use of relatively low-temperature processing, and the employment of easy-to-handle chemicals, we believe that this study provides important and new information for the field of chemical and material science and engineering.

2.5. References

[1] A.B.D. Nandiyanto, N. Hagura, F. Iskandar, K. Okuyama, Design of a highly ordered and uniform porous structure with multisized pores in film and particle forms using a template-driven self-assembly technique, Acta Materialia, 58 (2010) 282-289.

[2] F. Iskandar, A.B.D. Nandiyanto, K.M. Yun, C.J. Hogan, K. Okuyama, P. Biswas, Enhanced photocatalytic performance of brookite tio2 macroporous particles prepared by spray drying with colloidal templating, Advanced Materials, 19 (2007) 1408-1412.

[3] A.B.D. Nandiyanto, F. Iskandar, K. Okuyama, Macroporous anatase titania particle: Aerosol self-assembly fabrication with photocatalytic performance, Chemical Engineering Journal, 152 (2009) 293-296.

[4] A.B.D. Nandiyanto, K. Okuyama, Progress in developing spray-drying methods for the production of controlled morphology particles: From the nanometer to submicrometer size ranges, Advanced Powder Technology, 22 (2011) 1-19.

_____

[5] A.B.D. Nandiyanto, T. Ogi, F. Iskandar, K. Okuyama, Highly ordered porous monolayer generation by dual-speed spin-coating with colloidal templates, Chemical Engineering Journal, 167 (2011) 409-415.

[6] A.B.D. Nandiyanto, S.G. Kim, F. Iskandar, K. Okuyama, Synthesis of spherical mesoporous silica nanoparticles with nanometer-size controllable pores and outer diameters, Microporous and Mesoporous Materials, 120 (2009) 447-453.

[7] D. Kajiya, K. Saitow, Solvation structures of cis-and trans-1, 2-dichloroethylene in supercritical co2 investigated by raman spectroscopy and attractive energy calculations, The Journal of Physical Chemistry B, 113 (2009) 13291-13299.

[8] S. Takabayashi, K. Okamoto, H. Sakaue, T. Takahagi, K. Shimada, T. Nakatani, Annealing effect on the chemical structure of diamondlike carbon, Journal of Applied Physics, 104 (2008) 043512-043511 - 043512-043515.

[9] P. Zhang, J. He, X. Zhou, An ftir standard addition method for quantification of bound styrene in its copolymers, Polymer Testing, 27 (2008) 153-157.

[10] J.C. Yang, M.J. Jablonsky, J.W. Mays, Nmr and ft-ir studies of sulfonated styrene-based homopolymers and copolymers, Polymer, 43 (2002) 5125-5132.

[11] M. Davies, A. Edwards, Dielectric studies of mobility of polar molecules in polystyrene, Transactions of the Faraday Society, 63 (1967) 2163-2176.

[12] A. Palm, Raman spectrum of polystyrene, Journal of Physical Chemistry, 55 (1951) 1320 - 1324.

[13] S.F. Lascelles, S.P. Armes, P.A. Zhdan, S.J. Greaves, A.M. Brown, J. F.Watts, S.R. Leadley, S.Y. Luk, Surface characterization of micrometre-sized, polypyrrole-coated polystyrene latexes: Verification of a 'core-shell' morphology, Journal of Materials Chemistry, 7 (1997) 1349-1355.

[14] S.Z. Bas, S. Yildiz, Chemical modification kinetics of polystyrenes having various molecular weights, Colloids and Surfaces A: Physicochemical and Engineering Aspects, 298 (2007) 123-128.

[15] J. Xu, P. Li, C. Wu, Formation of highly monodispersed emulsifier-free cationic poly(methylstyrene) latex particles, Journal of Polymer Science: Part A: Polymer Chemistry, 37 (1999) 2069 - 2074.

[16] W. Lane, Determination of solubility of styrene in water and of water in styrene, Industrial & Engineering Chemistry Analytical Edition, 18 (1946) 295-296.

[17] C. Tseng, Y. Lu, M. El Aasser, J. Vanderhoff, Uniform polymer particles by dispersion polymerization in alcohol, Journal of Polymer Science Part A: Polymer Chemistry, 24 (1986) 2995-3007.

[18] T. Yamamoto, M. Nakayama, Y. Kanda, K. Higashitani, Growth mechanism of soap-free polymerization of styrene investigated by afm, Journal of colloid and interface science, 297 (2006) 112-121.

[19] A.B.D. Nandiyanto, F. Iskandar, T. Ogi, K. Okuyama, Nanometer to submicrometer magnesium fluoride particles with controllable morphology, Langmuir, 26 (2010) 12260-12266.

[20] J.W. Goodwin, J. Hearn, C.C. Ho, R.H. Ottewil, Studies on the preparation and characterization of

_____

monodisperse polystyrene lattice, Colloid Polymer Science, 252 (1974) 484-471.

[21] F. Iskandar, A.B.D. Nandiyanto, W. Widiyastuti, L.S. Young, K. Okuyama, L. Gradon, Production of morphology-controllable porous hyaluronic acid particles using a spray-drying method, Acta Biomaterialia, 5 (2009) 1027-1034.

Chapter 3

Effect of colloidal nanoparticles charge, size, and concentration on fabrication of self-organized porous silica particle

3.1. Introduction

The design of porous material has attracted a tremendous amount of attention.[1] The existence of pores can result in exceptional chemical and physical properties that differ markedly from those of bulk or dense material and have potential in many fields of applications: electronics, catalysis, drug delivery, sensing, pigmentation, and magnetic and optical material science.[2]

To produce a material with desirable porous structure, many strategies have been advanced.[3, 4] The commonest employs a self-assembly template technique that uses either an inorganic component[5, 6], a surfactant/organic molecule[7-12], or a template particle[2, 4, 13-20]. However, most reports described successful production of porous material with only partial information on charges, interactions, sizes, and compositions of the template and host materials.

Information about influences of self-assembly parameters (i.e. surface charge, size, and concentration of colloidal nanoparticles) on the formation of porous materials is still lacking. In fact, optimization of these parameters provides significant information towards producing better highly ordered porous materials. Although some studies have reported explanations regarding size and process conditions[21, 22], limitations in applicability are still found, such as to films only and not to particles. Furthermore, these did not incorporate colloidal particle charge effects. Indeed, this factor allows the formation of material with different porous configurations.

Chapter 3: Effect of colloidal nanoparticles charge, size, and concentration on fabrication of self-organized porous silica particle

_____

The relation between porous morphology and process conditions has been investigated experimentally and theoretically[18, 23, 24]. Here, the aim of this chapter is to spotlight influence of self-assembly parameters on porous material fabrication. Silica nanoparticles (as a host material model) and polystyrene (PS) spheres (as a template model) were used and self-assembled to produce porous material in film and particle forms. Spherical and monodispersed PS spheres can be completely removed using either calcination or solvent dissolution.[2] Thus, their inverse replication is effective to produce identical pore size, shape, and structure.[18] To precisely uncover the influences associated with the self-assembly parameters, preparations were performed under surfactant-free conditions, which typically are disregarded in current reports. The experimental results indicated that these self-assembly parameters were influential in controlling the porous structure and the pore size. A highly ordered porous structure was successfully created only if appropriate self-assembly parameter conditions are applied (i.e., PS surface charge $\leq$ -30 mV; silica-to-PS size ratio < 0.078; and silica-to-PS mass ratio of about 0.50). In contrast, deviation from optimum parameter conditions resulted in the formation of incomplete or brittle porous structures. To examine the successful formation of highly ordered pores in film and particle forms, a geometrical model related to tight packing of spheres in the material construction was also developed. In addition, the present chapter reports the influence of self-assembly parameters for porous material formation in film and particle forms. To the best of my knowledge, this report is the first to address the issue and could be relevant to other functional properties of porous materials.

Chapter 3: Effect of colloidal nanoparticles charge, size, and concentration on fabrication of self-organized porous silica particle

_____

3.2. Experimental Method

3.2.1. Raw materials

Porous material was produced from a precursor containing silica nanoparticles (Nissan Chemical Co. Ltd., Japan) with mean sizes of 5, 16, 32, 45, and 90 nm and PS spheres. The PS spheres were synthesized from a simple polymerization of styrene monomer (styrene; Kanto Chemical Co., Inc., Japan) under surfactant-free conditions. As the initiator in the styrene polymerization, potassium persulfate (KPS; Sigma-Aldrich, USA) or 2,2-azobis (isobutyramidine) dihydrochloride (AIBA; Sigma-Aldrich, USA) was used. To produce PS with different diameters and surface charges, concentrations of the styrene and the initiator were varied independently. The PS synthetic method has been detailed and explained in previous reports.[24] All chemicals were used without further purification.

3.2.2. Fabrication of film with porous structures

Porous film was prepared from a drop of the precursor onto a substrate (silicon wafer; size of 4×4 mm). This precursor was then dried at 40 °C to form a composite silica/PS film. A slow-drying temperature was used to allow sufficient time for silica and PS spheres to self-arrange into an ordered structure. After completing self-assembly, a white matrix film formed that was then subjected to template removal (calcined at 500 °C in the air atmosphere) to remove any remaining residual solvent and PS, leaving a porous film as the final product.

Chapter 3: Effect of colloidal nanoparticles charge, size, and concentration on fabrication of self-organized porous silica particle

_____

3.2.3. Production of particles with porous structures

To produce porous particles, a spray-drying method was used. Details of the apparatus has been described in the previous works.[2, 23] Briefly, the apparatus consisted of an ultrasonic nebulizer (model NE-U12, Omron Corp., Tokyo, Japan) operating at frequency 1.7 MHz, a ceramic tubular furnace (D = 13 mm and L = 1 m), and a filter. The nebulizer, which was equipped with a cyclone, was used to generate monodispersed droplets of several micrometers in diameter. These droplets were then introduced into a tubular furnace with two fixed temperature zones (200/600 °C) using a carrier gas (air flowing at 0.75 L/min). Thermalization in the tubular furnace had a dual purpose, (i) to evaporate solvent, producing composite silica/PS particles when the aerosol travelled through the first zone, and (ii) to remove the PS from the composite, creating porous inorganic particles in the second zone. The prepared particles were then collected using a filter.

3.2.4. Production of particles with porous structures

The prepared film and particles were characterized using a scanning electron microscope (SEM) (Hitachi S-5000, Hitachi Ltd, Japan) operating at 20 kV for examining their sizes and morphologies. The elemental and the physicochemical composition of the prepared materials were evaluated using a Fourier transform infrared (FTIR) spectrometer (Spectrum One System, Perkin-Elmer, USA) in the range 600–4000 cm^{-1} and a thermogravimetric and differential thermal analyzer (TG-DTA) (Exstar6000, Seiko Instruments Inc., Japan; heating rate = 5 °C/min; carrier gas: air, 200 mL/min). To characterize the charge of the colloidal particles, a zeta potential measurement (Malvern Zetasizer, Nano ZS, UK) was conducted.

3.3. Result and Discussion

3.3.1. Investigation of porous structuralization

Figure 3.1 shows SEM images of the colloidal particles used for the preparation of porous silica material. Relatively monodispersed particles with a spherical shape were observed. This result confirms that these colloidal particles can be used for precise investigations of the influences of self-assembly parameters on porous structuralization.
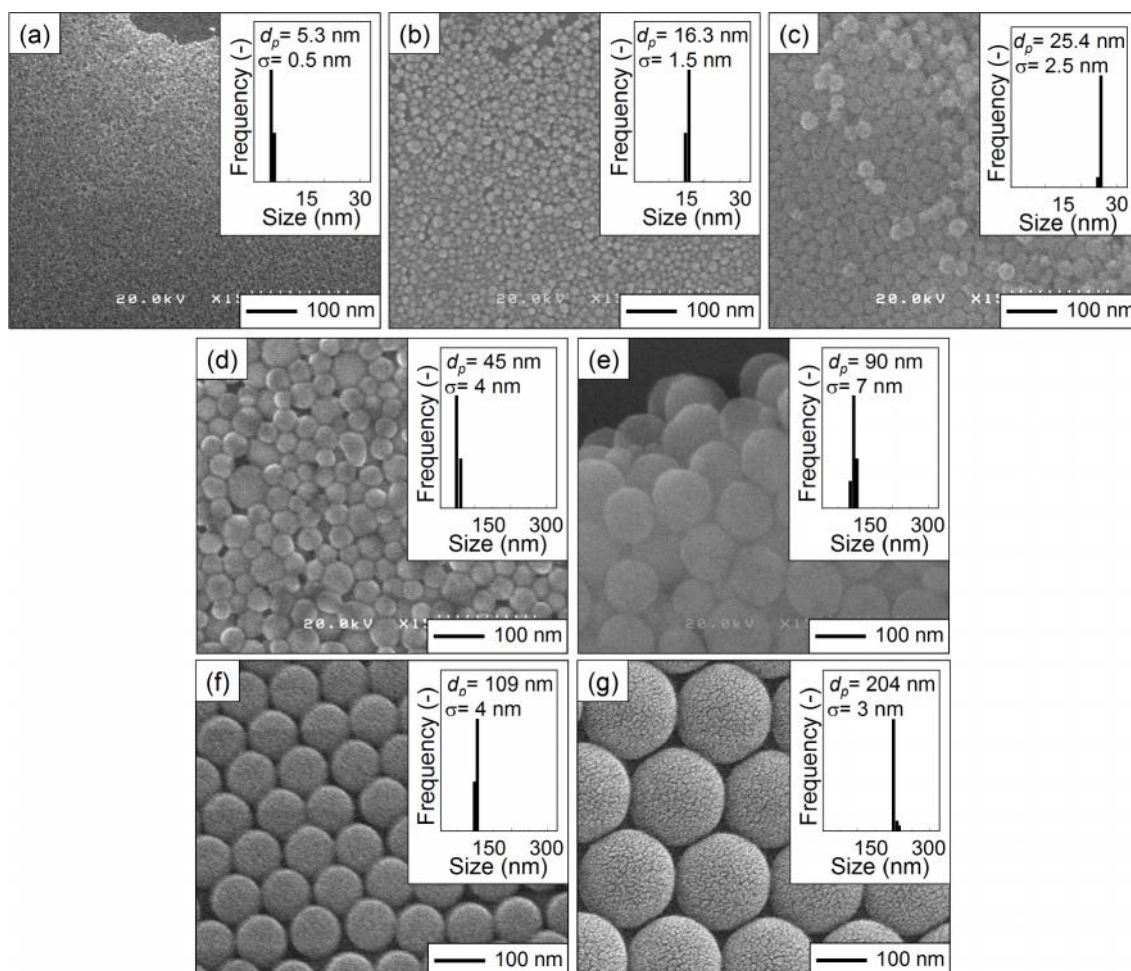
Figure 3.1.   SEM images of colloidal particles used in this study: (a) 5-nm silica, (b) 16-nm silica, (c) 25-nm silica, (d) 45-nm silica, (e) 90-nm silica, (f) 100-nm PS, and (g) 200-nm PS.

Chapter 3: Effect of colloidal nanoparticles charge, size, and concentration on fabrication of self-organized porous silica particle

_____

Figure 3.2 shows SEM images of the film before and after template removal. When dropping the precursor containing PS and silica, a composite film was produced (**Figure 3.2a**). PS and silica were self-assembled on the substrate. The PS spheres were clearly observed with the orientation of the hexagonal pattern, while the silica nanoparticles filled in the void space between the PS spheres. After applying the template removal to the composite film, the hole-structured film was prepared (**Figure 3.2b**). The low-magnified SEM image in **Figure 3.2c** shows that the porous morphologies, structures, and dimensions in all positions are identical. Thus, we infer that the present process is reliable with respect to uniformity of the porous structures in the final product.
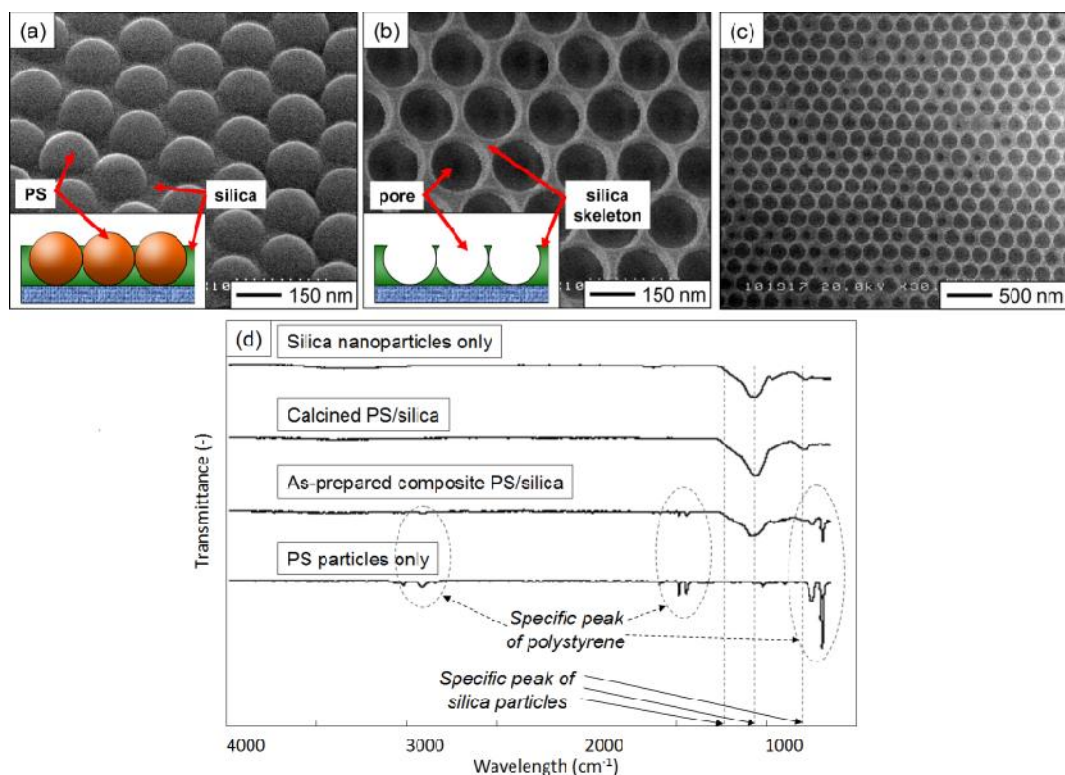
Figure 3.2. SEM images of the coated film before (a) and after template removal (b,c). Panel (c) is a low-magnification SEM image of the sample imaged for panel (b). Figure (d) shows the results from FTIR analysis of the prepared material. Insets in (a) and (b) are illustrations of the colloidal particle configuration. Samples were prepared using 200-nm PS and 5-nm silica.

_____

Figure 3.2d shows the FTIR spectra for the self-assembled film before and after template removal. As standards for comparisons, we also analyzed "PS only" and "silica only" samples. The FTIR spectra of as-prepared film detected the PS (at band 500–1000, 1400–1700, and 2800–3200 cm^{-1}) and the silica peaks (in the range 1000–1200 cm^{-1}). No other adsorption peaks (beside the peaks of silica and PS) appeared, indicating that PS spheres and silica nanoparticles were self-assembled by neither chemical reaction nor intermediate component formation. After the sample went through template removal, the film exhibited absorption peaks only in the range 1000–1200 cm^{-1}, which was identical to those of the "silica only" sample. These results indicate that all PS spheres are completely removed after template removal, retaining just silica in the final product. This finding is also confirmed by the TG analysis, presented in **Figure 3.3**.
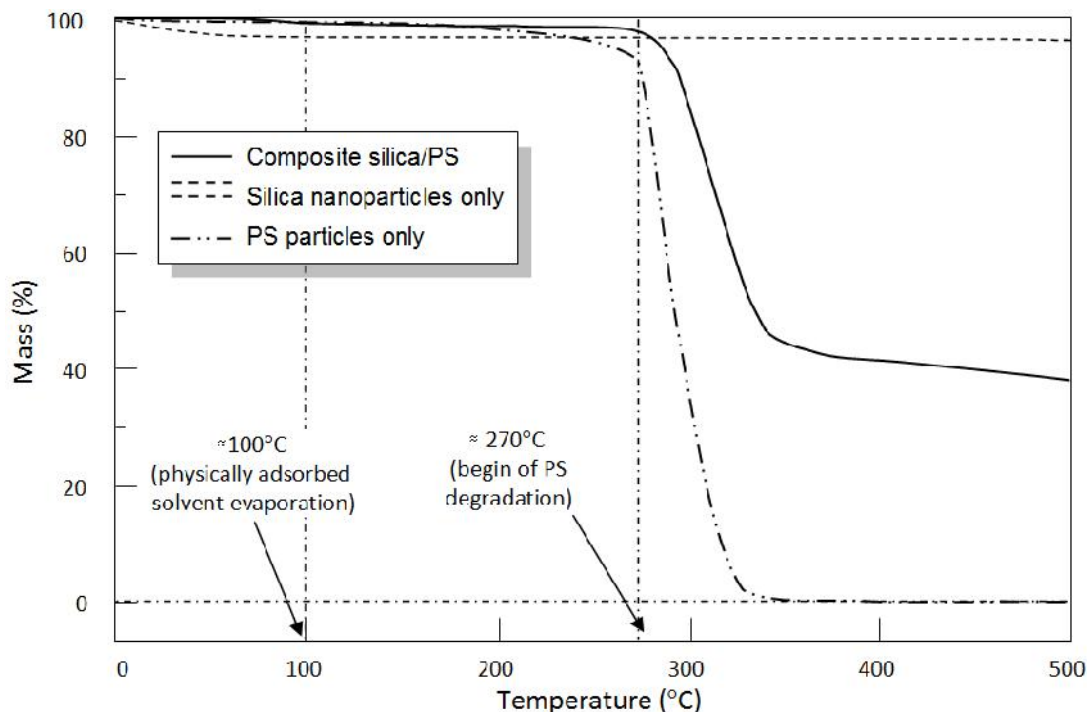
Figure 3.3. TGA analysis result of samples containing "silica only", "PS only", and "silica and PS". Sample containing "silica and PS" was prepared using a silica-to-PS mass ratio of 0.50. Silica and PS used in this analysis have a mean size of 5 and 200 nm, respectively.

Chapter 3: Effect of colloidal nanoparticles charge, size, and concentration on fabrication of self-organized porous silica particle

_____

In addition, we also found an interesting phenomenon in the TG analysis. For the pure silica sample, the mass loss at 500°C was due to condensation and loss of –OH (H_2O) groups. For a sample with silica-to-PS mass ratio of 0.50, the mass of the final residue at 500°C is near to 40% (not closer to 50%). The difference is likely due to the exothermic combustion of PS in the composite, which results in higher local temperatures than the furnace temperature and therefore giving more condensation of silica.

3.3.2. The influence of colloidal surface charge on porous structuralization

Figure 3.4 shows the influence of initiator type and concentration on the porous structuralization, examined with SEM analysis. A change of initiator type and concentration modifies the PS surface charge that greatly impacts the particle-to-particle interaction during self-assembly.[24, 25] Holes of about 200 nm in diameter were identified in all cases. A good hole configuration (hexagonal porous pattern) was formed when using PS spheres synthesized using KPS amounts of more than 0.0400 wt% (**Figure 3.4a,b**). Collapse of the hexagonal porous pattern was identified when employing PS synthesized from KPS with a concentration of 0.0080 wt% (**Figure 3.4c**). A failure in the formation of porous film was found when using PS spheres synthesized using AIBA (**Figure 3.4d**). As the size and shape of the PS templates are the same, the fundamental reason behind the successful formation of pores is due to the influence of initiator type and concentration on the silica-and-PS interaction during self-assembly.

Zeta potential analysis results of the colloidal particles are shown in **Figure 3.4e**. The zeta values of the PS spheres synthesized using KPS with concentrations of more than 0.0400 wt% were about -30 mV, whereas those with KPS of 0.0080 wt%

_____

were -27 mV. For PS synthesized using AIBA, the zeta value was +32 mV, whereas the zeta values of the silica colloidal nanoparticles (i.e., 5, 16, 25, 45, and 90 nm) were about -33 mV.

From the above results, successful porous structuralization was achieved only when using silica and PS particles with negative zeta values. Thus, we can conclude that the successful formation of porous film is due to repulsive interactions between the colloidal components (i.e., silica and PS).

Aside from needing the same surface charges in the colloidal components, the impact of PS charge values on the porous structure was also found. The PS with sufficient charge (surface charge $\leq$ -30 mV) leads to the creation of porous hexagonal arrangements, whereas those with less charge enable only a non-optimal porous configuration to form. These results provide useful information on what level of particle-and-particle interaction and repulsion forces are required to attain good self-assembly during the formation of porous material. In addition, although higher concentrations of KPS can potentially assist the hexagonal porous structure, the presence of ions from initiator degradation (i.e. K^+, SO_4^{2-}, and $S_2O_8^{2-}$) must be considered. Negative impacts from these ions on the electrostatics and interaction between colloidal particles (e.g., coagulation, flocculation, etc.)[26] can develop, causing problems in the porous structuralization and skeleton strength.
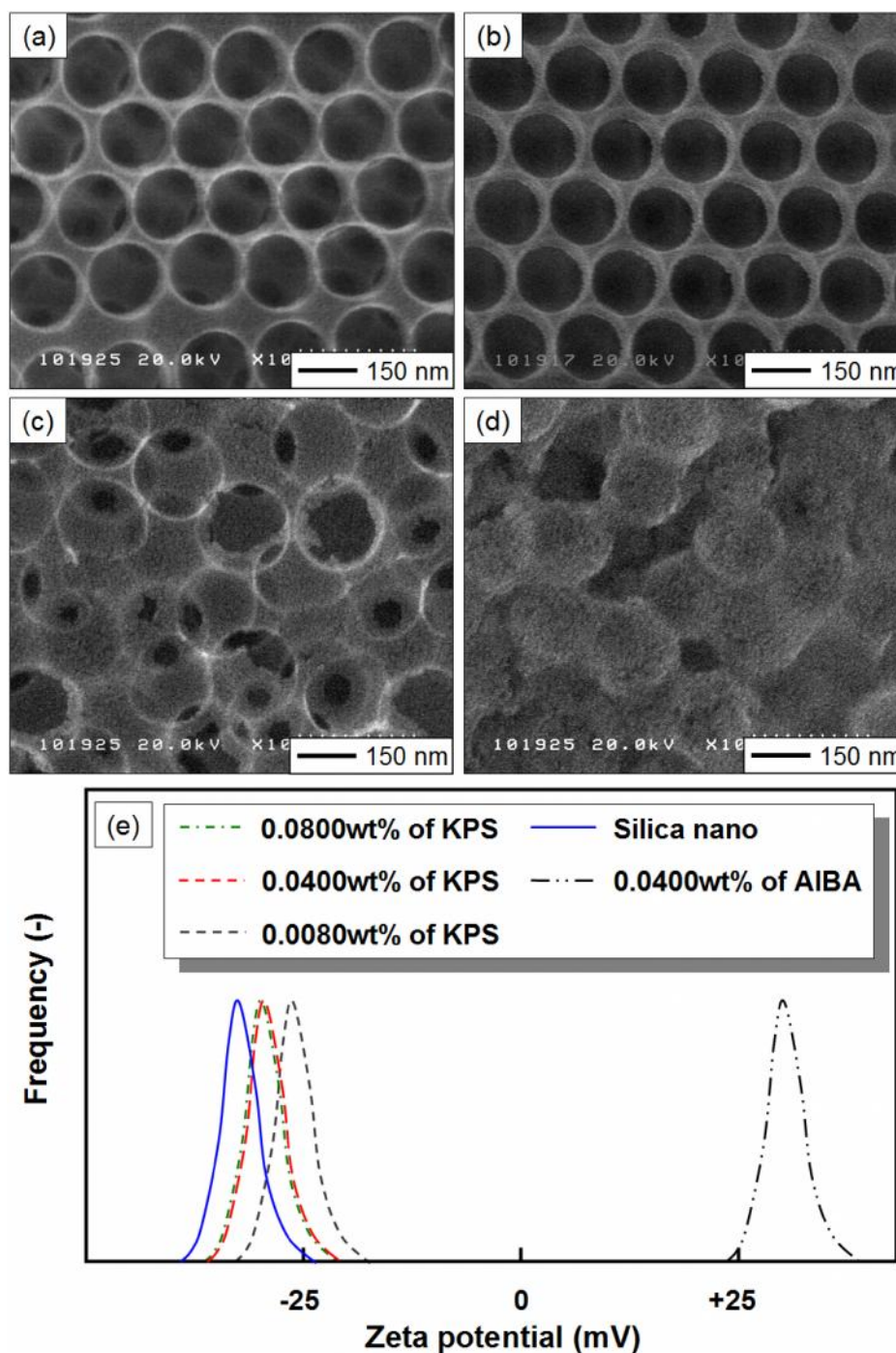
Figure 3.4. Porous structuralization results as a function of initiator type and concentration: (a) KPS = 0.0800 wt%, (b) KPS = 0.0400 wt%, (c) KPS = 0.0080 wt%, and (d) AIBA = 0.0400 wt%. Figure (e) presents the results from zeta-potential analysis of each initial colloid. Samples in panels (a)–(d) were prepared using 200-nm PS and 5-nm silica (silica-to-PS mass ratio of 0.50).

Chapter 3: Effect of colloidal nanoparticles charge, size, and concentration on fabrication of self-organized porous silica particle

_____

3.3.3. The influence of silica-to-PS mass ratio on the porous structuralization formation

Figure 3.5 shows the SEM images of films prepared with various silica-to-PS mass ratios. Self-assembled precursors without PS allowed the formation of film without macroporous structures (**Figure 3.5a**). The additional PS colloidal spheres in the precursor initiated the creation of film with pores (**Figure 3.5b, c**), with the number of pores increasing with increasing PS amounts. Further excess in the PS amount resulted in the formation of film with fragmented skeletal structures (**Figure 3.5d**). The results suggest that the skeletal network is from the aggregation of silica nanoparticles and the pores are from the inverse-replication of PS.
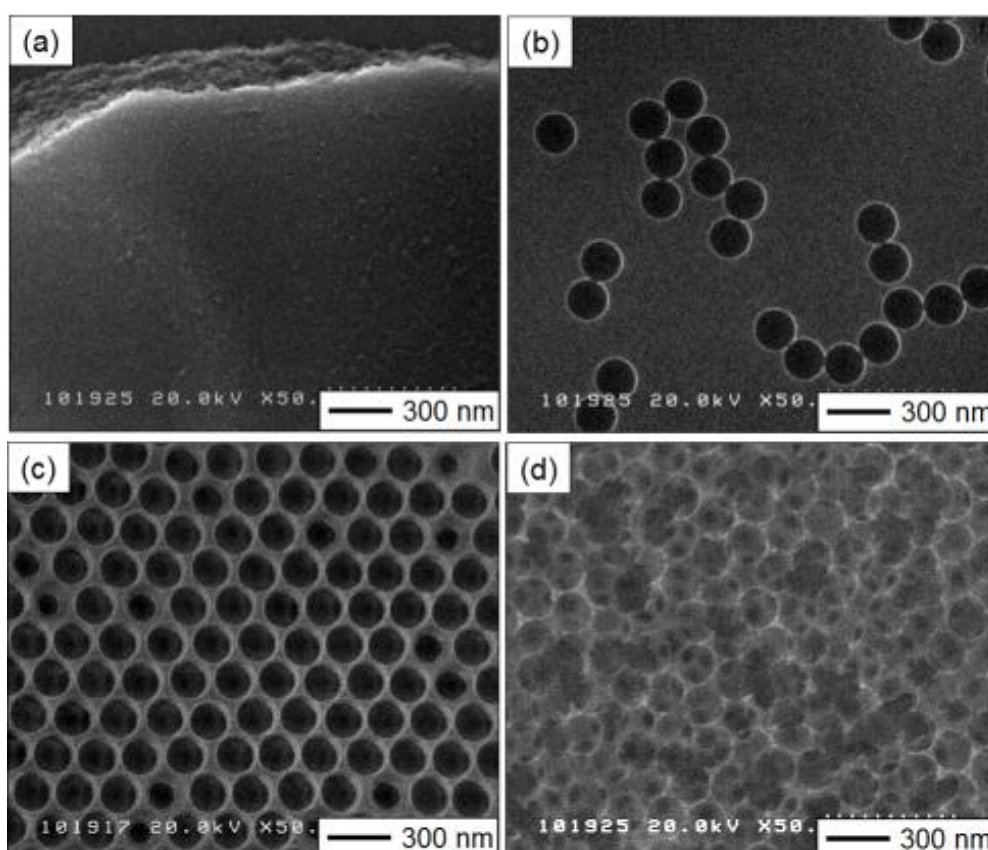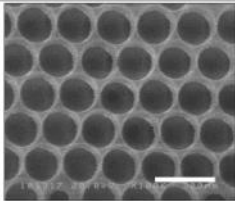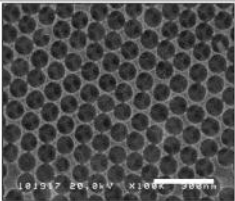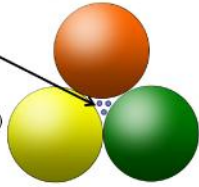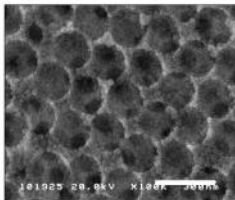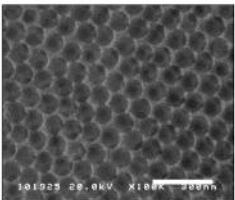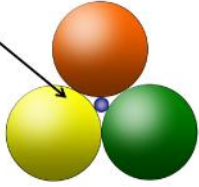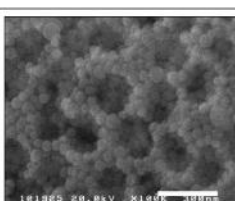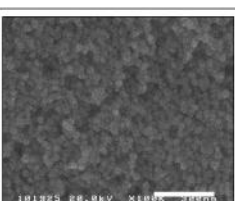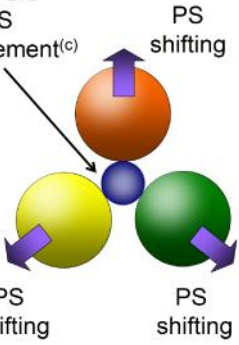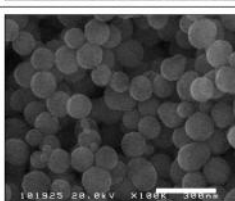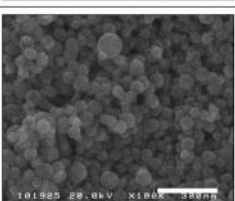
Figure 3.5. SEM images of the film prepared with various silica-to-PS mass ratios: (a) no PS, (b) 1.00, (c) 0.50, and (d) 0.10. Samples were prepared using 200 nm of PS and 5 nm of silica.

_____

Based on the Kepler conjecture,[18] the volume fractions of PS and silica are 74 and 19.24%, respectively, whereas the volume of un-occupied space is 6.74%. Adopting the standard densities of air (ρ_{air} = 0.0012 g/mL), colloidal silica nanoparticles (ρ_{silica} = 1.96 g/mL)[27], and PS spheres (ρ_{PS} = 1.05 g/mL), subsequent calculation resulted in the silica-to-PS mass ratio of 0.48. This result is in a good agreement with that obtained from **Figure 3.5**. The material with highly ordered pores is obtained if the ratio of silica/PS is near 0.48. Deviations from this mass ratio result in non-hexagonal pore structures.

3.3.4. The influence of colloidal size on porous structuralization

The SEM images of porous films prepared with various size ratios of silica (*d*) and PS (*D*) are listed in **Table 3.1**, along with an illustrative model of the colloidal particle arrangement. The SEM results showed that pores were detected in all samples. The size and shape of pores were identical to those of PS added in the initial precursor, conferring potential for the control of pore diameter by changing the size of initial PS spheres. According to the *d/D* ratio, different porous structures were identified. With *d/D* ratios below 0.08, films with highly ordered pores were obtained (group A). In the intermediate range *d/D* = 0.08–0.18, some fragmented silica skeletons in the porous structure were found (group B). Above *d/D* > 0.18, porous structures exhibited disordered arrangements (group C). These results verify that the colloidal size has a direct impact during self-assembly, as illustrated in this table.

Chapter 3: Effect of colloidal nanoparticles charge, size, and concentration on fabrication of self-organized porous silica particle

_____

Table 3.1.   SEM images and schematic topological models of porous film prepared by various size ratios of silica and PS (under silica-to-PS ratio of 0.50). Scale bars are 300 nm.

Note: [a]silica size << void area; [b]silica size ≈ void area; [c]silica size > void area

A schematic of a geometrical model based on the experimental analysis is shown in **Figure 3.6**. Experimental results show the composite contains a multilayer PS arrangement (**Figure 3.6a, b**). PS spheres facilitate mainly the material construction and pack with the multilayers, whereas silica nanoparticles only completely fill the voids between the arrangement of PS spheres. Because the arrangement of pores is a replication of those of PS in their composite form (**Figure 3.6c**), the geometrical model can be directly estimated from the composite silica/PS material.

Chapter 3: Effect of colloidal nanoparticles charge, size, and concentration on fabrication of self-organized porous silica particle

_____

Figure 3.6d>**f** shows illustration of the geometrical model used in this study. This model was used based on the well-known close packing of spheres.[21] We used combinations of silica and PS nanoparticles, in which the information about close packing of nanoparticles is typically non-existence. In this model, if nanoparticles are packed in their maximum arrangement, then the composite is constructed simply from a single tetrahedral unit (denoted by *T*) in the Euclidian space (see **Figure 3.6e**). Under ideal conditions, in which the silica nanoparticles assemble without changing/shifting the PS positions, each PS sphere is touching its nearest neighbors, as depicted in **Figure 3.6f**.

In regard to the void space between these four adjacent spheres of the *T* cell (**Figure 3.6e**), the maximum-diameter silica particle able to fit within the void space is determined from $d/D \approx \dfrac{1 - \cos(\theta/2)}{\cos(\theta/2)}$, where θ denotes the angle formed between any three adjoining spheres. For identical PS spheres, the size ratio is $d/D = 0.155$, which agrees with the previous results.[18] This value is a critical point, determining if silica is able to penetrate the void between PS spheres without disturbing their arrangement. In general, increases in this value enable non-hexagonal PS arrangements to form because the silica can shift the PS sphere from its position.
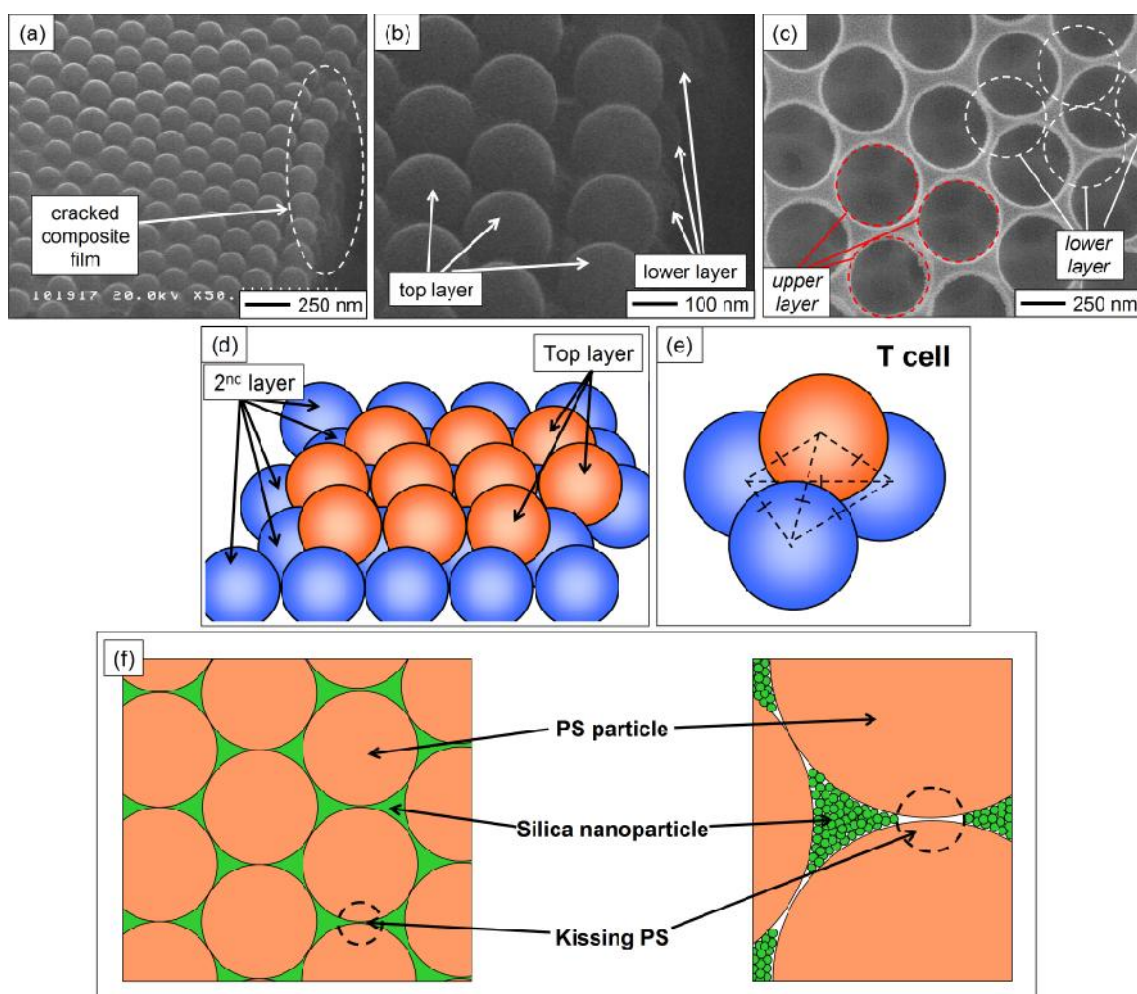
Figure 3.6. Topological analysis of self-assembly sphere packing: SEM images of experimental results before (a,b) and after template removal (c), a three-dimensional representation of a hexagonally packed composite PS/silica film (d), an illustration of a single unit of a tetrahedral structure (e), and a two-dimensional representation of packed composite PS/silica film (f). Figure (b) is the high-magnification SEM image of the sample imaged in Figure (a).

Besides being able to penetrate the void space, silica must be able to arrange tetrahedrally within the void space if highly ordered pores are to develop.[18] Adopting this condition, *d* is re-expressed as $d = 2d_c + c$, where d_c is the maximum diameter of silica (for a tetrahedral structure to form on the edge of the void) and *c* is the effective void diameter between the new tetrahedral silica. Thus, the size ratio can be estimated

Chapter 3: Effect of colloidal nanoparticles charge, size, and concentration on fabrication of self-organized porous silica particle

_____

as $\dfrac{d_c}{D} = \dfrac{1}{2}\left(\left[\dfrac{1-\cos\left(\frac{n}{2}\right)}{\cos\left(\frac{n}{2}\right)}\right] - \dfrac{c}{D}\right)$. As the value of c/D is small, the equation can be

simplified to $\dfrac{d_c}{D} \approx \dfrac{1-\cos\left(\frac{n}{2}\right)}{2\cos\left(\frac{n}{2}\right)}$, yielding a size ratio of $d_c/D = 0.078$. This value

determines the minimum requirement to produce material with highly ordered pores.

Correlations of the above results with outcomes from porous structuralization are illustrated in **Figure 3.7** based on this size ratio. Three zones are highlighted by shading: clear-, light-, and dark-patterned areas. The classification is in accord with the above two critical values (i.e., "solid line" (d/D = 0.078) and "dashed line" (d/D = 0.155)). Experimental results from films prepared with various silica-to-PS size ratios were also added. These showed that ratios below the "solid line" provide a useful criterion to obtain a successful formation of highly ordered pores ("open dot"). For ratios in the intermediate range (light-patterned area), formations of porous film with incomplete silica skeletal structures are found ("open triangle"). This result confirms that the light-patterned area represents a buffer zone in the preparation of porous materials. Silica particles can possibly invade the spaces between the PS spheres without changing the maximum PS arrangement. Ratios above the "dashed line" lead to the formation of disordered porous structures ("solid square"). Because silica needs to shift PS spheres from their positions, this region of the graph signifies that nascent ordered porous materials are impossible. This figure confirms that the above geometrical model is effective in qualitatively predicting the formation of highly ordered porous materials.
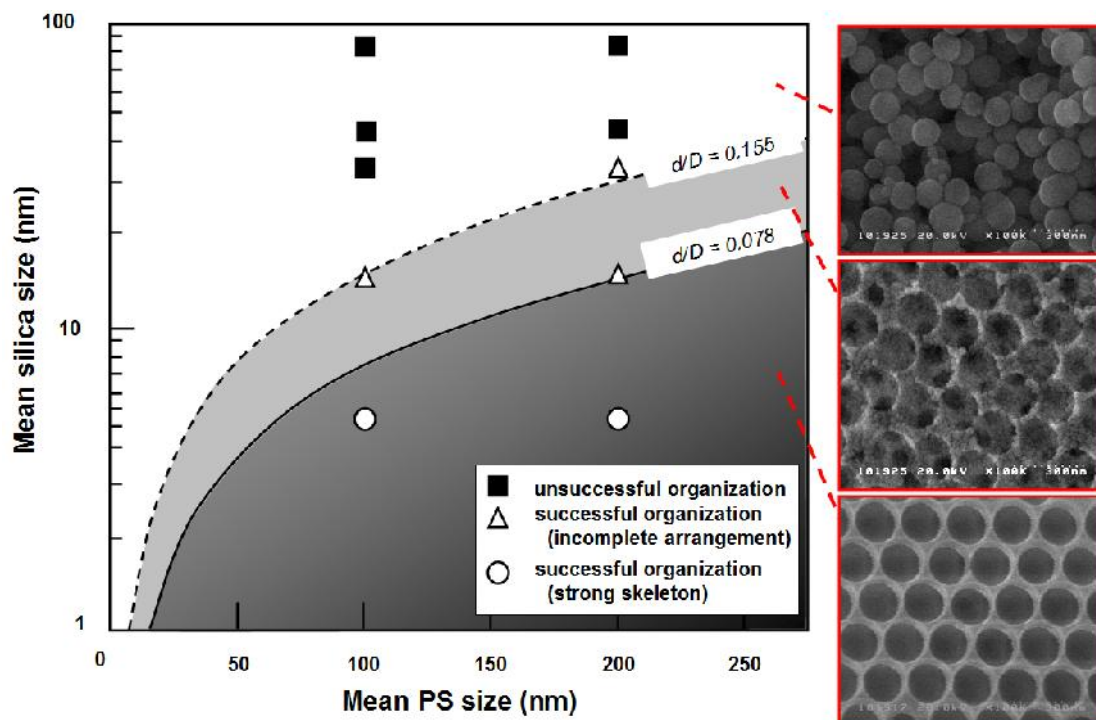
Figure 3.7.   Combinations of silica and PS sizes in successful and unsuccessful pore configurations

3.3.5. Discussion

A clarification of the above hypothesis for the preparation of porous particles examined by the SEM analysis is shown in **Figure 3.8**. The influences of self-assembly parameters (i.e. composition and size of colloidal nanoparticles) on the porous structuralization in the particle form were examined.

Spray-dried precursors with no additional PS resulted in the production of non-porous particles (**Figure 3.8a**), whereas those with PS allowed the formation of porous particles (**Figure 3.8b**). As an excess PS composition in the precursor led to the formation of a broken particle (**Figure 3.8c**), optimizing colloidal composition was then necessary to develop maximal pore arrangements in the particle. Thus, arrangements were obtained only if a silica-to-PS mass ratio of about 0.5 was used. This result is in a good agreement with the above experimental results.

Chapter 3: Effect of colloidal nanoparticles charge, size, and concentration on fabrication of self-organized porous silica particle

_____

Figure 3.8b, d>**f** are the SEM images of particles prepared with various PS surface charges under the same *d/D* value. The result showed that the use of negatively charged PS assisted the formation of porous particles (**Figure 3.8b, d, e**), whereas those of positively charged PS led to the creation of hollow particles (**Figure 3.8f**). We also checked the influence of different PS charge values. Although porous particles are producible, different configurations were found (shown in dashed red area). The use of high concentrations of KPS (high zeta values) resulted in porous materials with kissing holes (**Figure 3.8d**), whereas those obtained with lower KPS concentrations (low zeta values) exhibited fewer kissing holes (**Figure 3.8e**); a detailed explanation and mechanism will be given in a forthcoming report. These results are in a good correlation with the above charge hypothesis, summarized in **Figure 3.4**, verifying that the colloidal charge is effective in producing particles with different porous configurations.

The influence of colloidal size on porous structuralization is shown in **Figure 3.8g**>**i**. If silica-to-PS size ratios of less than 0.078 are used, particles with highly ordered pores were effectively produced (**Figure 3.8b**). The appearance of connecting holes between neighboring pores is observed, verifying that the PS particles kissed and packed in their maximal configurations. This unique porous structure has potential for enhancing particle density and surface area, making possible applications in catalysis, chromatography, filtration, and low density and low refractive index material sciences. Higher ratios (*d/D* of 0.155) resulted in the formation of porous particles (**Figure 3.8g**). However, some porous particles have lower coordination numbers of connecting holes (kissing PS). As discussed above on geometrical-model considerations, this ratio falls within the buffer area where silica exactly fits the void area. Displacements of PS by silica are not strong enough because the void area can still facilitate the filling with silica. Ratios above the threshold ratio (*d/D* > 0.155) permit the production of porous

particles with incomplete silica skeletons (**Figure 3.8h**). Thus, silica begins to dominate the self-assembly process. The space between the PS spheres is insufficient to accommodate more silica in forming strong silica structures. Higher ratios resulted in the formation of particles with non-hexagonal porous structures (**Figure 3.8i**). PS particles also fail in maintaining their structure caused by the disruption of silica nanoparticles. As a consequence, the PS structures inside the particle collapse and the resultant particles do not have highly ordered macropores.
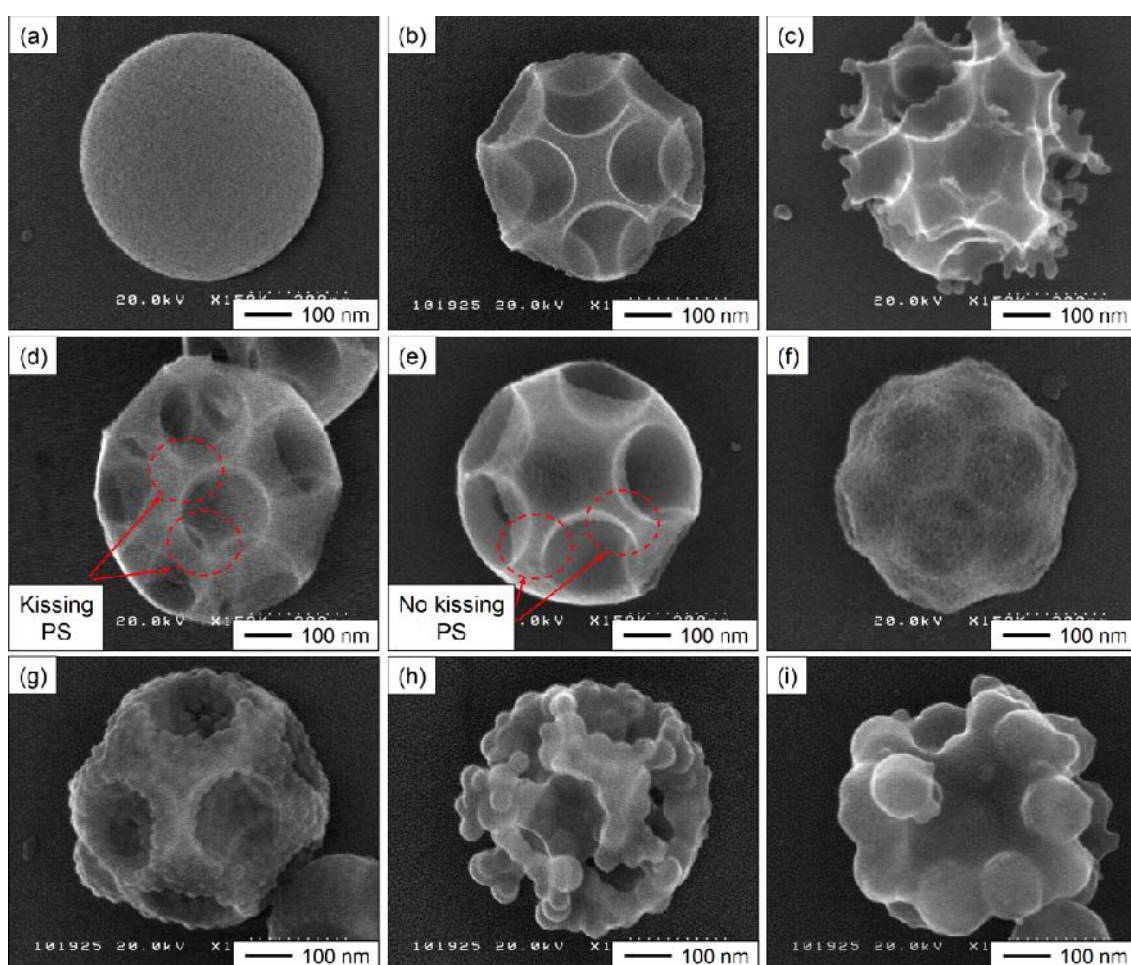
Figure 3.8.   SEM images of particles prepared from the precursor containing "silica only" (a) and "silica and PS particles" (b–i). Panels (b, d–i) are SEM images of particles prepared with a silica-to-PS mass ratio of 0.50, whereas panel (c) is that of particles with ratio 0.30. Panels (d–f) correspond to samples prepared with various initiator types / compositions (wt%) / charges (mV): (d) KPS/0.0800/(-31); (e) KPS/0.0080/(-27); and (f) AIBA/0.0400/(+30).

_____

Panels (b–f), (g), (h), and (i) are samples prepared with *d/D* values <0.025, 0.155, 0.225, and 0.450, respectively.

The above results confirm the above conceptual findings, where the self-assembly parameters have the potential to control outcomes, i.e., the porous structure and pore size in both film and particle. However, further studies are still required for direct applications in the self-assembled porous material fabrication from colloidal nanoparticles with different characteristics.

3.4. Conclusions

The influence of self-assembly parameters (i.e. size, surface charge, and concentration of colloidal nanoparticles) on the self-organized porous material fabrication has been systematically investigated. The experimental results indicate that these parameters are effective in controlling the porous structure and the pore size. Materials containing highly ordered pores were successfully created only if the process was conducted under appropriate self-assembly parameter conditions. In contrast, variations of these parameter conditions resulted in the formation of materials with either incomplete or brittle porous structures. A geometrical model based on the tight packing of spheres in the material structures was also developed to examine the successful formation of highly ordered pores in film and particle forms. Because the optimization of these self-assembly parameters provides significant information on practical uses, the results of this report could have further applicability to functional properties of porous materials.

3.5. References

[1] A. Taguchi, F. Schüth, Ordered mesoporous materials in catalysis, Microporous and Mesoporous Materials, 77 (2005) 1-45.

_____

[2] A.B.D. Nandiyanto, K. Okuyama, Progress in developing spray-drying methods for the production of controlled morphology particles: From the nanometer to submicrometer size ranges, Advanced Powder Technology, 22 (2011) 1 - 19.

[3] O.D. Velev, A.M. Lenhoff, Colloidal crystals as templates for porous materials, Current Opinion in Colloid & Interface Science, 5 (2000) 56-63.

[4] A. Stein, R.C. Schroden, Colloidal crystal templating of three-dimensionally ordered macroporous solids: Materials for photonics and beyond, Current Opinion in Solid State and Materials Science, 5 (2001) 553-564.

[5] Q. Wei, S.L. James, A metal–organic gel used as a template for a porous organic polymer, Chemical communications, (2005) 1555-1556.

[6] S. Kim, B. Liu, M. Zachariah, Synthesis of nanoporous metal oxide particles by a new inorganic matrix spray pyrolysis method, Chemistry of materials, 14 (2002) 2889-2899.

[7] C. Kresge, M. Leonowicz, W. Roth, J. Vartuli, J. Beck, Ordered mesoporous molecular sieves synthesized by a liquid-crystal template mechanism, nature, 359 (1992) 710-712.

[8] D. Zhao, J. Feng, Q. Huo, N. Melosh, G.H. Fredrickson, B.F. Chmelka, G.D. Stucky, Triblock copolymer syntheses of mesoporous silica with periodic 50 to 300 angstrom pores, science, 279 (1998) 548-552.

[9] A.B.D. Nandiyanto, S.G. Kim, F. Iskandar, K. Okuyama, Synthesis of spherical mesoporous silica nanoparticles with nanometer-size controllable pores and outer diameters, Microporous and Mesoporous Materials, 120 (2009) 447-453.

[10] Y. Hoshikawa, H. Yabe, A. Nomura, T. Yamaki, A. Shimojima, T. Okubo, Mesoporous silica nanoparticles with remarkable stability and dispersibility for antireflective coatings, Chemistry of materials, 22 (2009) 12-14.

[11] J.M. Kim, Y. Sakamoto, Y.K. Hwang, Y.-U. Kwon, O. Terasaki, S.-E. Park, G.D. Stucky, Structural design of mesoporous silica by micelle-packing control using blends of amphiphilic block copolymers, The Journal of Physical Chemistry B, 106 (2002) 2552-2558.

[12] X. Liu, Q. Hu, Z. Fang, Q. Wu, Q. Xie, Carboxyl enriched monodisperse porous fe3o4 nanoparticles with extraordinary sustained-release property, Langmuir, 25 (2009) 7244-7248.

[13] S.A. Johnson, P.J. Ollivier, T.E. Mallouk, Ordered mesoporous polymers of tunable pore size from colloidal silica templates, science, 283 (1999) 963-965.

[14] P. Jiang, J. Cizeron, J.F. Bertone, V.L. Colvin, Preparation of macroporous metal films from colloidal crystals, Journal of the American Chemical Society, 121 (1999) 7957-7958.

[15] O.D. Velev, E.W. Kaler, Structured porous materials via colloidal crystal templating: From inorganic oxides to metals, Advanced Materials, 12 (2000) 531-534.

[16] H. Yan, C.F. Blanford, B.T. Holland, W.H. Smyrl, A. Stein, General synthesis of periodic macroporous solids by templated salt precipitation and chemical conversion, Chemistry of materials, 12 (2000) 1134-1141.

[17] J. Lee, J. Kim, T. Hyeon, Recent progress in the synthesis of porous carbon materials, Advanced Materials, 18 (2006) 2073-2094.

[18] A.B.D. Nandiyanto, N. Hagura, F. Iskandar, K. Okuyama, Design of a highly ordered and uniform porous structure with multisized pores in film and particle forms using a template-driven self-assembly technique, Acta Materialia, 58 (2010) 282-289.

[19] C. Wang, Q. Wang, T. Wang, Simple method for preparation of porous polyimide film with an ordered surface based on in situ self-assembly of polyamic acid and silica microspheres, Langmuir, 26 (2010) 18357-18361.

[20] J. Cheng, Y. Zhang, P. Gopalakrishnakone, N. Chen, Use of the upside-down method to prepare porous polymer films with tunable surface pore sizes, Langmuir, 25 (2008) 51-54.

[21] C. Martin, D. Bouvard, Isostatic compaction of bimodal powder mixtures and composites, International journal of mechanical sciences, 46 (2004) 907-927.

[22] A. Stein, B.E. Wilson, S.G. Rudisill, Design and functionality of colloidal-crystal-templated materials—chemical applications of inverse opals, Chemical Society Reviews, (2013).

[23] L. Grado , S. Janeczko, M. Abdullah, F. Iskandar, K. Okuyama, Self-organization kinetics of mesoporous nanostructured particles, AIChE journal, 50 (2004) 2583-2593.

[24] A.B.D. Nandiyanto, A. Suhendi, T. Ogi, T. Iwaki, K. Okuyama, Synthesis of additive-free cationic polystyrene particles with controllable size for hollow template applications, Colloids and Surfaces A: Physicochemical and Engineering Aspects, 396 (2012) 96 - 105.

[25] A.B.D. Nandiyanto, Y. Akane, T. Ogi, K. Okuyama, Mesopore-free hollow silica particles with controllable diameter and shell thickness via additive-free synthesis, Langmuir, 28 (2012) 8616-8624.

[26] L. Günther, W. Peukert, Control of coating properties by tailored particle interactions: Relation between suspension rheology and film structure, Colloids and Surfaces A: Physicochemical and Engineering Aspects, 225 (2003) 49-61.

[27] Y. Xu, Q. Li, Multiple fluorescent labeling of silica nanoparticles with lanthanide chelates for highly sensitive time-resolved immunofluorometric assays, Clinical chemistry, 53 (2007) 1503-1510.

Chapter 4

Development of a high stability and controllability charged droplets generation system

4.1. Introduction

Electrohydrodynamic spraying (electrospray) is a well-known method to produce micron-sized charged droplets from the tip of an emitter by applying an electric field. This has attracted great attention due to its potential application in many areas including mass-spectrometry, nanoparticle synthesis, drug delivery, bio-materials, ink-jet printing and protein printing.[1-6]

Electrospray droplets are typically used as an ion source in mass spectroscopy analysis, while in the particle synthesis electrospray are used as a particle source. The electrospray generated droplets can be resulted from various operational modes, which some of them are spindle, pulsating, cone-jet and multi-jet modes. The operational modes in an electrospray system are critical to deliver a required amount of aerosol during electrospray, for which a cone-jet is the most favored of all operational modes during electrospraying. The cone-jet mode is reliable for delivering aerosol in a high precision volume in a femtoliter order.[7, 8] Prior studies on electrospray have shown that an electric voltage between electrodes was kept constant to obtain a cone-jet mode. In fact, I observed that the cone-jet meniscus was unstable for electrospray operations of a relatively long duration. Furthermore, after a period of time, the liquid cone-jet would spurt from the emitter to the electrode, which resulted in a corona discharge and a fluctuation in the volume of the liquid-droplets delivered during electrospray. Although this phenomenon has been observed by Cloupeau et. al.,[9] no control has been proposed

_____

to overcome this problem. Gapeev et. al. reported current control for a stable ion source application[10]. However, the stability of the cone shape was neglected and the controlled charges distribution was tend to shift toward higher charges. In fact, the instability of a cone-jet is thought to be influenced by the fluctuation of the electric current during electrospray.[11, 12] For this reason, study on the cone jet morphological control and stability in the current controlled electrospray is important.

In this thesis I present the control of cone-jet geometry during electrospray by an electric current and to demonstrate their applications for droplet and particle generation. I used polyethylene glycol as a model for particle generation using this method. Although it was hypothesized that a constant current maintains cone-jet stability, as far as could be ascertained, the present study is the first report of a real-time observation of cone-jet stability during electrospray. I also examined the correlation between cone-jet geometry and electric current applied to the electrospray system. The cone jet length could be controlled easily by applying the appropriate constant current. In order to keep the electric current at a certain value, a proportional-integral-derivat (PID) control was employed to the electrospray system. In addition, the system is suitable for continuous flow applications, which require long period of control and disturbance resistant. I believe that the present study will be very useful for the future application of electrospray, particularly for high precision aerosol generators and particle synthesis.

4.2. Experimental Setup and Method

Precursor solutions were prepared by dissolving a known amount of polyethylene glycol (PEG, Mw = 20000 g/mol, Wako Pure Chemical industries Ltd.) in an equivolume mixture of deionized water and ethanol. All precursors were stirred at

room temperature for several hours until clear and transparent solutions were obtained. A liquid precursor solution was then placed in a hypodermic syringe (Gastight, Hamilton, USA) with a 27 Gauge needle at a fixed distance of 5 cm from the cathode.

The needle was connected to a variable high-voltage-source (HVS, HSR-10P (A), Matsusada, Japan). The HVS was capable of delivering dc voltage of up to 10 kV and was controlled using an analog-to-digital-digital-to-analog system (ADDA, AIO-160802AY-USB, Contec, Japan). A syringe pump (Harvard Apparatus PHD 2000, USA) was used with online control via an RS-232 serial communication port for modifying the solution flow rate. The cone-jet dynamics during electrospray was monitored using a CCD Camera (Mintron, Taiwan) connected to a video-to-universal serial bus (USB) device (PCA-DAV2, Japan) for automatic image capture. The configuration of the present system is illustrated in **Figure 4.1**. The environmental temperature during the electrospraying process was kept at 30 °C with humidity below 10%. The electric current was determined by placing a resistor, R, in a series circuit between the cathode and ground to monitor the voltage drop across the resistor via real-time measurement using the ADDA. Finally, the digital data were sent to a computer. The morphology of the collected particles was observed using a scanning electron microscope (SEM, S-3100, Hitachi, Japan).

_____
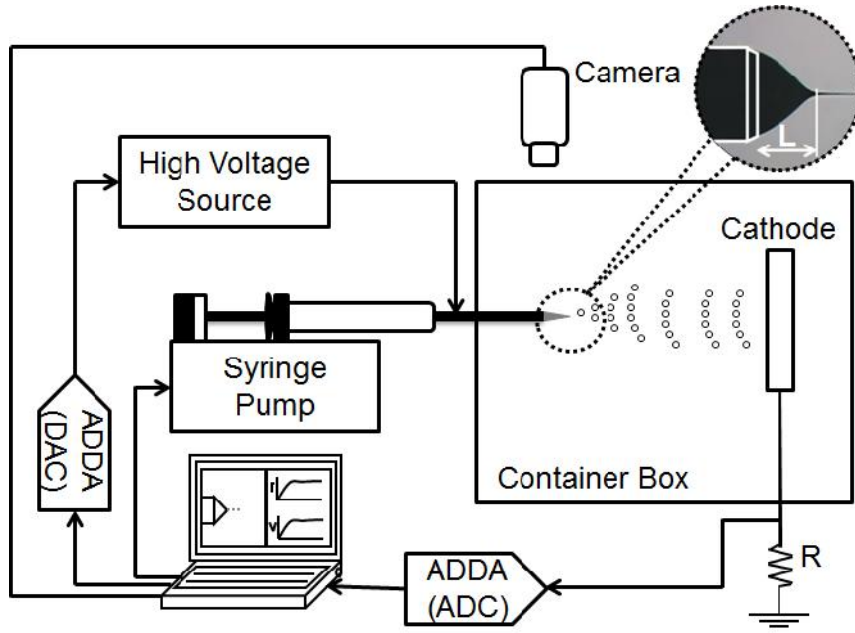
Figure 4.1.   Schematic diagram of the electrospray system.

4.3. Result and Discussion

The PID controller was used as a control system, and had a control signal, $u(t)$, that can be describes, as follows[13]:

$$u(t) = K_p \left[e(t) + \frac{1}{T_i} \int_0^t e(t)dt + T_d \frac{de(t)}{dt} \right],$$

(1)

where $e(t)$ is the difference between the set-point current (I_{SP}) and the real-time current ($I(t)$), defined as $e(t) \equiv I_{SP} - I(t)$. K_p, T_i, and T_d are the proportional constant, the integral and the derivative action times, respectively. For the best control action, tuning of these parameters is required. The Ziegler-Nichols (ZN) tuning method was used to find the best control parameters. The method was based on the idea of characterizing the process with fewer parameters and calculating the control parameters using a simple formula with the process characteristics. The ZN method

introduces the ultimate gain (K_u) and the ultimate period of oscillation (T_u) for determining the controller parameters previously reported. The present system has values of 12 and 0.2 for K_u and T_u, respectively. By using the K_u and T_u, and the previously reported [14] constants for the three conditions (i.e.: classic, some-overshoot, and no-overshoot).

The step responses of the PID controller for a set point current of 35 nA are shown in **Figure 4.2a**. Three types of responses were shown after the ZN tuning method was applied, and were labeled as classic-PID, some-overshoot-PID, and no-overshoot-PID. The settling times for those conditions, labeled as t_c (classic), t_s (some-overshoot), and t_n (no-overshoot) were 1, 0.3, and 0.8 s, respectively. These settling times were faster than those recorded in previous work.[13] A good control system provides a quick response for a change in output conditions, as shown by a short settling time. The control response for various set points for the some-overshoot PID type is shown in **Figure** 4.2b. The set point for electric current was varied from 62 to 78 nA, and the real-time electric current followed accordingly with no significant disturbance. In the longer period of electrospray process, the fluctuation of the current was different from a few second after step transition (**Figure** 4.2). The fluctuation was caused mainly by evaporation of droplets before reaching the cathode and some loss droplets. Moreover, the rate of change in current due to instability of the volume delivered from the syringe pump and evaporation rate may also cause the increase in the current fluctuations. For these reasons, the some-overshoot condition was chosen for further utilization because its short settling time and minimum overshoot.

_____
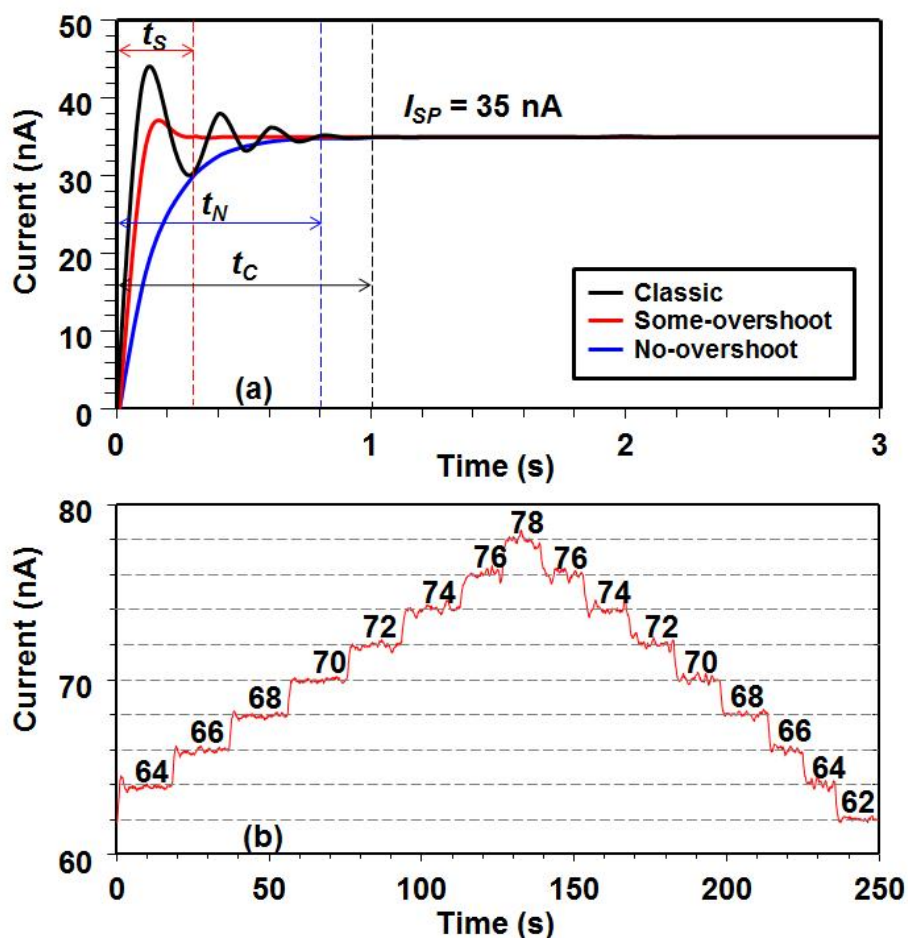
Figure 4.2. PID Controller examination: (a) Finding optimum parameters using the Ziegler Nichols methods for step response of 35 nA set point and (b) Control responses for various current set points ranging from 62 to 78 nA using some-overshoot condition.

Measurements for the electric current during electrospray using both the conventional and the present system are shown in **Figure** 4.3. The measurements were done for 4,000 s with a set point of 96 nA. The present system clearly was more robust than the conventional system in maintaining the electric current at a certain value. In addition, the cone-jet geometry of the controlled-system was very stable during measurement with no change in the shape. This observation was contrary to the conventional system that showed an unstable cone-jet geometry during relatively long-term experimentation. The dynamics of a cone-jet shape could be ascribed to the molecules that escape on the surface into the gas phase, disturbing the electrostatic

_____

force per unit area and causing the electric current to fluctuate. The fluctuations of these measurements ranged from 0.55 to 2.93 nA for the present and the conventional systems, respectively. Fluctuation in the controlled system was due to noise during measurement.
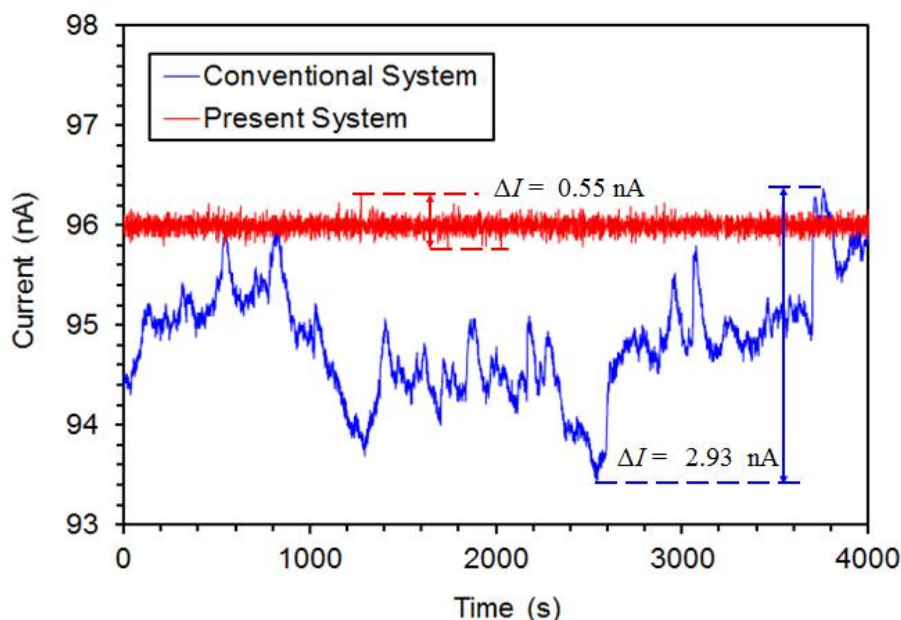
Figure 4.3.   Electric current measurement using the conventional and present system.

 Figure 4.4 illustrates the successful application of the present system to control the cone-jet geometry during electrospray using a precursor containing 15 wt% of polymer, and delivered at a constant flow rate of 12 µL/min. The cone jet length, which defined as a distance from the needle end as a cone base to the cone apex was measured for different current value .The cone-jet length was reduced with the increment of electric current, which agrees with the Rutledge model predicting that the cone length decreases with an increase in electric current.[15] A robust and stable cone-jet is important for the generation of femtoliter droplets with a constant volume. Based on the phenomena observed in this study, I hypothesize that the present system will deliver a fluid at a constant volume. Further investigation on the droplet volume delivered during electrospray using the present system will be reported in the near future.
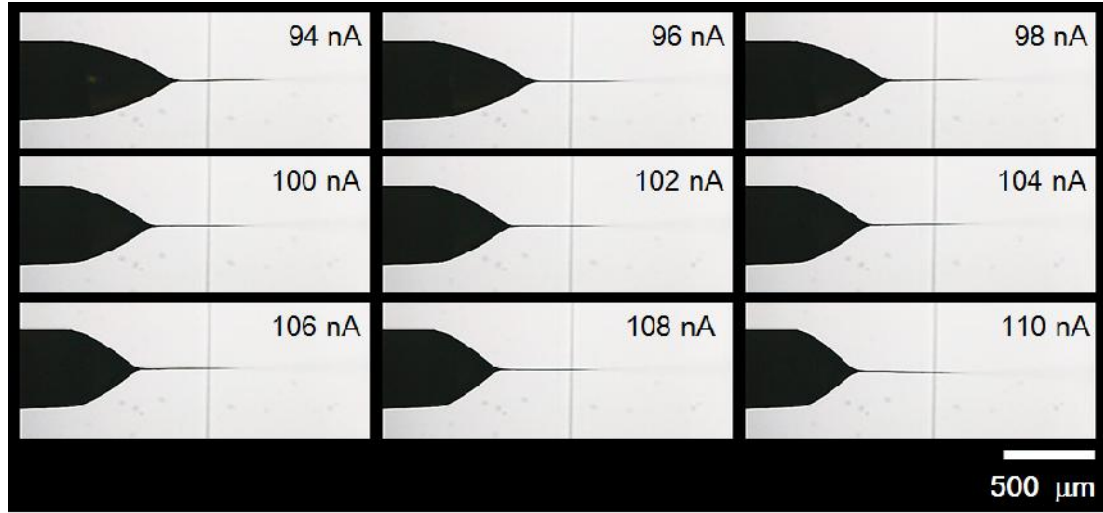
Figure 4.4. Images of cone-jet shapes during a constant-current electrospraying process for various current values.

To further investigate the correlation between cone jet length and electric current, experiments were conducted at various solution flow rates that ranged from 4-20 μL/min. Rutledge and co-workers derived the correlation between terminal jet radius and inverse volume charge density as follows:[15]

$$\log h_t = C_1 \log\left(\frac{Q}{I}\right) + C_2 \tag{2}$$

where h_t is the terminal jet radius (m), Q is the solution flow rate (m³/s), I is the electric current (A), C_1 is the constant that theoretically has a value of 0.667, and C_2 is the constant that can be determined from the solution properties. I assume that terminal jet radius has a linear relationship with cone-jet length i.e.

$$L = \alpha\, h_t \tag{3}$$

where α is the linearization constant. Thus the correlation between cone-jet length and inverse volume charge density can be defined as:

$$\log L = C_1 \log\left(\frac{Q}{I}\right) + C_3 \tag{4}$$

where C_3 is a constant containing C_2 and α.

_____
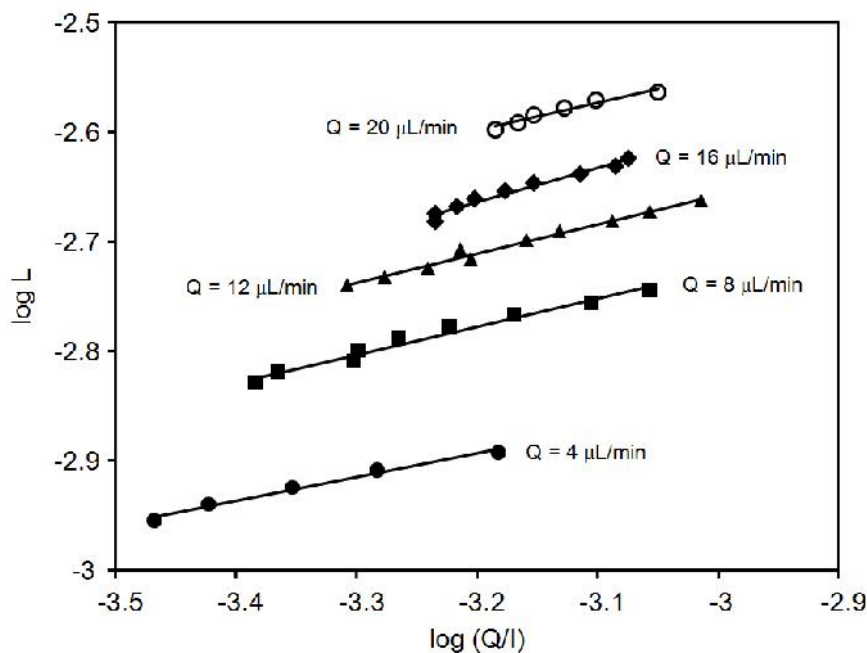
Figure 4.5.   Log-log plot of L and (Q/I) for various flow rates.

The log-log plots of L and (Q/I) for various flow rates are shown in **Figure 4.5**. The values of C_1 and C_3 for all flow rates are tabulated in **Table** 2. The values of C_1 ranged from 0.215 to 0.313, and differed with predicted values, which may have been due to the high evaporation rate of the solvent used in the experiment. Similar results were obtained for electrospinning experiments with a power scaling that ranged from 0.7 to 0.9[15]. The log-log plots had good linear correlations, which was indicated by a correlation coefficient of R^2 ~1. Good correlation coefficient R^2 shows that the assumption of linear coefficient α was acceptable. It can be concluded that the cone-jet length and the inverse volume charge density follow a power law: $L \sim (Q/I)^{C_1}$.

Based on the above result, the length of the cone jet was a function of the inverse volume charge density. Then, the inverse volume charge density had also a correlation with the droplet size.[16] Because the droplet size is important in the aerosol process,[17] I believe that the present study will be useful for further development (i.e. the particle and aerosol generator).

_____

Figure 4.6a and b show the SEM images of particles produced by electrospray with and without current control respectively. The particles were nearly spherical, agglomeration free, and had a monodisperse size distribution. The insets show the size distributions of the particles. The size distributions show that the particles generated using current controlled electrospray system was found to have a smaller standard deviation value of 40 nm than the conventional system which has a value of 80 nm. The additional information about the verification for the successful synthesis of various polymer is important. However, in this chapter I focused on the control of the cone jet geometry by the electric current for droplet generation.
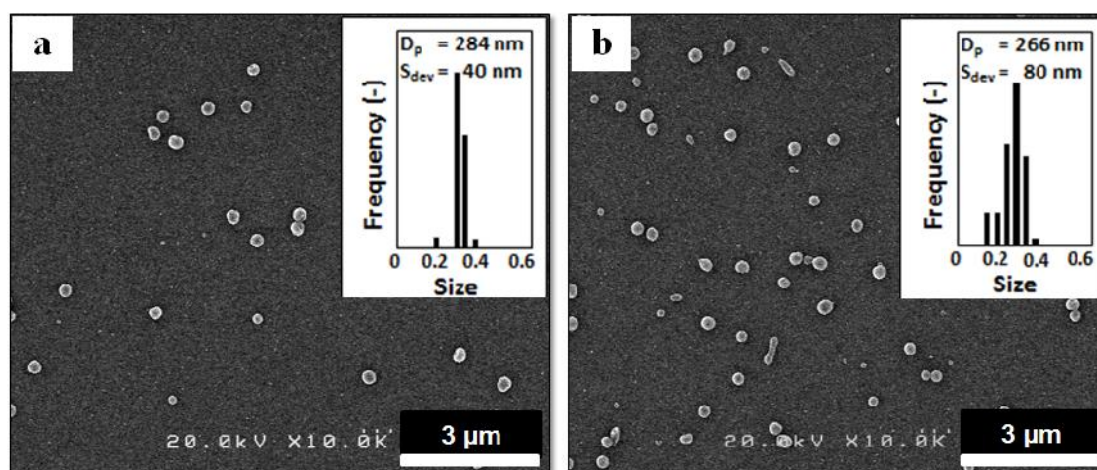
Figure 4.6.   SEM images of particles generated using electrospray (a) with and (b) without current control.

In the case of electrospray as an aerosol generator, ring type grounded electrode is commonly used. For this system, different measurement configuration could be employed i.e.: measurements of the current flow through the ring and total current flow through the anode. The droplets/particles pass through the ring is proportional to the current of the total current subtracted by the current flow through the ring.

4.4. Conclusions

In conclusion, I have developed a current-controlled electrospray system to control the cone-jet geometry. The present system is robust and maintains electric current at a certain value. The cone-jet geometry is strongly influenced by electric current. The correlation between cone-jet geometry and electric-current was studied and was found to follow a power law. The ability of the present system to control cone jet geometry over extended periods of time creates a great opportunity for the development of a high-precision droplets and particle generator.

4.5. References

[1] J.B. Fenn, M. Mann, C.K. Meng, S.F. Wong, C.M. Whitehouse, Electrospray ionization for mass spectrometry of large biomolecules, Science, 246 (1989) 64 - 71.

[2] K. Okuyama, I. Wuled Lenggoro, Preparation of nanoparticles via spray route, Chemical Engineering Science, 58 (2003) 537 - 547.

[3] A. Suhendi, A.B.D. Nandiyanto, T. Ogi, K. Okuyama, Agglomeration-free core-shell polystyrene/silica particles preparation using an electrospray method and additive-free cationic polystyrene core, Materials Letters, 91 (2013) 161-164.

[4] D.R. Chen, C.H. Wendt, D.Y.H. Pui, A novel approach for introducing bio-materials into cells, Journal of Nanoparticle Research, 2 (2000) 133 - 139.

[5] K. Wang, M.D. Paine, J.P.W. Stark, Fully voltage-controlled electrohydrodynamic jet printing of conductive silver tracks with a sub-100 µm linewidth, Journal of Applied Physics, 106 (2009) 0249071 - 0249074.

[6] J. Barron, H. Young, D. Dlott, M. Darfler, D. Krizman, B. Ringeisen, Printing of protein microarrays via a capillary-free fluid jetting mechanism, Proteomics, 5 (2005) 4138 - 4144.

[7] D. Wang, S. Jayasinghe, M. Edirisinghe, High resolution print-patterning of a nano-suspension, Journal of Nanoparticle Research, 7 (2005) 301 - 306.

[8] O. Yogi, T. Kawakami, M. Yamauchi, J.Y. Ye, M. Ishikawa, On-demand droplet spotter for preparing pico-to femtoliter droplets on surfaces, Analytical Chemistry, 73 (2001) 1896 - 1902.

[9] G. Joffre, M. Cloupeau, Stabilizing effect of emitted charges on the cone-like shapes of electrified menisci, Journal de Physique, 47 (1986) C7354 - C7359.

[10] A. Gapeev, A. Berton, D. Fabris, Current-controlled nanospray ionization mass spectrometry, Journal of the American Society for Mass Spectrometry, 20 (2009) 1334 - 1341.

[11] V. Gundabala, N. Vilanova, A. Fernández-Nieves, Current-voltage characteristic of electrospray processes in microfluidics, Physical Review Letters, 105 (2010) 1545031 - 1545034.

[12] R. Samatham, K.J. Kim, Electric current as a control variable in the electrospinning process, Polymer Engineering and Science, 46 (2006) 954 - 959.

[13] M.M. Munir, F. Iskandar, K. Okuyama, A constant-current electrospinning system for production of high quality nanofibers, Review of Scientific Instruments, 79 (2008) 0939041 - 0939044.

[14] A.S. Mccormack, K.R. Godfrey, Rule-based autotuning based on frequency domain identification, IEEE Transactions on Control Systems Technology, 6 (1998) 19.

[15] S.V. Fridrikh, J.H. Yu, M.P. Brenner, G.C. Rutledge, Controlling the fiber diameter during electrospinning, Physical Review Letters, 90 (2003) 1445021 - 1445024.

[16] A. Gomez, K. Tang, Charge and fission of droplets in electrostatic sprays, Physics of Fluids, 6 (1994) 404 - 414.

[17] A.B.D. Nandiyanto, K. Okuyama, Progress in developing spray-drying methods for the production of controlled morphology particles: From the nanometer to submicrometer size ranges, Advanced Powder Technology, 22 (2011) 1 - 19.

Chapter 5

Effect of droplet size and colloidal nanoparticle composition on the formation of core-shell silica/PS particles

5.1. Introduction

The synthesis of silica coated particles has been attracted great attention[1] due to its wide application in thermal insulation, paint, composite material, and drug delivery. Silica is thermally stable, inexpensive, harmless, and chemically inert.[2]

There are many methods to prepare silica coating[1-3]. However, they have to use additive (i.e. polymer, salt, surfactant, etc.) to enhance the encapsulation efficiency[2], which in turn create contamination and agglomeration problems[4]. To overcome these problems, many researchers suggest the combination of the additive-free process and the charge-based interaction phenomenon. Schmid et. al. reported additive-free process with the use of silica nano particles[5]. Unfortunately, there still some agglomerates in the final product. Another process was reported by Hotta et. al[6]. However, they employed acid condition (pH<4) to control the component charge, which caused difficulty in handling process. Moreover, above methods used a liquid-phase synthesis method, which required multi-step preparation and time-consuming process. Therefeore, a simple yet effective methods in term of preparation time and handling is necessary.

Based on previous chapter (**chapter 4**) on generating charged droplets, the purpose of this chapter was to introduce a new method for preparing core-shell particles with agglomeration free, and controllable core size and morphology. Cationic PS particles were used as a core model and silica nanoparticles were

employed as a shell model. Different from other methods, electrospray was used to facilitate the development of core-shell structure. The electrospray was chosen due to its capability to produce small droplets[7]. The electrospray can produce "one core particle per one drop"[8], which leads the perfect coating on the core material and avoid the agglomeration phenomena. I also added the control of the particle diameter and morphology in this report. The control of the particle size was obtained by only changing the initial PS core size. The morphological control could be realized by varying the mass ratio of silica/PS. Furthermore, the study on the successful and unsuccesful conditions (imperfect coating, silica aggregates formation, etc.) was also described, which would be important for further developments.

5.2. Experimental method

To produce core-shell particles, PS suspension (prepared using the method in the **chapter 2**, +39 mV) and silica nanoparticles (Fuso chemical Co. ltd, 6 nm, -30 mV) were diluted in equivolume water/ethanol suspension and electrosprayed into collection electrode. The suspension was varied in silica/PS mass ratios of 0.13, 0.20, 0.29, 0.40, and 1.00.

The configuration of the electrospray system is shown in **Figure 5.1**. It consists of a syringe with 27 Gauge needle, a syringe pump, a variable dc high-voltage source, and a box chamber made of visible fiberglass with a dimension of 45x30x30 cm^3. The syringe capillary passes through a hole on the box and contacts the anode. The positive terminal of the high-voltage source (Matsusada HER 10R3), which is capable of delivering a dc voltage of up to 10 kV, is connected to the anode while its negative terminal and the collecting electrode is fixed to the ground. The distance between the needle and the collecting electrode is 6 cm. The temperature and relative humidity

inside the chamber was maintained at 40 °C and less than 30%, respectively. The solution was electrosprayed on to a collecting electrode inside the chamber. The electrospray voltage was kept around 3 kV to maintain the cone jet. To monitor the shape of the cone jet, a video camera was used.
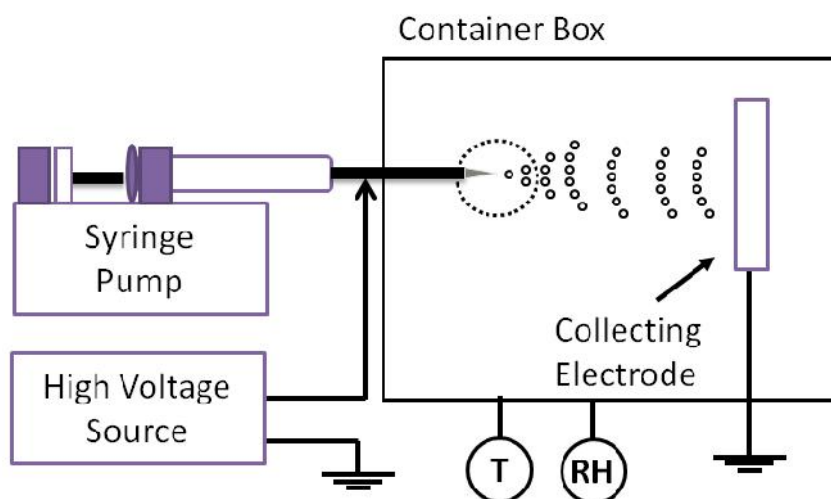
Figure 5.1. Experimental setup

The prepared particles were characterized using a scanning (SEM, Hitachi S-5000, 20 kV, Japan) and a transmittance electron micrograph (TEM; JEM-3000F, 300 kV, Japan) for examination of particle size, morphology and structure.

5.3. Results and Discussion

Figure 5.2 shows SEM and TEM images of particles before and after the electrospray process. The as-synthesized PS particles were spherical and well-dispersed (**Figure 5.2a**). After electrospraying, the surface of the particles becomes rough (**Figure 5.2b**). To confirm the structure inside the particles, the TEM images are shown in **Figure 5.2c** and **d**. **Figure 5.2c** reveals dense and spherical PS particles. The outer diameter of the prepared particles were identical to those of particles in **Figure 5.2a**. **Figure 5.2d** shows that PS particles were coated by silica nanoparticles. High magnification image show a spherical and rough particle with hairy style.
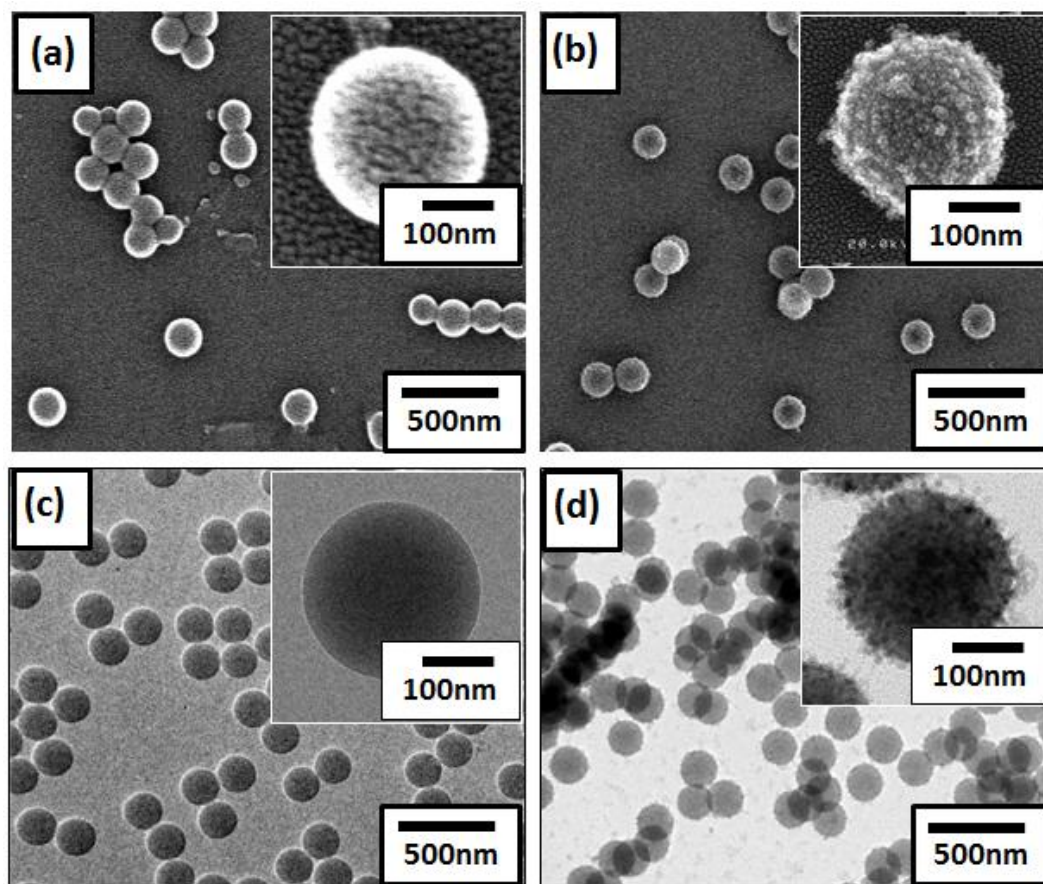
Figure 5.2   SEM (a,b) and TEM (c,d) images of particles before (a,c) and after (b,d) the electrospray process.

Figure 5.3 shows SEM analysis images of PS-coated silica particles under different process conditions. **Figures 5.3a-e** show the effect of silica/PS mass ratio (Cs), while **Figure 5.3f** reveals the effect of initial PS size on core-shell morphology. When Cs=0.13, few numbers of silica were attached on the PS surface (**Figure 5.3a**). High magnification of SEM image shows that some parts of the PS surface were smooth. When Cs=0.20, particles with rough surface were found (**Figure 5.3b**). Increasing more ratio (Cs=0.29) caused the formation of particles with rougher surface (**Figure 5.3c**). For Cs=0.40, small and irregular particles appeared (**Figure 5.3d**). Further excess ratio (Cs=1.00) resulted in the formation of more number of irregular particles with various sizes and forms (**Figure 5.3e**). To confirm that the PS was coated by silica nanoparticles, PS with size of about 90 nm was used (**Figure 5.3f**). Rough particles with the size of

about 90 nm were detected, confirming that the outer diameter was from the initial PS size.
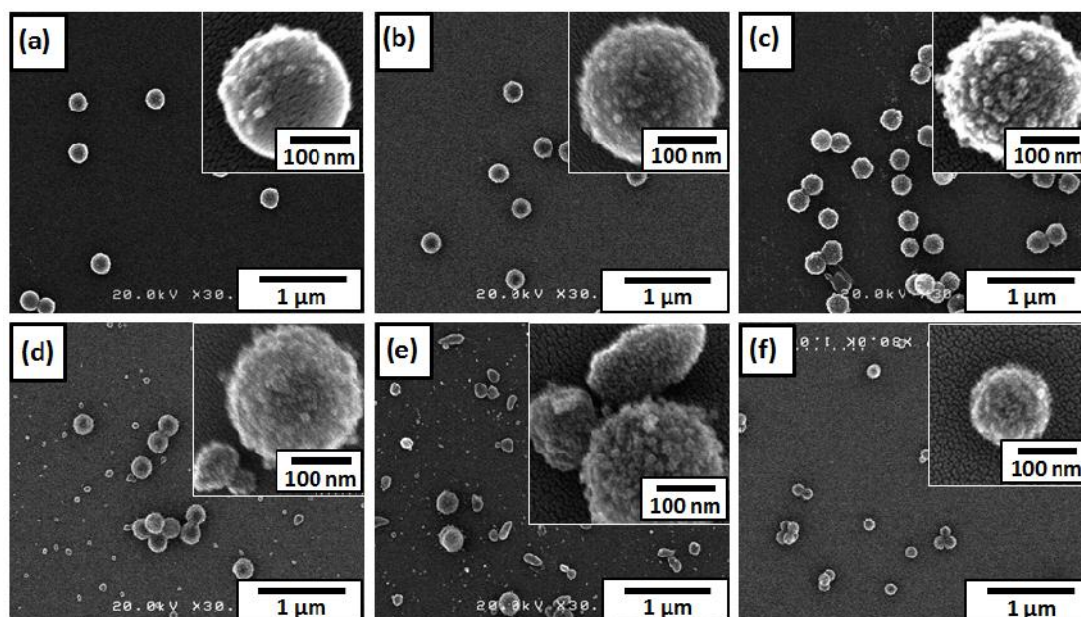
Figure 5.3.   SEM images of the effect of silica-to-PS ratio on the core-shell morphology: (a) 0.13, (b) 0.20, (c) 0.29, (d) 0.40, and (e) 1.00. Samples (a-e) prepared using PS with a mean size of 220 nm. Sample (f) prepared using silica/PS ratio of 0.57 and PS with a mean size of 90 nm.

The structure inside the particles is shown in **Figure 5.4**. When Cs=0.13, only small number of silica nanoparticles attached to the PS surface (**Figure 5.4a**). On higher ratio, the PS was completely coated by the silica nanoparticles (**Figure 5.4b**). However, high-magnification image shows that the hairy structure was found. For Cs=0.40 (**Figure 5.4c**), the formation of various particles size was found. Two types of particles were detected: one was core-shell particle and the other was silica aggregates. **Figure 5.4d** shows PS-coated silica with a core diameter of 90 nm. High magnification image shows the PS particles were coated completely by silica particles. The above results confirmed that the control of the morphology and particle diameter could be achieved by adjusting the silica/PS ratio and varying the size of the cationic PS, respectively.
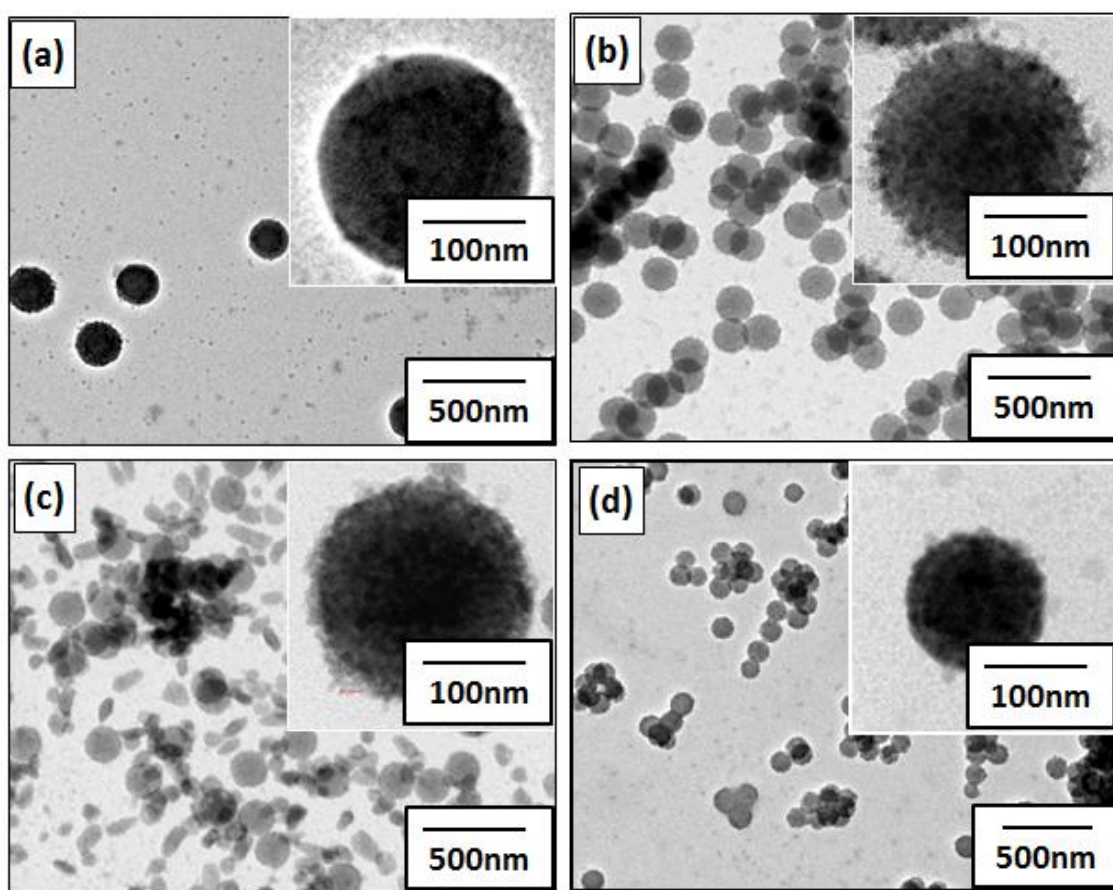
Figure 5.4.   TEM images of the effect of silica-to-PS ratio on the core-shell morphology: (a) 0.13, (b) 0.29, and (c) 1.00. Samples (a-e) prepared using PS with a mean size of 220 nm. Sample (d) prepared using silica/PS ratio of 0.57 and PS with a mean size of 90 nm.

The successful PS coating was due to the opposite charge between PS and silica particles. This polarity difference creates an attractive force between PS and silica, which made the silica nanoparticles to be attracted on the PS surface. This hypothesis was confirmed by the chemical and the elemental analysis using TG-DTA and FTIR as shown in **Figures 5.5** and **5.6**, respectively.
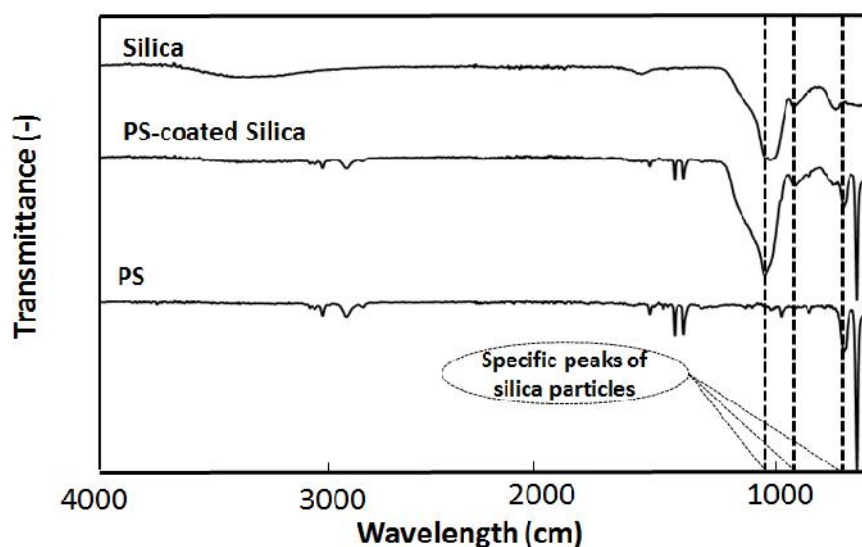
Figure 5.5.   FTIR analysis of PS, PS-coated silica, and silica particles.

However, beside the PS-silica attraction phenomenon, the silica/PS mass ratio should be also considered. This ratio affects the successful coating process. When the ratio is too low, silica number was inadequate to cover the PS surface completely. However, when the ratio is too high, the silica aggregates were formed. The formation of this aggregate is due to the probability for some droplets to contain silica colloid only (no PS inside the droplet), resulting the formation of some aggregated silica in the final product (as shown in **Figure 5.3d**).
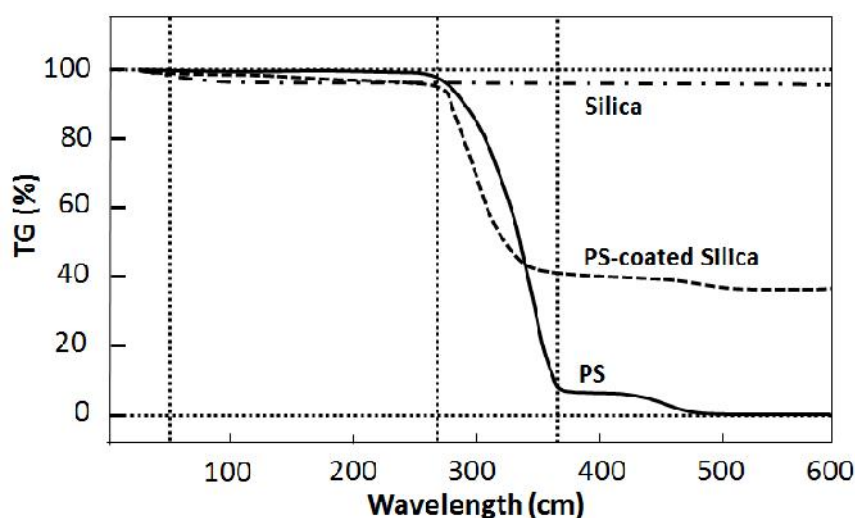
Figure 5.6.   Thermal analysis of PS, PS-coated silica, and silica particles.

Chapter 5: Effect of droplet size and colloidal nanoparticle composition on the formation of core-shell silica/PS particles

_____

I summarized the particles formation, based on silica/PS mass ratio, in **Figure 5.7**. When the ratio of less than 0.15 was used, almost no coating was obtained. For ratio between 0.15 and 0.25, all PS were fully coated by silica. When the ratio was increased to Cs=0.25 - 0.35, the PS was fully coated with hairy structure. Adding more silica (Cs=0.35 - 0.50) results the appearance of small silica aggregates in addition to the formation core-shell particles. Further additional silica (Cs>0.50) leads the formation of larger and irregular aggregates.
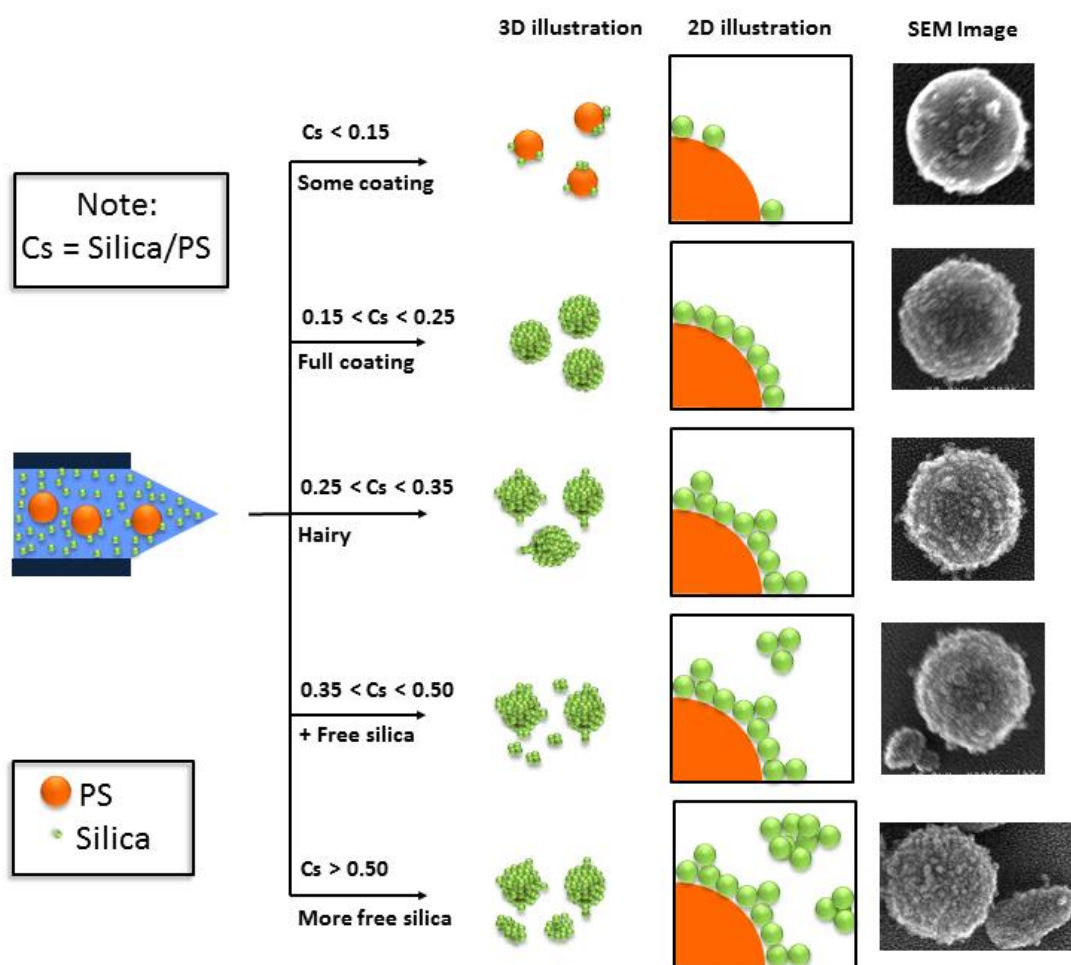
Figure 5.7.   Summary of the preparation of core-shell particles with different morphologies.

Chapter 5: Effect of droplet size and colloidal nanoparticle composition on the formation of core-shell silica/PS particles

_____

5.4. Conclusions

I have successfully developed a new method for the preparation of agglomeration-free core-shell PS/silica particles with controllable size and morphology using the electrospray method and under the additive-free process. Control of size and morphology could be achieved by changing the initial PS core and varying the silica/PS ratio, respectively. I believe that further insights gained from research such as the present study should make other fabrication innovations possible.

5.5. References

[1] Y.B. Zhang, X.F. Qian, H.A. Xi, J. Yin, Z.K. Zhu, Preparation of polystyrene core–mesoporous silica nanoparticles shell composite, Materials Letters, 58 (2004) 222-225.

[2] A.B.D. Nandiyanto, Y. Akane, T. Ogi, K. Okuyama, Mesopore-free hollow silica particles with controllable diameter and shell thickness via an additive-free synthesis, Langmuir, 28 (2012) 8616-8624.

[3] H. Sertchook, D. Avnir, Submicron silica/polystyrene composite particles prepared by a one-step sol-gel process, Chemistry of Materials, 15 (2003) 1690-1694.

[4] Y. Zhang, H. Chen, Q. Zou, Anionic surfactant for silica-coated polystyrene composite microspheres prepared with miniemulsion polymerization, Colloid & Polymer Science, 287 (2009) 1221-1227.

[5] A. Schmid, S. Fujii, S.P. Armes, C.a.P. Leite, F. Galembeck, H. Minami, N. Saito, M. Okubo, Polystyrene-silica colloidal nanocomposite particles prepared by alcoholic dispersion polymerization, Chemistry of Materials, 19 (2007) 2435-2445.

[6] Y. Hotta, P.C.A. Alberius, L. Bergström, Coated polystyrene particles as templates for ordered macroporous silica structures with controlled wall thickness, J. Mater. Chem., 13 (2003) 496-501.

[7] A.B.D. Nandiyanto, K. Okuyama, Progress in developing spray-drying methods for the production of controlled morphology particles: From the nanometer to submicrometer size ranges, Advanced Powder Technology, 22 (2011) 1 - 19.

[8] I.W. Lenggoro, B. Xia, K. Okuyama, J.F. De La Mora, Sizing of colloidal nanoparticles by electrospray and differential mobility analyzer methods, Langmuir, 18 (2002) 4584-4591.

[9] A.B.D. Nandiyanto, A. Suhendi, T. Ogi, T. Iwaki, K. Okuyama, Synthesis of additive-free cationic polystyrene particles with controllable size for hollow template applications, Colloids and Surfaces A: Physicochemical and Engineering Aspects, 396 (2012) 96 - 105.

Chapter 6

Effect of droplet size and concentration on the formation of spherical hollow particle

6.1. Introduction

Hollow particles have received considerable attention due to their wide range applications: catalysts, fuel cell electrodes, thermal insulation materials, sensors, and drug delivery.[1, 2] Several methods have been proposed to prepare hollow particles.[1-7] However, current methods have noted several disadvantages: (1) their limitation in the production of irregular form and non-uniform particle size; (2) their dependence in the use of additive (i.e. surfactant, polymer, salt, etc.) for achieving the hollow structurization; (3) mostly using a liquid-phase synthesis method, which requires multi-step, complicated, and time-consuming procedures; and (4) disregardance of the agglomeration of final products.

In the previous chapter (chapter 5), I succeeded in preparing silica/polystyrene core-shell particles with controllable morphology using an electrospray method. The successfulness of core coating was due to composition and charge interaction between core and shell materials. As a continuation of those work, here in this chapter, I reported the preparation of agglomeration-free hollow particles with spherical shape and controllable size (from 90 to 200 nm). Commercial silica nanoparticles and cationic PS spheres were used as a model of shell and core materials, respectively. Spherical, monodispersed, and positively charged PS spheres can be effective to attract silica onto PS surface.[8] Thus, their inverse replication of PS can promote the production of hollow particles with identical hole size, shape,

_____

and structure. To gain the facile preparation of agglomeration-free particles, an electrospray method followed by template removal process was used. Experimental results showed that control of particle size and agglomeration condition was achieved only by varying PS core diameter, electrospray flow rate, and precursor concentration.

6.2. Experimental method

Hollow silica particles were prepared from a precursor containing of PS suspension (prepared using the method in **chapter 2**, 200 nm, $\zeta = +32$ mV) and silica nanoparticles (Nissan chemical Co. Ltd., 5 nm, $\zeta = -30$ mV) in equivolume water/ethanol solution. Silica-to-PS mass ratio was fixed at 0.20, which was the optimum value to gain complete PS coating with a good structure. The mixed solution was electrosprayed onto a collection electrode, in which detailed experimental apparatus is described in the previous chapter. The collected particles were put into template removal process (heating at 500 °C).

The prepared particles were characterized using a scanning (SEM, Hitachi S-5000, 20 kV, Japan) and a transmission electron microscopes (TEM; JEM-2010, 300 kV, Japan) to examine particle size, morphology and structure. The elemental and the physicochemical composition of the prepared particles were evaluated using a Fourier transform infrared (FTIR) spectrometer (Spectrum One System, Perkin-Elmer, USA).

6.3. Result and discussion

6.3.1. Preparation of particles with different morphologies

Figure 6.1 shows SEM and TEM images of PS, PS/silica composite, and hollow silica particles. As-synthesized PS particles were spherical and well-dispersed

(**Figure 6.1(a,1)**). **Figure 6.1(b,1)** and **(c,1)** show electrosprayed particles before and after the template removal process. Size and shape of the electrosprayed particles were identical to those of the initial PS particles. The surface of the electrosprayed particles were rough.
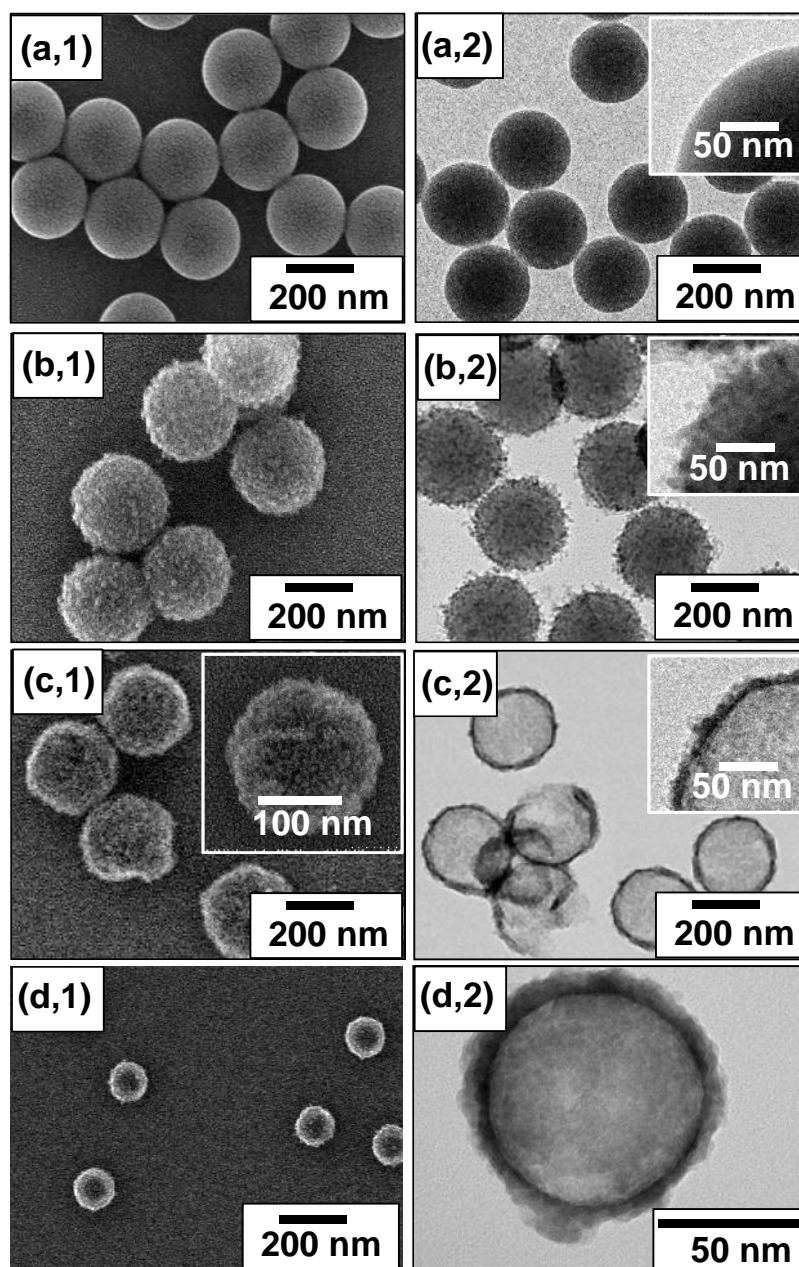
Figure 6.1. Electron microscope images of PS (a), PS/silica composite (b), and hollow silica (c and d). Figures (a,1), (b,1), (c,1), and (d,1) are the SEM analysis results, while Figures (a,2), (b,2), (c,2), and (d,2) are the TEM analysis results. Figure (a-c) and (d) are samples prepared using PS spheres with a mean size of 200 and 90 nm, respectively.

_____

To confirm the internal structure of the particles, TEM images are shown in **Figure 6.1(a,2), (b,2)** and **(c,2)**. **Figure 6.1(a,2)** shows that the structure of the PS particles are spherical and dense. **Figure 6.1(b,2)** reveals core-shell structure. Silica nanoparticles were well-distributed onto the PS particles surface. **Figure 6.1(c,2)** results that after the template removal process, particles with hollow structure are obtained. A high magnified TEM image indicates that the shell has uniform thickness and a rough surface. This confirm that the present method is effective to produce spherical hollow particles.

Figure 6.1(d,1) and **(d,2)** shows SEM and TEM images of hollow silica particles prepared using smaller PS template. Smaller particle sizes were observed (**Figure** 1(d,1)). Hollow structure was clearly obtained (**Figure 6.1(d,2)**). Sizes of the hollow particles were identical to those of the initial PS, confirming that control of the hollow particle diameter could be achieved only by varying the size of the initial PS spheres.

FTIR analysis results of hollow silica, PS/silica composite, and PS particles are shown in **Figure 6.2**. Different peaks among the samples were revealed. For the PS sample, the peaks were observed at wavenumber of 500-1000, 1400-1700, and 2800-3200 cm^{-1}. For PS/silica composite sample, new peaks appeared at 1200 and 900 cm^{-1}, in addition to those peaks in PS sample. The FTIR analysis of hollow silica nanoparticles shows that the appeared peaks are in exact match with those of peaks in pure silica nanoparticles, verifying that the prepared hollow particles are silica.

_____
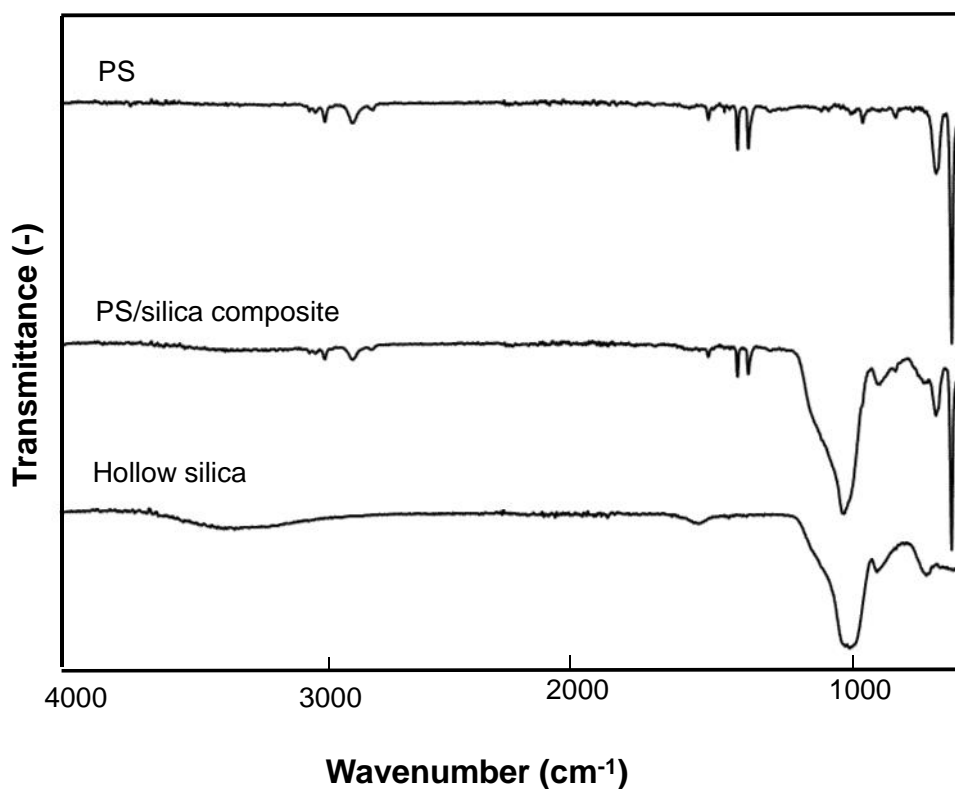
Figure 6.2. FTIR analysis of PS, PS/silica composite, and hollow silica particles.

SEM images of the particles produced with various flow rates (Q) under the same precursor concentration (0.10 wt.%) are shown **Figure 6.3a-c**. When $Q \leq 1.00$ μL/min, agglomeration-free spherical hollow particles were produced (**Figure 6.3a**). By increasing the Q (> 1.00 μL/min), aggregated particles were obtained (**Figure 6.3b-c**). The Q is essential to control the droplet size. Because droplet contains nanoparticles, larger droplet can hold more nanoparticles and lead the production of agglomerated hollow particles.

_____
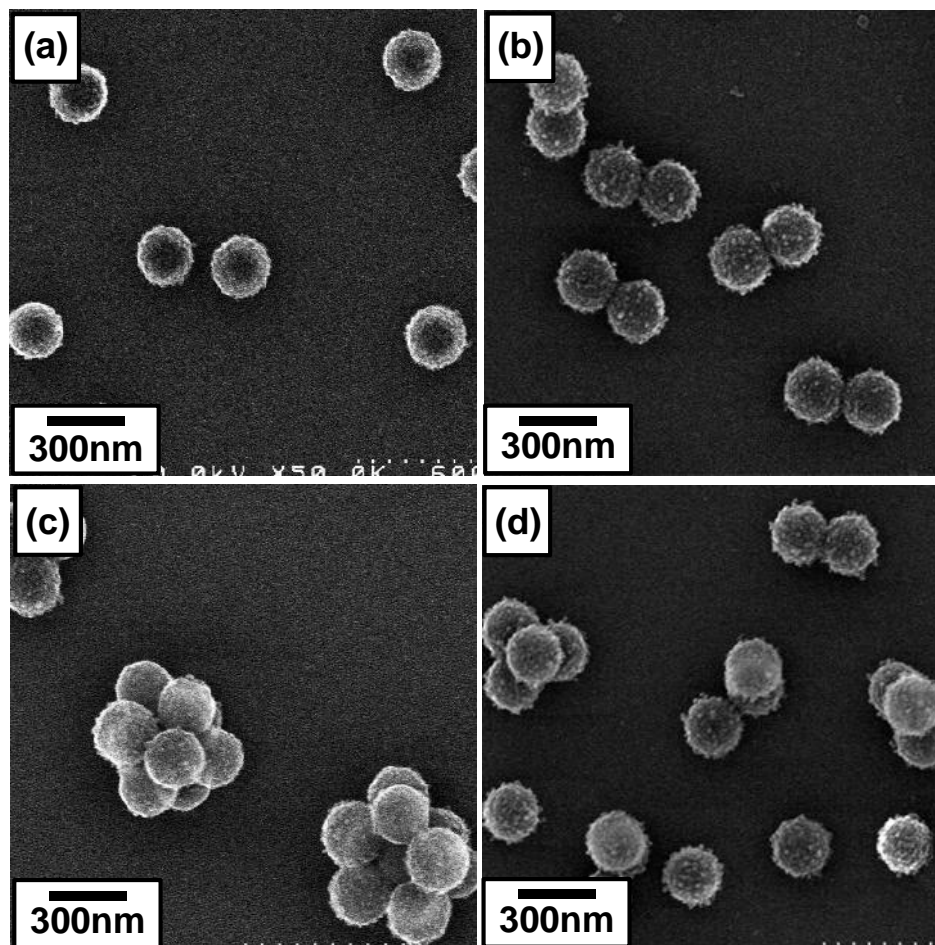
Figure 6.3. SEM images of particles generated with various *Q/C* values (μL/min)/(wt%): (a) 1.00/0.10;(b) 2.00/0.10; (c) 6.00/0.10; and (d) 1.00/1.00.

Figure 6.3a and **d** show SEM images of particles generated with various precursor concentrations (*C*). When $C \leq 0.20$ wt%, individual hollow particles were created. When $C > 0.20$ wt%, agglomerated particles were produced. *C* value determines number of nanoparticles inside the droplet. Thus, too high *C* value results the failure in the production of agglomeration-free hollow particles.

Based on the above experimental results, I proposed the particle formation mechanism in **Figure 6.4**. After the solution is sprayed (due to high voltage between needle and collection electrode), the droplet is produced. The droplet is then travelling to the collection electrode. During aerosol travel, solvent is evaporated and

_____

self-assembly of nanoparticles occurs. After the template removal process, hollow

particle can be produced. Using variation of Q and C values, hollow particle formation

can be divided into four main routes. When Q   5.00 µL/min and C   0.20 wt%,

aggregated hollow particles are produced (R1). These hollow particles contain many

spherical holes. When $Q = 1.00$-5.00 µL/min and C 0.20 wt%, mixtures of aggregated

and individual hollow particles are obtained (R2). For Q 1.00 µL/min and C 0.20

wt%, individual hollow particles are created (R3). For the case of Q 1.00 µL/min and

$C > 0.20$ wt%, aggregation of the hollow particles occurs (R4). Thus, from these results,

agglomeration-free hollow particles can be produced only when process parameters fall

within the appropriate condition (Q 1.00 µL/min and C 0.20 wt%).
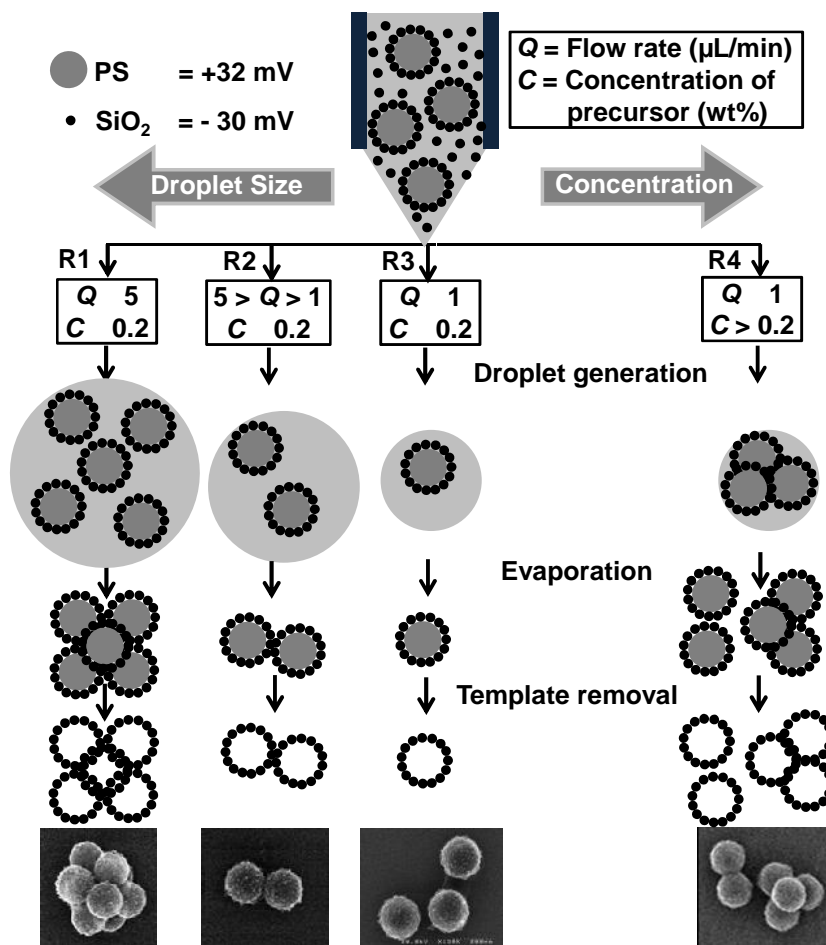
Figure 6.4.   Hollow particle formation mechanism.

_____

6.4. Conclusion

In summary, agglomeration-free hollow silica particles have successfully prepared using the electrospray method followed by the template removal process. The experimental results indicate that the PS size, the Q, and the C are effective in controlling the hollow particle size and the agglomeration condition. The agglomeration-free spherical hollow particles could be obtained using low flow rate (Q 1.00 µL/min) with low precursor concentration (C 0.20 wt%). I believe that further insights gained from research such as the present study should make further particle fabrication innovations possible.

6.5. References

[1] T. Nomura, Y. Morimoto, H. Tokumoto, Y. Konishi, Fabrication of silica hollow particles using escherichia coli as a template, Materials Letters, 62 (2008) 3727-3729.

[2] S. Nagamine, A. Sugioka, Y. Konishi, Preparation of tio$_2$ hollow microparticles by spraying water droplets into an organic solution of titanium tetraisopropoxide, Materials Letters, 61 (2007) 444-447.

[3] J.H. Park, C. Oh, S.I. Shin, S.K. Moon, S.G. Oh, Preparation of hollow silica microspheres in w/o emulsions with polymers, Journal of colloid and interface science, 266 (2003) 107-114.

[4] F. Caruso, R.A. Caruso, H. Möhwald, Nanoengineering of inorganic and hybrid hollow spheres by colloidal templating, Science, 282 (1998) 1111-1114.

[5] G. Hadiko, Y.S. Han, M. Fuji, M. Takahashi, Synthesis of hollow calcium carbonate particles by the bubble templating method, Materials Letters, 59 (2005) 2519-2522.

[6] G. Li, Z. Zhang, Synthesis of submicrometer-sized hollow titania spheres with controllable shells, Materials Letters, 58 (2004) 2768-2771.

[7] Y. Du, Z.X. Cheng, S. Xue Dou, D.J. Attard, X. Lin Wang, Fabrication, magnetic, and ferroelectric properties of multiferroic bifeo< inf> 3</inf> hollow nanoparticles, Journal of applied physics, 109 (2011) 073903-073903-073905.

[8] A.B.D. Nandiyanto, A. Suhendi, T. Ogi, T. Iwaki, K. Okuyama, Synthesis of additive-free cationic polystyrene particles with controllable size for hollow template applications, Colloids and Surfaces A: Physicochemical and Engineering Aspects, 396 (2012) 96 - 105.

Chapter 7

Effect of droplet charge on the fabrication of self-organized hollow silica particles

7.1. Introduction

Studies on fabrication of hollow particles have attracted a great amount of attention. Excellent performances gained from the existence of the hole structure make this material useful in various applications, such as catalysts, thermal insulators, sensors, printing materials, and drug delivery systems.[1, 2]

To produce particles with desirable hole structures, many methods have been reported.[3-6] Although the current development methods are effective, these methods are still insufficient for practical use due to the obligation from the use of additive (e.g. surfactant, polymer, etc).[7, 8] In fact, this additive may reduce performance, strength, and purity of the final product. Although several researchers reported the synthesis of hollow particles via an additive-free process,[9] the suggested methods still have limitations, such as agglomeration phenomena, uncontrollable hollow structure, multistep and complicated synthetic procedures, and impurities.

To address the above problems, spray-drying of colloidal nanoparticles is a good candidate technique.[10] Different from other methods, the spray-drying process offers simple and facile synthetic method, control of crystallinity, and avoid of agglomeration of the final product.[11] Typically, the hollow particles are produced from combination of host material and template component.[12] This combination is effective to create hollow particles with controllable hole size. However, outer shape of the prepared particles are spherical only, and their reports describe on the successful hollow particle synthesis with only partial information about self-organization

_____

parameters (i.e. colloidal particle surface charge, size, and composition). Further, their reports did not perform the self-organization process under charged droplet. In fact, the charge of droplet plays important role in the self-assembly of the component in the droplet.[10]

Based on the previous chapters on the fabrication of hole-structured particles, here, the purpose of this chapter was to report effects of droplet charge on the fabrication of self-organized hollow particles from spray-drying of colloidal nanoparticles. The effects of this droplet charge under various self-organization parameters (i.e. flow rate, surface charge, size, and composition of colloidal nanoparticles) were investigated experimentally, and the results are qualitatively explained. To achieve production of hollow particles under the charged droplet condition, I used an electrospray-assisted spray-drying method. Experimental results showed that the droplet charge played an important role in controlling self-organization of colloidal components in the formation of hollow particles. Particles containing hollow structures were effectively created for all variations, except for the process under a specific condition (droplet and colloidal particles are in the same charge polarity). The present method is also possible for producing hollow particles with controllable outer shape, hole number, shell thickness, and internal structure. In addition, to the best of my knowledge, this report is the first to address the droplet charge issue with colloidal nanoparticle consideration and could be relevant to other functional properties of hollow materials.

7.2. Hypothetical effects of droplet charge on the particle structure

Main principle of spray-drying method is to deliver and rapidly heat an initial solution/slurry via direct injection of very small droplets,[11] namely atomization

_____

process (**Figure 7.1a**). Because the common spray-drying method provides the atomization process by physical forces, no charge exists on the generated droplet. Therefore, self-organization of components in the formation of particles is based on charge of colloidal nanoparticles only.[13] For instance, when particles were prepared from spray-drying of precursor containing silica nanoparticles and PS spheres, possible particle formation mechanism can be classified by two routes. Combination of precursor containing negatively charged silica and anionic PS results in the production of porous-structured particles, whereas those combination of silica nanoparticles with cationic PS spheres allows the creation of hollow particles.[12]
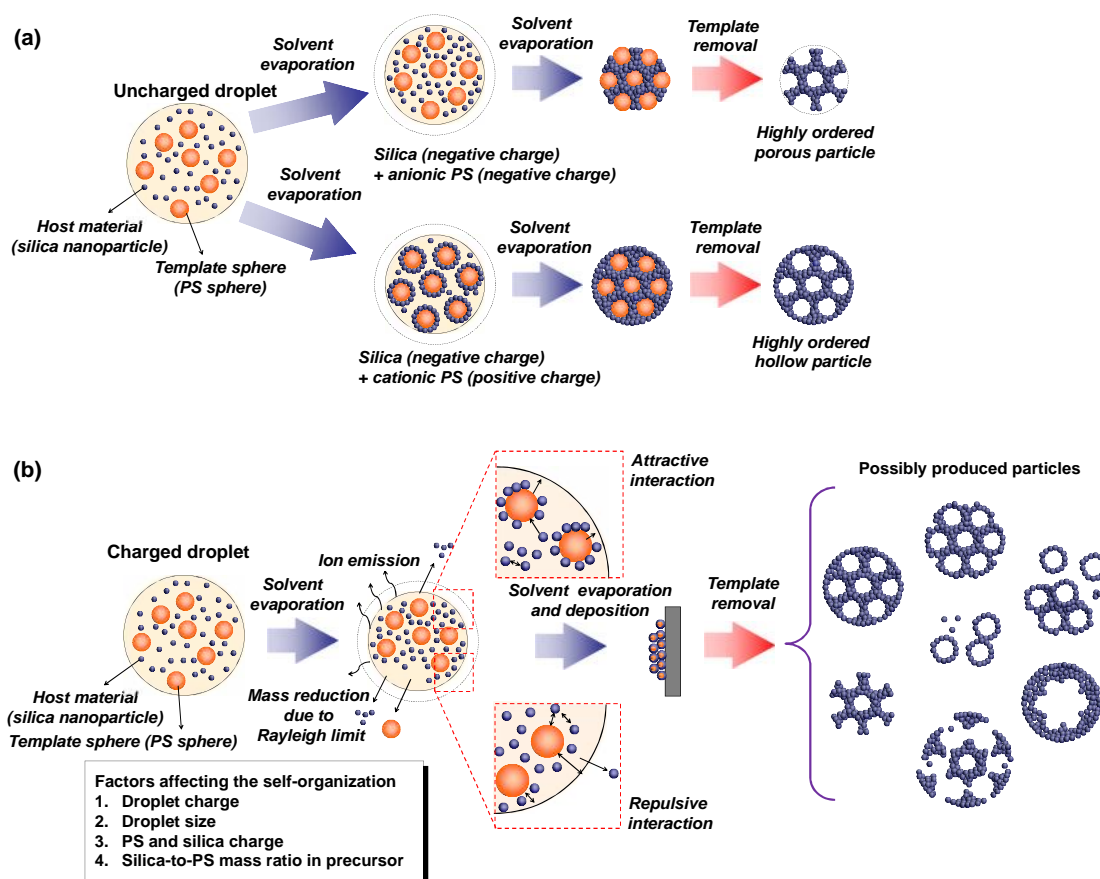
Figure 7.1. Schematic illustration of self-organization of colloidal particle inside uncharged (a) and charged (b) droplets.

When the spray-drying method is processed under charged droplet condition, additional factors in the colloidal self-assembly phenomena should be considered

_____

(**Figure 7.1b**).[10] Droplet charge adds electrostatic interactions to the colloidal nanoparticles during the self-organization process. Therefore, in addition to the solvent evaporation and the colloidal-to-colloidal interactions, several phenomena happen: attractive-and-repulsive interactions between colloidal particle and droplet surface[14], ion emission, and mass reduction due to Rayleigh limit theory.[11, 15] Combination of those factors can result particles with unique morphologies, which are different from common spray-drying method.

7.3. Experimental Section

7.3.1. Raw materials

Hollow particles were produced from silica nanoparticles (Nissan Chemical Co. Ltd.; a mean size of 5 and 15 nm) and PS spheres. PS spheres were synthesized from a simple polymerization of styrene monomer (styrene; Kanto Chemical Co., Inc.) under surfactant-free conditions. As the initiator in the styrene polymerization, potassium persulfate (KPS; Sigma-Aldrich) or 2,2-azobis (isobutyramidine) dihydrochloride (AIBA; Sigma-Aldrich) was used, which was effective to produce PS spheres with negative or positive surface charge, respectively. To produce PS spheres with different diameters, concentrations of the styrene were varied. Detailed PS synthetic method is explained in **Chapter 2**.[12] All chemicals were used without further purification.

7.3.2. Production of hollow particles

To produce hollow particles, a mixture of silica nanoparticles and PS spheres were diluted in ethanol with a concentration of 0.15 wt%, namely a precursor. The precursor was then put into the spray-drying apparatus. I used two types of spray-drying equipments, in which these equipments were used for supporting electrospray-assisted

_____

and ultrasonic-assisted spray-drying methods (**Figure 7.2**). The electrospray-assisted spray-drying method was used to produce particles under charged droplet condition, whereas the ultrasonic-assisted spray-drying method was under uncharged droplet condition.
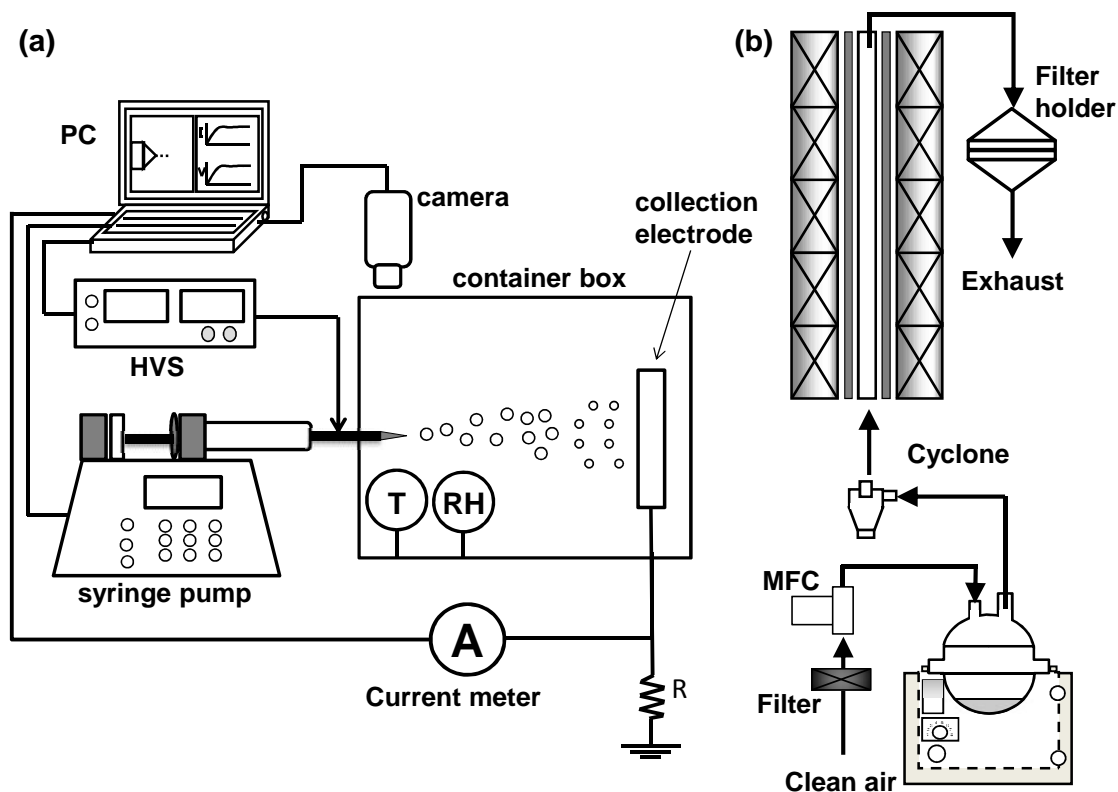
Figure 7.2.   Experimental apparatuses for generating particles using the electrospray-assisted (a) and the ultrasonic nebulizer-assisted (b) spray drying methods, respectively.

7.3.2.1. Production of particles using electrospray-assisted spray-drying method

Experimental system for electrospray-assisted spray-drying method is shown in **Figure 7.2a**. This spray-drying system was similar to that used in **Chapter 1**.[16-18] The apparatus consists of a syringe (Hamilton, Gastight 1000 µl; with a 27 Gauge needle), a syringe pump (Harvard apparatus, PHD2000), a controllable DC high-voltage source (HVS; Matsusada HER 10R3; conducted at 3.00 kV), a box chamber (a

_____

temperature of 40 ºC and relative humidity of less than 30%), and a collection electrode (situated at 7.00 cm away from the needle and connected to the ground).

In briefly, after the precursor was added into the syringe, the precursor was sprayed, forming droplet. Droplet flew to the collection electrode due to electrostatic force. During droplet travel, solvent evaporated, producing particles that were deposited onto the collection electrode. The produced particles were then put into the template removal process (heat treatment at 500°C; heating rate = 2°C/min; holding time = 10 minutes).

7.3.2.2. Production of particles using ultrasonic-assisted spray drying method

To produce particles under uncharged droplet, the ultrasonic-assisted spray-drying method was used (**Figure 7.2b**). Detailed synthetic apparatus and process are described in **chapter 1**.[12] The apparatus consists of an ultrasonic nebulizer (model NE-U12, Omron Corp.; equipped with a cyclone at operating frequency of 1.7 MHz), a ceramic tubular furnace (diameter of 13 mm and length of 100 mm; two fixed temperature zones (200/600°C)), and a filter.

In short, after the precursor was added into the ultrasonic nebulizer, micrometer-sized droplet was produced. Then, with the flow of nitrogen gas (0.75 L/min), the droplet travelled to the tubular furnace (to evaporate solvent and to remove PS), forming particles. After leaving the tubular furnace, particles were collected by the filter.

7.3.3. Characterizations

The prepared particles were characterized using a scanning electron microscope (SEM, Hitachi S-5000; operated at 20 kV) and a transmission electron

_____

microscope (TEM, JEM-2010; operated at 200 kV) to examine their size and morphology. The elemental and the chemical compositions of the prepared particles were evaluated using a Fourier transform infrared spectroscopy analysis (FTIR, PerkinElmer, Spectrum One System; in the range of 600-4000 cm^{-1}). The particles were also characterized using a thermogravimetric and differential thermal analyzer (TG-DTA, Exstar6000, Seiko Instruments Inc.; heating rate of 5°C/min). The charges of the colloidal nanoparticles were measured using a zeta potential measurement system (Malvern Zetasizer, Nano ZS).

7.4. Results and Discussion

7.4.1. Investigation of physicochemical properties of colloidal nanoparticles

Physical properties of the initial colloidal nanoparticles in the precursor solution are presented in **Figure 7.3**. SEM images revealed that monodispersed nanoparticles with a spherical shape were observed. Zeta potential results indicated that 5 and 15 nm of silica nanoparticles had a zeta value of -30 and -29 mV, respectively. The zeta potential of 200 nm of cationic PS spheres was +31 mV, whereas 90 and 200 nm of anionic PS spheres were -35 and -32 mV, respectively. These results confirm that these colloidal nanoparticles can be used for investigation of hollow particle production.[13]

_____
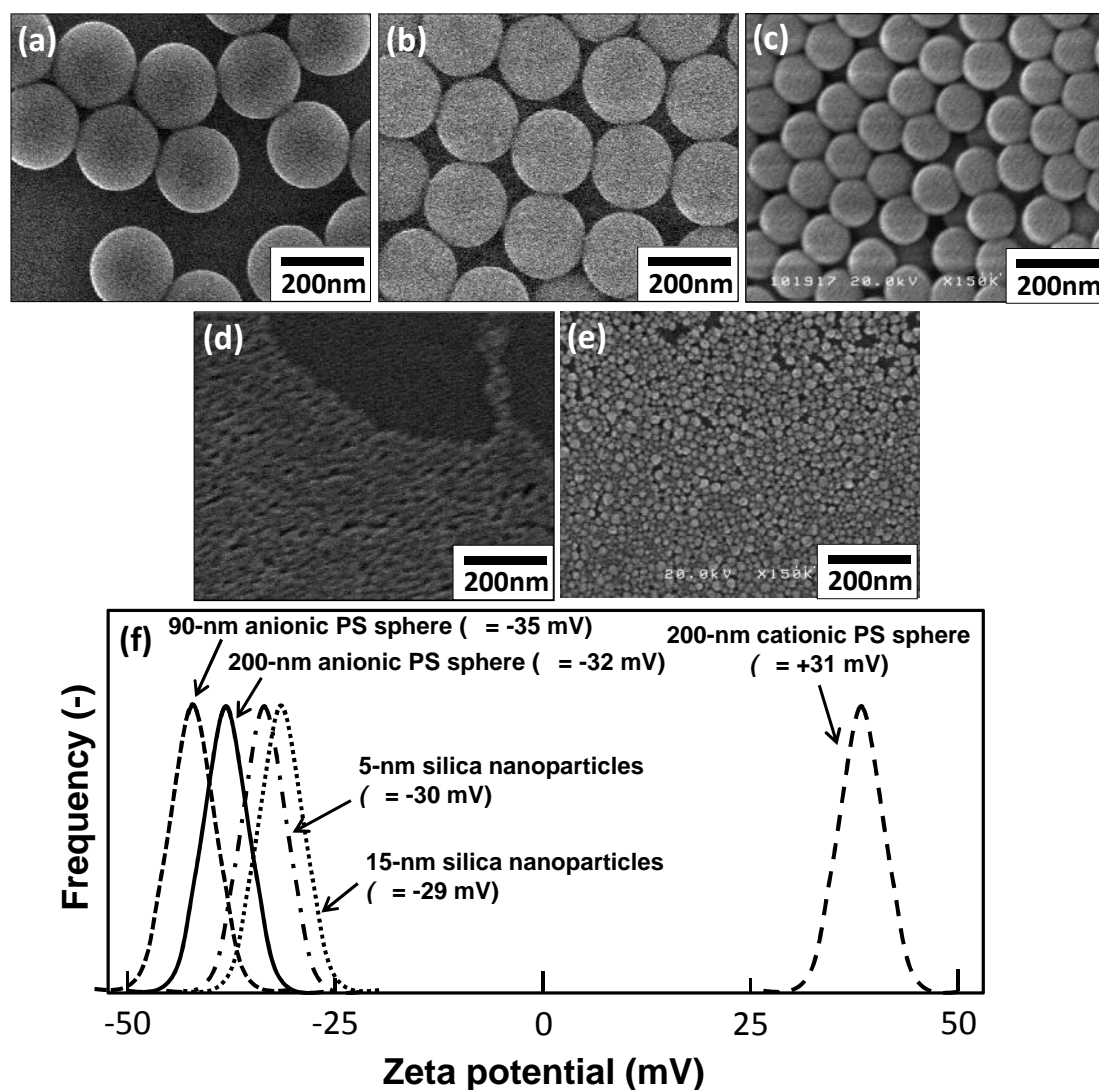
Figure 7.3.   Physical properties of the initial colloidal nanoparticles used in the precursor. SEM images of colloidal particles: (a) 200-nm cationic PS, (b) 200-nm anionic PS, (c) 90-nm anionic PS, (d) 5-nm silica, and (e) 15-nm silica. Figure (f) is the zeta potential measurement results.

Figure 7.4 shows physicochemical properties of the electrosprayed silica/PS particles before and after the template removal process. As a reference, I also analyzed particles prepared from a precursor containing "silica only" and "PS only".

_____
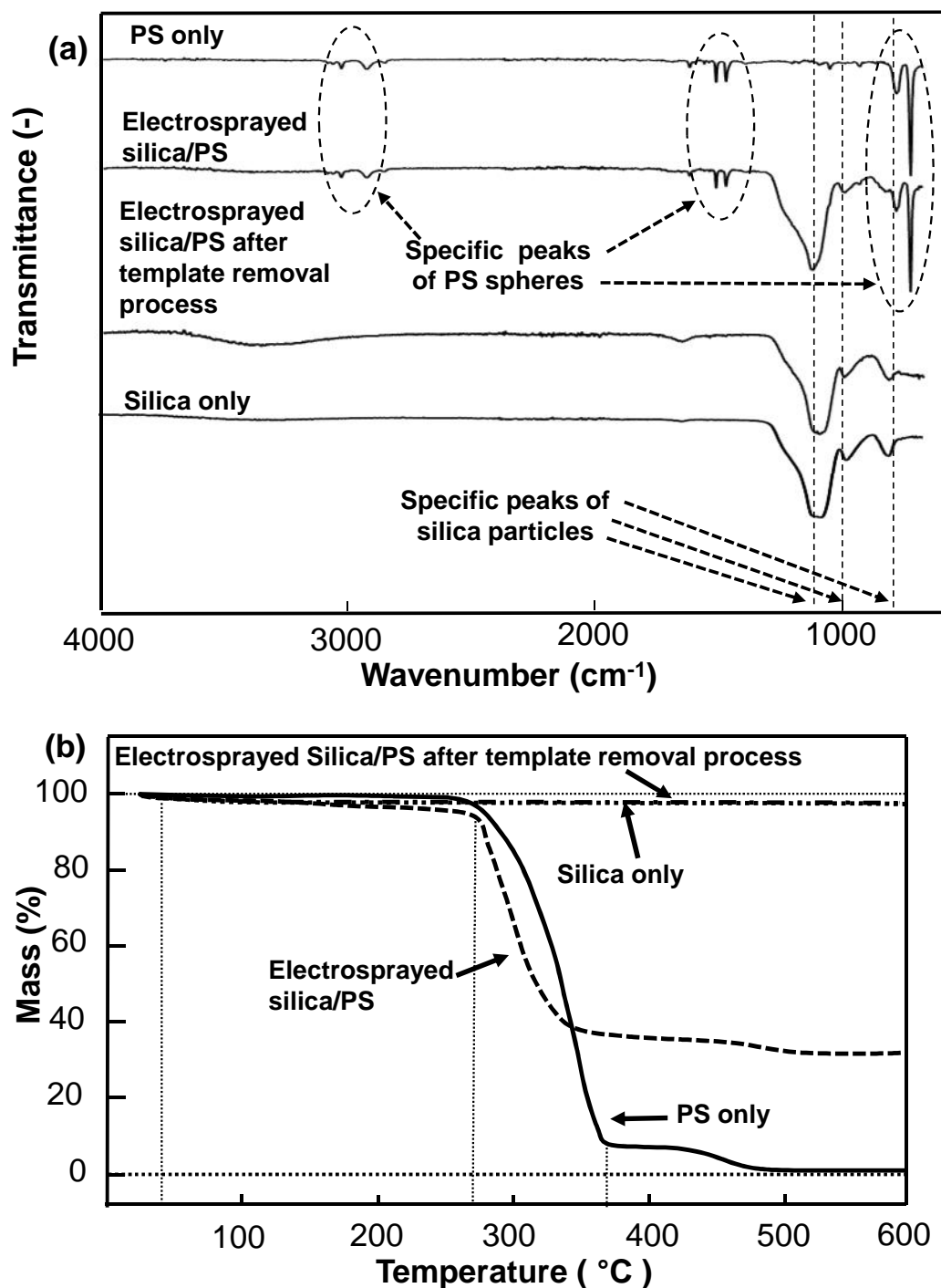
Figure 7.4. Physicochemical properties of electrosprayed particles using: (a) FTIR and (b) TG/DTA analysis. Samples were prepared using 5-nm silica nanoparticles and 200-nm PS spheres.

Figure 7.4a shows the FTIR spectra results for all samples. A sample containing "electrosprayed silica/PS" had two main peaks, where these peaks were combination peaks of silica (in the range 1000–1200 cm⁻¹) and PS (at band 500–1000,

_____

1400–1700, and 2800–3200 cm^{-1}), as confirmed by the reference samples. After the silica/PS composite were put into the template removal process, PS peaks disappeared. This result verifies that the silica and the PS colloidal particles self-assembly during the electrospray process. Then, after the particles are heated, PS spheres are removed, remaining silica in the final product.

Figure 7.4b presents TG/DTA analysis results. TG/DTA analysis results of "electrosprayed silica/PS after the template removal process" and "silica only" samples indicated relatively constant in mass for wide range of temperatures, giving evidences that the samples were silica. In the case of "electrosprayed silica/PS" and "PS only" samples, the TG/DTA results detected a significant decrease in mass from 275°C. Then, after reaching the temperature of 360°C, the mass was stable. The final masses of "electrosprayed silica/PS" and "PS only" samples were 35 and 0 wt%, respectively. This result confirms that the template removal process is effective to completely remove all PS components, and the remaining mass in the "silica/PS" sample was due to the presence of the silica mass fraction.

7.4.2. Effects of colloidal surface charge and flow rate

Figure 7.5 shows effect of colloidal surface charge on hollow structurization examined with TEM analysis. Holes of about 200 nm in diameter were identified in all cases, verifying that these holes were from the inverse replication of PS spheres. A change in the colloidal surface charge impacts greatly to the colloidal-to-colloidal interaction during the self-assembly process.[13] Different hole configurations were found, which could be observed by the existence of silica wall between the holes (shown as red-dashed line in **Figure 7.5a-b**). In short, when silica and cationic PS colloidal nanoparticles were electrosprayed, hollow particles with silica wall were

produced (**Figure 7.5a**). On the other hand, when silica and anionic PS spheres were used, hollow particles with no silica wall were found (**Figure 7.5b**). Different internal structures are found because of attractive and repulsive effects between the colloidal nanoparticles and the droplet surface. To confirm the above colloidal charge effects, I also investigated the process that performed under different flow rates of precursor. Experimental results showed that changes in the flow rate influenced the number of holes only but had no impact to the internal structures in the final hollow particles (shown **Figure 7.5c-d**).
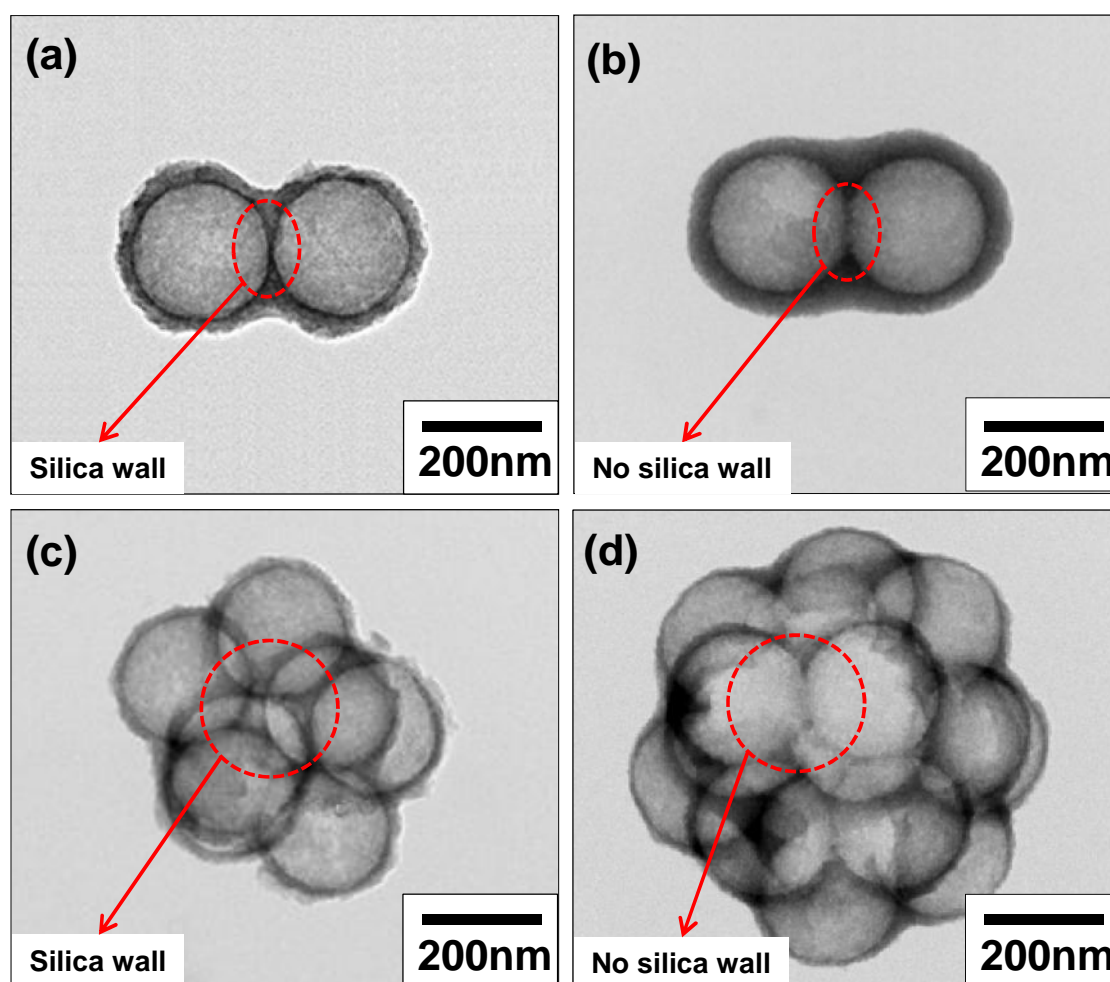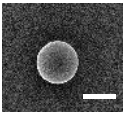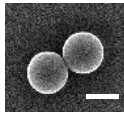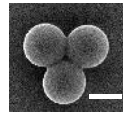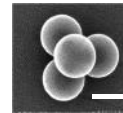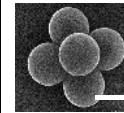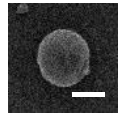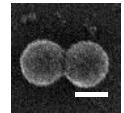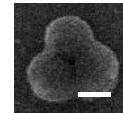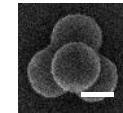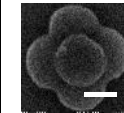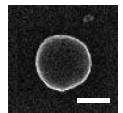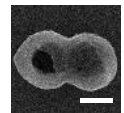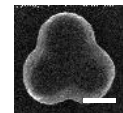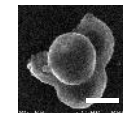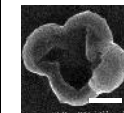
Figure 7.5.   TEM images of the particles prepared with various colloidal surface charges and flow rates. Samples in Figures (a) and (c) were prepared using cationic PS, whereas Figure (b) and (d) were using anionic PS. Figures (a) and (b) were prepared using Q=2 µL/min and Figure (c) and (d) were using 6 µL/min.

_____

Table 7.1.   SEM images and schematic models of electrosprayed particles prepared using anionic PS spheres with various flow rates. Scale bars are 200 nm.

Group sample		Hole number (*n*)				
		n=1	n=2	n=3	n=4	n=5
Electrosprayed anionic PS only	SEM images					
	Model					
Electrosprayed silica / anionic PS	SEM images					
	Model					
Electrosprayed silica / anionic PS after template removal process	SEM images					
	Model					

Detailed effect of flow rate on the hollow structurization is shown in **Table 7.1 and 7.2**. **Table 7.1** presents about the particles prepared using silica and anionic PS nanoparticles, whereas **Table 7.2** discusses about the particles produced using silica and cationic PS nanoparticles. The result showed that the number of the spherical components (*n*) depended on the adjustment of flow rate, in which this result was in a good agreement with **Chapter 5**.[17] When the process was conducted in the same flow rate, the number of *n* for all groups was identical. Outer surface and diameter of particles prepared from "silica/PS" suspension were different from those from "PS only" solution. When heat treatment was added to the as-prepared silica/PS particles, no change in outer shape, structure, and diameter was found. These results reply that during the process, the PS plays as a main building block in the hollow particle formation,

while silica covers the arranged PS spheres. Therefore, when the PS components are removed, hollow-structured particles are created. In addition, different internal structures were found when I used different charges of PS spheres, confirming the result in **Figure 7.5a-b**.

Table 7.2. SEM images and schematic models of electrosprayed particles prepared using cationic PS spheres with various flow rates. Scale bars are 200 nm.

Group sample		Hole number (*n*)				
		n=1	n=2	n=3	n=4	n=5
Electrosprayed cationic PS only	SEM images					
	Model					
Electrosprayed silica / cationic PS	SEM images					
	Model					
Electrosprayed silica / cationic PS after template removal process	SEM images					
	Model					

7.4.3. Effects of the silica/PS mass ratio

Figure 7.6 shows morphologies of the generated particles prepared with various silica/PS mass ratios. Peanut-like particles were observed. The SEM images in **Figure 7.6a-b** revealed that the mass ratio influenced outer diameter but had no impact to outer shape and surface. To verify the hole structure inside the particle, TEM analysis

_____

was conducted (**Figure 7.6c-d**). As shown in the figures, the TEM images indicated that the prepared particles contained two holes, confirming change in silica/PS mass ratio did not affect to self-organization of colloidal nanoparticles in the formation of hollow particle. Ferret analysis from TEM images implied that the thickness increased from 15 to 27 nm. Increases in silica/PS mass ratio influences how much silica is attached on the surface of PS. In addition, although the present result show their successful synthesis of hollow particles, the mass ratio of host and template components must be considered. Too much deviation from the optimal mass ratio leads the unsuccessful formation of hollow particles, in which this is explained in detail in **Chapter 5**.[18]
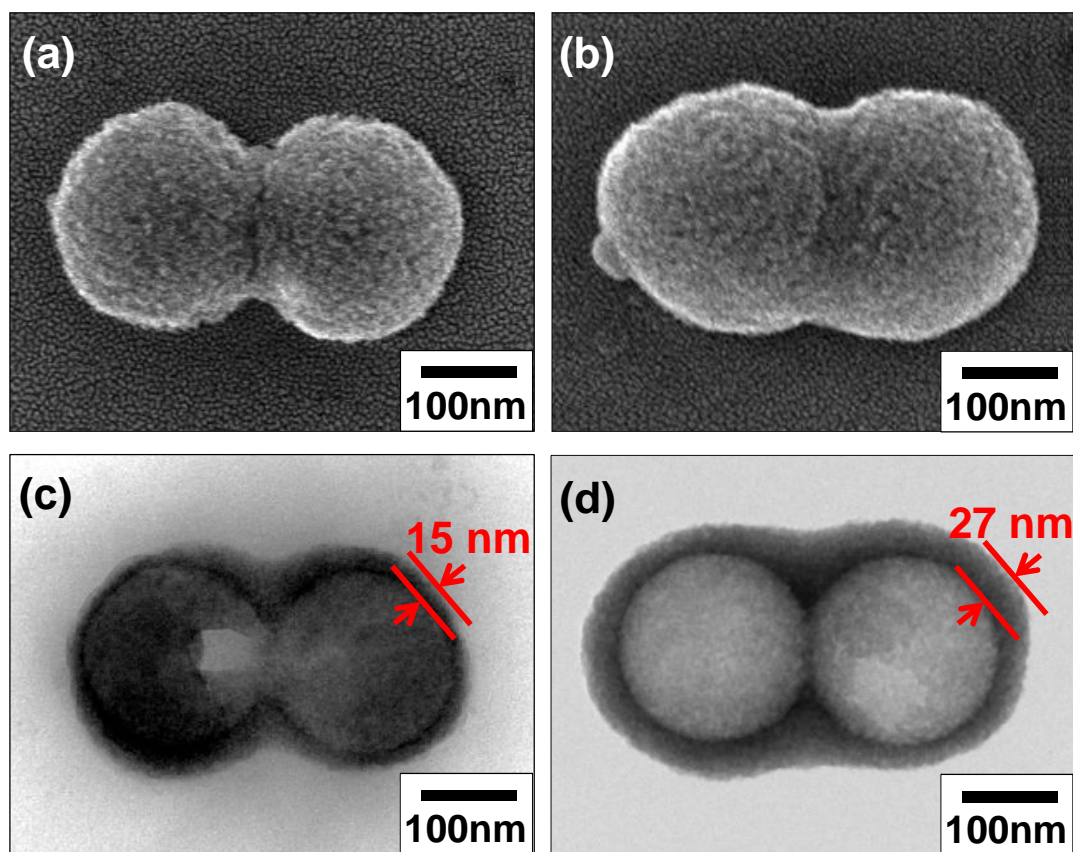
Figure 7.6. SEM and TEM images of the electrosprayed particles prepared with various silica/PS mass ratios. Samples in Figures (a) and (c) were prepared using a silica/PS mass ratio of 0.33, whereas Figures (b) and (d) were 0.50.

_____

7.4.4. Effects of the silica/PS size ratio

Figure 7.7 shows the TEM images of the generated particles produced with various silica/PS size ratios. Experimental results showed the strong relationship between component size and hollow particle structurization. When using a silica/PS size ratio of 15/200, hollow particles with a hole size of 200 nm and a shell thickness of 42 nm were produced (**Figure 7.7a**). When the silica size reduced down to 5 nm, shell thickness became thinner (thickness of 15 nm), whereas the hole size was retained (**Figure 7.7b**). By changing a silica/PS size ratio to 5/90, hollow particles with a hole size of 90 nm and a shell thickness of 15 nm were prepared (**Figure 7.7c**). I found that if the PS size was varied but the silica nanoparticles were maintained, no significant change in the shell thickness was observed. To confirm the component size parameter, I also performed the process under different flow rates (**Figure 7.7d-e**). The TEM result revealed that the flow rate had no effect on controlling hole size and shell thickness. From above results, it concludes that the PS and the silica sizes provide the change in the hole size and the shell thickness, respectively. In addition, although the size ratio can be used as a modified parameter for controlling hole size and shell thickness, the adjustment of size ratio have some limitations. If the size of silica and PS are almost the same, it results the fail in maintenance of silica to be arranged on the PS surface. Detailed information about the colloidal size parameter in the self-organization of colloidal nanoparticles is explained in **Chapter 3**.
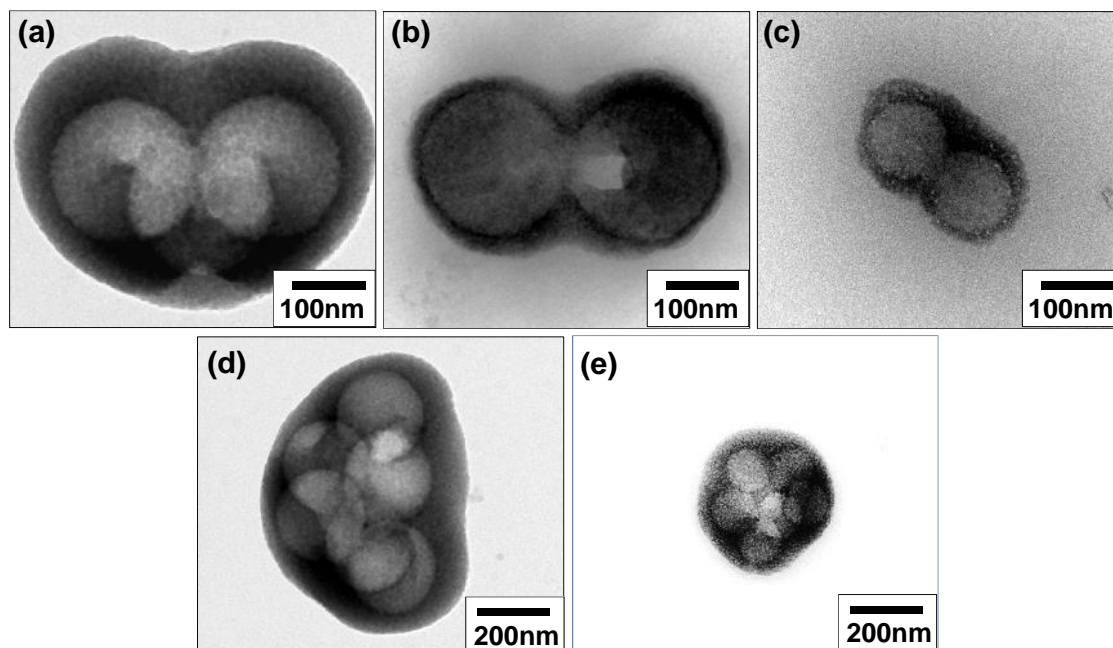
Figure 7.7. TEM images of the hollow particles prepared with various silica/PS size ratios and flow

rates. Samples in Figures (a, d), (b), and (c, e) were prepared using a silica/PS size ratio of

15/200, 5/200, and 5/90, respectively. Samples in Figures (a)-(c) were prepared using flow

rate of 2 µL/min, while Figures (d) and (e) were using 6 µL/min.

7.4.5. Effect of droplet charge
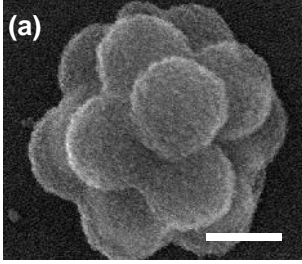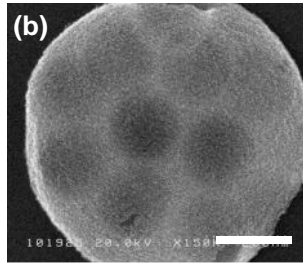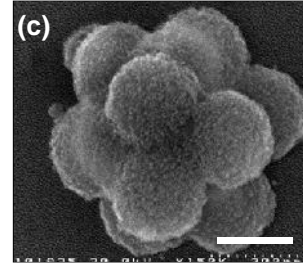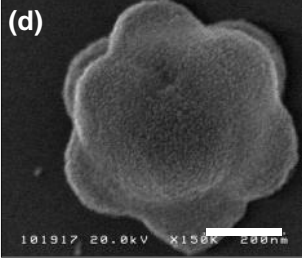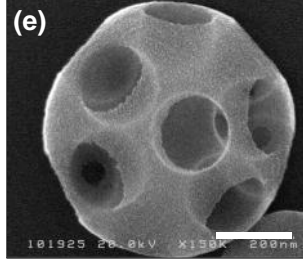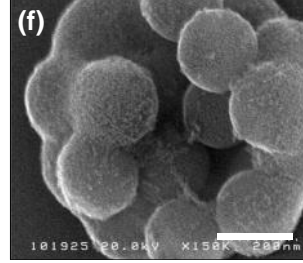
To confirm the hollow structurization due to droplet charge effect, I

investigated the hollow particle formations under different droplet charges (**Table 7.3**).

Particles with hole sizes of 200 nm were produced for all cases, confirming that the PS

spheres were effective to lead the hollow structurization. Since silica has a negative

charge, the present investigation was focused on the effect of charges in droplet and

colloidal PS spheres.

When silica nanoparticles and cationic PS spheres (positive zeta charge) were

used for producing hollow particles under different droplet charges, different types of

hollow particles were obtained. When positively charged droplet was applied, grape-like

*Chapter 7: Effect of droplet charge on fabrication of self-organized hollow particles
from electrospray-drying of colloidal nanoparticles*

_____

hollow particles were produced (inset **Figure a** in **Table 7.3**). When decreasing droplet charges into zero condition, spherical-shaped hollow particles were fabricated (inset **Figure b** in **Table 7.3**). Further decreasing the charge down to negative values, aggregated hollow particles were created (inset **Figure c** in **Table 7.3**). The successful formation of hollow particles can be obtained for all variations. The attractive interaction between silica and PS are strong enough to maintain the hollow structure against droplet charge.

When silica nanoparticles and anionic PS spheres (negatively zeta value) were used, different hole configurations were obtained. When positive droplet charge was implemented, daisy-shaped hollow particles were produced (inset **Figure d** in **Table 7.3**). However, when zero-charged droplet was applied, porous-structured particles were created (inset **Figure e** in **Table 7.3**). Further adjustment of droplet charged down to negative values results the production of particles with irregular structure (inset **Figure f** in **Table 7.3**). From these results, it can be concluded that the droplet charges provide effect on hollow structurization. The hollow particles are failed in the zero- and negative-charged droplet condition because the repulsive interaction between colloidal-to-colloidal nanoparticles dominates in the manipulation of particle formation. Colloidal nanoparticles would rather staying solitary than combining with other nanoparticles. Then, with the occurrence of solvent evaporation, the colloidal nanoparticles are forced to be self-assembly into their most stable condition under repulsive condition.

_____

Table 7.3.   Effect of droplet and PS surface charges on hollow particle morphology. Samples were prepared using 5-nm silica and 200-nm PS spheres with a silica/PS mass ratio of 0.50. Scale bars are 200-nm.

PS charge	Droplet charge		
	Positive	**Zero**	**Negative**
Positive	(a)	(b)	(c)
Negative	(d)	(e)	(f)

7.4.6. Proposed mechanism on the formation of hollow particles

Based on above experimental results, I proposed the particle formation mechanism in charged and uncharged droplets in **Figure 7.8**. **Figure 7.8a and b** show the cases of positively and negatively charged droplets, respectively, while **Figure 7.8c** shows the cases of uncharged droplet.

Route **R1(+)** describes the process that is conducted using combination of negative PS and positive droplet charges. Attractive interaction between colloidal nanoparticles and droplet surface happens because of their opposite charge values. Colloidal nanoparticles attract and move to the surface of droplet, forming a shell-like film in the droplet. Because the Brownian motion of silica is faster than those of PS spheres, the silica nanoparticles can reach the surface earlier than the PS spheres.

Therefore, outer surface of droplet can be filled mostly by silica nanoparticles. With the existence of solvent evaporation phenomenon, shell (that is formed by the self-assembly of colloidal nanoparticles) is forced to the center of the droplet. The PS spheres are trapped and self-arranged to the center of droplet, while silica nanoparticles follow and cover the arranged PS spheres. As a consequence, hollow particle with no silica wall is produced in the final product.

Route **R2(+)** shows the particle formation when using cationic PS spheres and positive droplet charge. Different from route **R1 (+)**, silica wall is found in the inner structure of the produced particle. This is because during the process, silica nanoparticles and PS spheres have attracted each other since the early stage of the droplet formation, creating core-shell PS/silica nanoparticles. Therefore, during electrospray process, the core-shell nanoparticles are mainly self-assembled in the droplet and the remained free silica nanoparticles fill the spaces between the arranged core-shell nanoparticles. As a result, hollow particle with silica wall is created.

In route **R3(-),** the droplet and the PS sphere charges are negative. All colloidal nanoparticles repel each other due to the same charge polarity. As a consequence, some of the colloidal nanoparticles are easily expelled, creating an incomplete sphere-packing phenomenon in the final product.

Route **R4(-)** shows the particle formation when using cationic PS spheres and negative droplet charge. Similar to route **R2(+)**, silica nanoparticles and PS spheres attract each other, forming core-shell nanoparticles since the early stage of droplet formation. Therefore, although the charge of the droplet creates repulsive action to the silica nanoparticles, hollow particle with silica wall structure is still obtained.
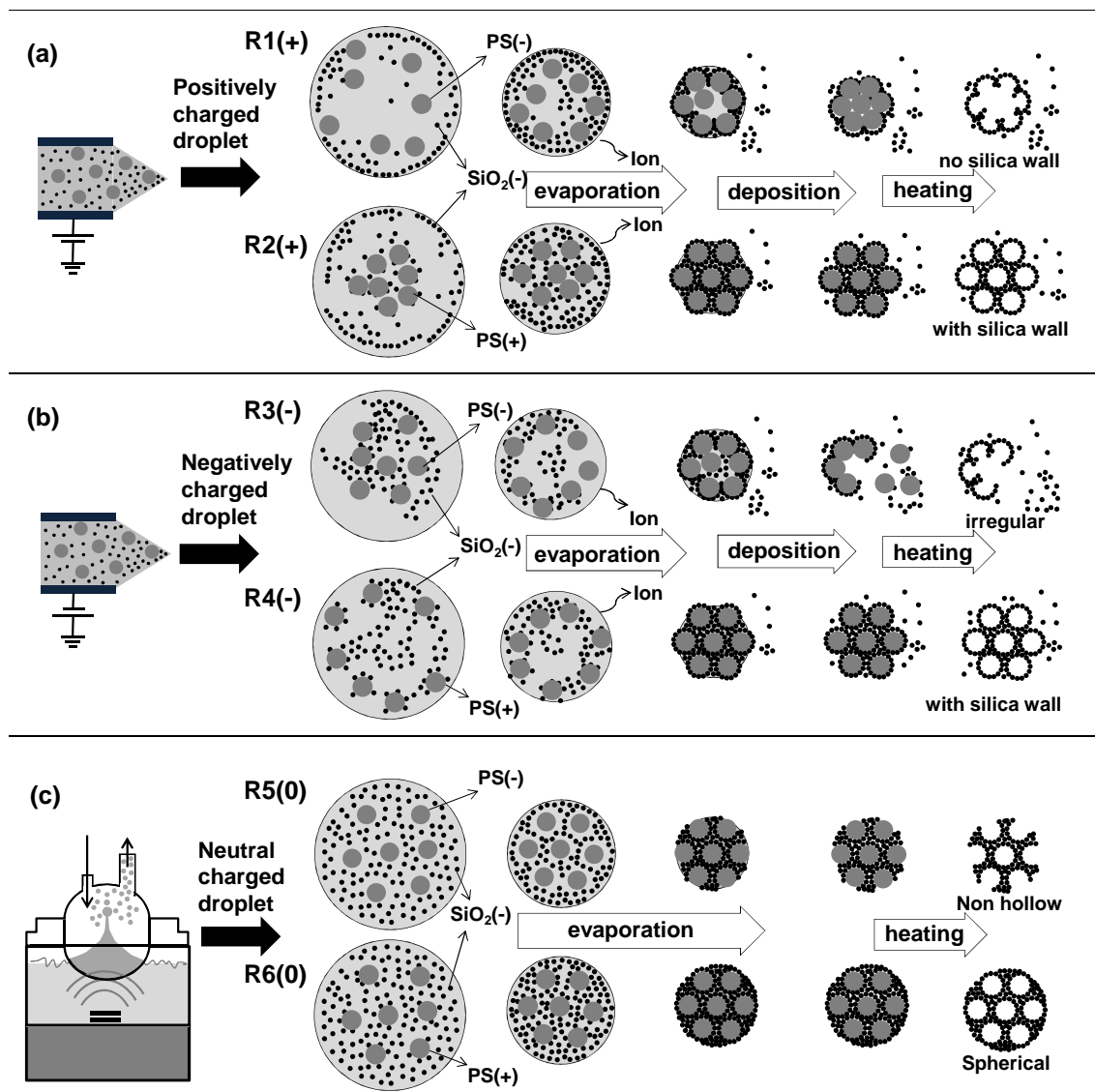
Figure 7.8. Schematic illustrations of hollow particle formation mechanism under different droplet and PS colloidal charges. Figures (a), (b), and (c) are using positive, negative, and neutral droplet charge, respectively.

To complete the consideration of the particle formation due to droplet charge factor, I also refer the cases of particle formation under the lack of electrostatic charge on the droplet surface (routes **R5(0)** and **R6(0)**). Similar to **Chapter 3**, when silica nanoparticles and anionic PS spheres were used, non-hollow structure was produced (**route R5(0)**). On the contrary, when silica nanoparticles and cationic PS spheres were

used, hollow particle with smooth surface and spherical shape is obtained (**route R6(0)**).

In addition, the present method (charged droplet; routes from **R1(+)** to **R4(-)**) allows the production of particles with daisy-shaped structure, in which this is different from common spray-drying method (routes **R5(0)** and **R6(0)**). Unnecessary nanoparticles can be ejected due to Rayleigh limit theory.

7.5. Conclusion

Effects of droplet charge on fabrication of self-organized hollow silica particles from spray-drying of colloidal nanoparticles has been studied. The hollow particles were produced using combination of the spray-drying method and the template removal process. As a model of colloidal component, silica nanoparticles (as a host material) and PS spheres (as a template) were used. The effects of this droplet charge under various self-organization parameters (i.e. flow rate, surface charge, size, and composition of colloidal nanoparticles) were investigated experimentally, and the results are qualitatively explained based on the available theory. Experimental results showed that the droplet charge played an important role in the formation of hollow particles. Hollow particles containing various interior structures were effectively created in all droplet charge variations, except when the process parameters fell within a specific condition (droplet and colloidal nanoparticles are in the same charge polarity). The present method allowed the production of hollow particles with controllable outer shape, hole number, shell thickness, and internal structure. I also proposed a particle formation mechanism during the spray-drying method under various droplet charge conditions. I believe that this information can make a significant extension of the production of functional nanostructured particles using the aerosol-assisted spray-drying process.

_____

7.6. References

[1] J.H. Lee, Gas sensors using hierarchical and hollow oxide nanostructures: Overview, Sensors and Actuators, B: Chemical, 140 (2009) 319-336.

[2] J. Yang, J. Lee, J. Kang, K. Lee, J.S. Suh, H.G. Yoon, Y.M. Huh, S. Haam, Hollow silica nanocontainers as drug delivery vehicles, Langmuir, 24 (2008) 3417-3421.

[3] Y. Zhao, L. Jiang, Hollow micro/nanomaterials with multilevel interior structures, Advanced Materials, 21 (2009) 3621-3638.

[4] X. Ding, K. Yu, Y. Jiang, H. Zhang, Z. Wang, A novel approach to the synthesis of hollow silica nanoparticles, Materials Letters, 58 (2004) 3618-3621.

[5] B. Tan, S.E. Rankin, Dual latex/surfactant templating of hollow spherical silica particles with ordered mesoporous shells, Langmuir, 21 (2005) 8180-8187.

[6] Y.-Q. Yeh, B.-C. Chen, H.-P. Lin, C.-Y. Tang, Synthesis of hollow silica spheres with mesostructured shell using cationic-anionic-neutral block copolymer ternary surfactants, Langmuir, 22 (2006) 6-9.

[7] I. Tissot, J. Reymond, F. Lefebvre, E. Bourgeat-Lami, Sioh-functionalized polystyrene latexes. A step toward the synthesis of hollow silica nanoparticles, Chemistry of Materials, 14 (2002) 1325-1331.

[8] A. Khanal, Y. Inoue, M. Yada, K. Nakashima, Synthesis of silica hollow nanoparticles templated by polymeric micelle with core-shell-corona structure, Journal of the American Chemical Society, 129 (2007) 1534-1535.

[9] A. Paudel, Z.A. Worku, J. Meeus, S. Guns, G. Van Den Mooter, Manufacturing of solid dispersions of poorly water soluble drugs by spray drying: Formulation and process considerations, International Journal of Pharmaceutics, (2012 (In press)).

[10] N.B. Cech, C.G. Enke, Effect of affinity for droplet surfaces on the fraction of analyte molecules charged during electrospray droplet fission, Analytical Chemistry, 73 (2001) 4632-4639.

[11] D.C. Taflin, T.L. Ward, E.J. Davis, Electrified droplet fission and the rayleigh limit, Langmuir, 5 (1989) 376-384.

[12] A.B.D. Nandiyanto, A. Suhendi, T. Ogi, T. Iwaki, K. Okuyama, Synthesis of additive-free cationic polystyrene particles with controllable size for hollow template applications, Colloids and Surfaces, A: Physicochemical and Engineering Aspects, 396 (2012) 96 - 105.

[13] W. Peukert, H.-C. Schwarzer, F. Stenger, Control of aggregation in production and handling of nanoparticles, Chemical Engineering and Processing: Process Intensification, 44 (2005) 245-252.

[14] J. Suh, B. Han, K. Okuyama, M. Choi, Highly charging of nanoparticles through electrospray of nanoparticle suspension, Journal of Colloid and Interface Science, 287 (2005) 135-140.

[15] A. Gomez, K. Tang, Charge and fission of droplets in electrostatic sprays, Physics of Fluids, 6 (1994) 404 - 414.

[16] A. Suhendi, M.M. Munir, A.B. Suryamas, A.B.D. Nandiyanto, T. Ogi, K. Okuyama, Control of

_____

cone-jet geometry during electrospray by an electric current, Advanced Powder Technology, 24 (2013) 532-536.

[17] A.B.D. Nandiyanto, A. Suhendi, O. Arutanti, T. Ogi, K. Okuyama, Influences of surface charge, size, and concentration of colloidal nanoparticles on fabrication of self-organized porous silica in film and particle forms, Langmuir, 29 (2013) 6262-6270.

[18] A. Suhendi, A.B.D. Nandiyanto, T. Ogi, K. Okuyama, Agglomeration-free core-shell polystyrene/silica particles   preparation using an electrospray method and additive-free cationic polystyrene core, Materials Letters, 91 (2013) 161-164.

_____

Chapter 8
Summary

Critical issues associated with the self-assembly during spray-drying method to obtain the effective strategies in designing nanostructured particle with various morphologies had been discussed. The colloidal nanoparticles properties (composition, size, and charge) and the droplet properties (size, concentration and charge) played significant roles in the fabrication of nanostructured particles.

The effectiveness of this method in controlling particle morphologies that include aggregates, core-shell, porous, hollow (spherical, daisy-shape), and hairy forms had been described along with theoretical explanation. A summary of the strategies in designing particle could be simply explained in the following:

(i)   The spray-drying under uncharged droplet conditions was a good method to produce particles with controllable morphology. The control of size and shape could be achieved simply by the change of composition, size and charges of the colloidal nanoparticles. In this study, several particles with different shapes produced by this synthesis method could be comprised:

- Basic explanation on the self-organization and spray-drying on particles fabrication with its current strategies to achieve this control is described in **Chapter 1**.

- Spherical-shaped cationic polystyrene particles with controllable size (from tens to hundreds nanometer) were successfully synthesized, in which this control could be achieved by the manipulation of reactant concentration (i.e. monomer and initiator) and processing temperature (**Chapter 2**).

- Colloidal nanoparticle properties (amount of charge, concentration, and size)

_____

was discussed in **Chapter 3**. Particles containing highly ordered pores were successfully created only if the process was conducted under appropriate self-assembly parameter conditions. In contrast, variations of these parameter conditions resulted in the formation of particles with either incomplete or brittle porous structures.

(ii)   The spray-drying method under charged droplet condition could be used as a good alternative way to produce particles with high degree of control. The control provides possibility to produce particle with various outer shape, shell thickness and different inner structure. Detailed result in this study could be described in the following:

- Current controlled electrospray system has been developed. The system provides control over droplets size and distribution. (**Chapter 4**). This control is available due to the constant delivery of charge to mass ratio of the electrosprayed solution.

- Core-shell silica/PS particles were prepared using electrospray-assisted spray-drying method (**Chapter 5**). The core-shell structure was developed due to the charge interaction between colloidal particle charges and was enhanced due to the existence of charge in the droplet. The outer morphology of the hollow particle can be controlled by the adjustment of the composition of the colloidal nanoparticles.

- Aggregate-free spherical hollow particles were produced by spray-drying and template removal process (**Chapter 6**). The aggregate-free condition was obtained by selecting the droplet size to the minimum.

- Effect of droplet size on the self-organization of nanoparticles during spray-drying process was thoroughly elaborated in **Chapter 7**. Effects of

_____

droplet charge and colloidal nanoparticles properties were described.

The various morphologies of particles fabricated from spray-drying of colloidal nanoparticles exhibit great potential for applications in future technology. Enhancement of particle performance could be achieved by the change in morphology.

Finally, I believed that this report would contribute new information to the fields of chemical and material engineering because the methods, which were studied and reviewed, had shown that broad applications could be born from nanostructured particles fabricated from self-assembly of the colloidal nanoparticles. In addition, self-assembly of colloidal nanoparticles inside charged droplets with controllable size and morphology is of both great significance and challenge, and need to be further explored.

Appendix I: List of Figures

Appendix II: List of Tables

Appendix III: List of Publications

1. Suhendi, A., Nandiyanto, A.B.D., Munir, M.M., Ogi, T., and Okuyama, K. Materials Letters, 91, 161-164 (2013).

2. Suhendi, A., Munir, M.M., Suryamas, A.B., Nandiyanto, A.B.D., Ogi, T., and Okuyama, K., Advanced Powder Technology, 24(2), 532-536 (2013)

3. Suhendi, A., Nandiyanto, A.B.D., Ogi, T., and Okuyama, K., Materials Letters, 106, 432-435 (2012)

4. Nandiyanto, A.B.D., Suhendi, A., Arutanti, O., Ogi, T., and Okuyama, K., Langmuir, 29 (21), 6262–6270 (2013)

5. Nandiyanto, A.B.D., Suhendi, A., Ogi, T., Iwaki, T., and Okuyama, K., Colloid Surface A: Physicochemical and Engineering Aspects, 396, 20, 96–105 (2012)

6. Munir, M.M., Suhendi, A., Ogi, T., Iskandar, F., and Okuyama, Advanced Powder Technology, 24(1), 143-149, (2013).

7. Munir, M.M., Suhendi, A., Ogi, T., Iskandar, F., and Okuyama, Journal of Chemical Physics 133, 124315, (2010).